2003

Quantifying habitat quality of larval bay anchovy (Anchoa mitchilli) in Chesapeake Bay by linking an individual-based model with spatially-detailed field data

Aaron Thomas Adamack
Louisiana State University and Agricultural and Mechanical College

QUANTIFYING HABITAT QUALITY OF LARVAL BAY ANCHOVY (*ANCHOA MITCHILLI*) IN CHESAPEAKE BAY BY LINKING AN INDIVIDUAL-BASED MODEL WITH SPATIALLY-DETAILED FIELD DATA

A Thesis

Submitted to the Graduate Faculty of the
Louisiana State University and
Agricultural and Mechanical College
in partial fulfillment of the
requirements for the degree of
Master of Science

in

The Department of Oceanography and Coastal Sciences

by
Aaron Thomas Adamack
B.Sc., University of British Columbia, 1999
December 2003

ACKNOWLEDGEMENTS

I will begin by thanking my major professor, Dr. Kenny Rose, for his encouragement, guidance and patience over the past four years, which helped me tremendously in completing this thesis. I thank my committee members Dr. Jaye Cable and Dr. Jim Cowan for their support, helpful comments and advice. I would also like to thank Dr. Jim Cowan and Dr. Ed Houde for their advice on analyzing the initial results of the simulations and for their suggestions that improved the accuracy of the model's mortality rate predictions. Additionally, I thank Chris Rilling and Dr. Ed Houde for providing me with access to their data, without which this project could not have happened. Thank you, Carol Fleeger, for your help in navigating the bureaucracy of LSU.

Thanks to Brian Milan, Sean Keenan, Megan Peabody, and the people at the Dauphin Island Sea Lab (Jessica McCawley, Melissa Woods and others) for giving me the opportunity to see what actual fish look like. Thanks to Shaye Sable for helping to ease my transition to this new country by providing me with furniture and rides. I really appreciate the friendship and support of the students in the Rose lab: Shaye Sable, Cheryl Murphy, Laura Althauser, and John Augustine. I also want to thank all of the friends that I've made over the past four years who've helped to make my life in Louisiana enjoyable, in particular: the dancing crowd, the poker guys, and the MER football fans. Thanks to Kristen Laursen for helping me to survive the process of writing my thesis and for providing her ongoing encouragement and support.

I would like to thank my parents Tom and Beverly Adamack, my sister Denene (Deni), and my grandma, Helen Adamack, for their continued support, encouragement and the many hours of discussions over the phone. Finally, this thesis is dedicated to my grandma, Helen Adamack, and to the memory of my grandparents, Roy and Edith Elander and Nick Adamack.

TABLE OF CONTENTS

LIST OF TABLES

LIST OF FIGURES

ABSTRACT

Larval bay anchovy (*Anchoa mitchilli*) habitat quality in Chesapeake Bay was predicted using an individual-based model applied to spatially-detailed field data from Rilling and Houde (1999). Habitat quality was predicted using the ratio of instantaneous mortality rate to instantaneous growth rate. Model predictions of habitat quality were compared to field estimates of habitat quality derived from the spatially-detailed field data. Three sets of one-day simulations were performed to estimate larval growth and mortality rates throughout Chesapeake Bay during June and during July 1993. Field-based simulations used field data to estimate the model inputs of water temperature, zooplankton densities, and the densities and sizes of bay anchovy larvae and gelatinous predators (*Mnemiopsis leidyi* and *Chrysaora quinquecirrha*). Standardized larvae simulations used the same field data, but standardized larval sizes and densities throughout the Bay. A third set of simulations was performed to determine the relative importance of six factors in determining the bay-wide spatial variation in predicted growth and mortality rates. Model predictions from the field-based simulations produced spatial patterns of habitat quality in the Bay that sometimes conflicted with the otolith-based predictions of Rilling and Houde. Field estimates of anchovy egg and larvae abundances were generally high in regions predicted to have low M/G ratios, but low in regions with low otolith-estimated M/G ratios. The standardized larvae simulations generally supported the conclusions of the field-based simulations. The effect of habitat quality on larval production was evaluated using the predicted mortality rates from the two sets of simulations. Initial larval abundances dominated the percent of survivors projected 20-days into the future that a region would produce, but when larvae were standardized across the bay, differences in habitat quality among regions was important in determining the relative contributions of survivors by region. Initial larval length and zooplankton densities were the

most important factors determining the spatial variation in growth rate, while predator density was most important for mortality rate. Future research should focus on field and laboratory data collection to resolve the discrepancy between model-predicted and otolith-estimated M/G ratios.

INTRODUCTION

Small changes in the growth and mortality rates of larval fish can have order of magnitude effects on larval recruitment (Houde 1987). A number of physical and biological factors may affect larval growth and mortality rates (Heath 1992). Physical factors include water temperature (Houde 1989), vertical structure of the water column, and dissolved oxygen (Breitburg et al. 2003). Biological factors include the availability of appropriate zooplankton prey (Rilling and Houde 1999), and the densities and sizes of predators (Paradis and Pepin 2001; Cowan et al. 1996). The relative importance of these different factors can vary in time and space. Growth rate can also affect cumulative mortality during the larval stage because mortality rate often decreases with larval length (Pepin 1993, Rice et al. 1993).

High primary productivity in estuaries results in high fish production for resident species, and for marine species whose young utilize estuaries as nursery grounds (Houde and Rutherford 1993). However, human impacts in coastal areas increasingly result in decreased fish habitat through a combination of degraded water quality, loss of sea grass beds and marshes, and an increased extent of hypoxia (Schmitten 1999, National Research Council 1999). Due to this loss of habitat, there is a growing need to identify and protect essential fish habitat, as mandated by the Sustainable Fisheries Act (Schmitten 1999). Most analyses of fish habitat quality rely on the correlation between fish densities and environmental factors (i.e., more fish implies better habitat) (Minello et al. 2003). Quantifying the quality of habitat for larval fish in estuaries such as Chesapeake Bay is especially difficult because of the dynamic nature of the pelagic zone, and is complicated by a lack of appropriate data (e.g., sizes and densities of prey and predators of bay anchovy larvae).

One approach that is used to determine habitat quality is associating the growth and mortality rates of larvae during their recent past to environmental conditions. Otoliths can be used to determine the age of individual larvae (Leak and Houde 1987). Growth rates of larvae are obtained by regressing the measured weights or lengths of larvae on their ages, and using the slope of the regression line as an estimate of mean larval growth rate. Larval mortality rates are estimated by regressing larval abundances on age, and using the slope as an estimate of mortality rate (Rilling and Houde 1999). Combining individual larvae into geographic regions based upon their capture location can then be used to estimate region-specific growth and mortality rates. These estimates of growth and mortality rates are based on days to weeks of past experiences of the larvae, and are indicative of habitat quality over broad geographic areas. Whether these estimates are indicative of habitat quality on local (less than regional) spatial scales depends on the mobility of larvae and the degree to which environmental and biological conditions vary in space and time.

A second approach to examining habitat quality has been the use of spatially-explicit bioenergetics models (e.g. Brandt and Kirsch 1993, Luo and Brandt 1993, Logerwell et al. 2001, Tyler and Brandt 2001). These models use growth as a fitness currency (Tyler and Brandt 2001) to measure the quality of habitat in pelagic environments. Data on the densities of prey species are obtained by using either physical sampling (i.e. plankton nets or Niskin bottles) or by the use of acoustic surveys (Brandt and Kirsch 1993). Growth rate potentials, the growth rate of a fish if it were present in a location, for specific size classes of fish are predicted by applying foraging and bioenergetics models to the prey density data. One assumption of this approach is that the fish of interest are located everywhere there are prey in the system, hence the term growth rate potential (Brandt and Kirsch 1993). This assumption makes comparison of predicted growth

rates to observed growth rates difficult. Also, only recently have there been attempts to predict mortality rates in conjunction with growth rate potential (e.g. Höök et al. 2003).

This study combines data from an extensive field monitoring effort with an individual-based model to predict larval bay anchovy growth and mortality rates at specific stations in Chesapeake Bay. The field data consist of the environmental variables of temperature, salinity, and dissolved oxygen, and the biological variables of zooplankton densities, and the sizes and densities of bay anchovy larvae (*Anchoa mitchilli*), ctenophores (*Mnemiopsis leidyi*), and sea nettles (*Chrysaora quinquecirrha*). Environmental and biological variables were measured at 46 stations in June and at 48 stations in July of 1993 in the Chesapeake Bay (Rilling 1996). The individual-based model simulates the growth of individual larvae based upon their encounters with zooplankton, and predicts mortality based on their encounters with individual gelatinous predators. One-day model simulations are performed using the field data to predict instantaneous growth (G) and mortality (M) rates for the surface and bottom layers at each station for June and July.

The primary objective of this study is to quantify habitat quality for larval bay anchovy in Chesapeake Bay. I used an individual-based model to obtain station-specific estimates of growth and mortality rates, which were aggregated to assess regional habitat quality. Thus, my approach differs from that based on otoliths, which first requires aggregating larvae and then obtaining regional growth and mortality rates. The individual-based modeling approach also uses conditions at the time of capture to predict growth and mortality rates, thereby minimizing the reliance on past history. Finally, by using field data on prey, bay anchovy larvae, and predators, the individual-based modeling approach allows for comparison of predicted growth and mortality rates to measured values. I use the modeling results to identify which areas of the Bay

are best for larval growth and survival, and which biological factors are most influential in determining the spatial variation in larval growth and mortality rates. I also compare my predictions of regional habitat quality to those obtained by Rilling (1996) based on otolith analyses. I conclude with recommendations on data collection and additional modeling that could improve the predictions of larval growth and mortality rates and their use in quantifying larval fish habitat.

Chesapeake Bay and Bay Anchovy

Chesapeake Bay (Bay) is the largest estuary in the United States (Kimura et al. 2000; Chesapeake Bay Program 2002), extending 250 km from north to south and 58 km (at its widest) from west to east. Geomorphically, it is described as a coastal plain estuary (Day et al. 1989), having formed approximately 10,000 to 15,000 years ago during the last eustatic sea level rise. On average, the Bay is relatively shallow with an average depth of approximately 6.5 m. Less than 10% of the Bay's area is deeper than 18 m, and approximately 50% of the Bay is less than 6 m deep (Jung 2002). The Bay is classified hydrographically as a partially mixed estuary (Baird and Ulanowicz 1989). Physical conditions in the Bay vary widely throughout its extent with a well-defined salinity gradient (Carter and Pritchard 1988); riverine flow is dominant in the northern extremes of the estuary (salinity of 0.2 ppt) while oceanic flow is dominant near the Bay mouth (salinity of 23.7 ppt) (Carter and Pritchard 1988, Rilling 1996). More than 80% of the freshwater entering Chesapeake Bay is from tributaries on it's northern and western sides. The Susquehanna River, which is located at the head of the Bay, provides half of Chesapeake Bay's freshwater inflow. The estuarine turbidity maximum is variably located between 39°10' and 39°28'N, and typically extends 10 to 30 km along the north to south (N-S) axis of the Bay (Roman and Holliday 2001). Water temperature in Chesapeake Bay ranges between about 6° to

17°C during the spring and between about 21° to 29°C during the summer (Baird and Ulanowicz 1989). During late spring and summer, the Bay develops thermohaline stratification (Keister et al. 2000) that isolates much of the bottom layer from the rest of the water column (Breitburg et al. 1999). Stratification, coupled with excess primary production due to high nutrient flow into the Bay leads to hypoxia and anoxia in the bottom layer as unconsumed phytoplankton sinks and is decomposed through microbial respiration, which rapidly consumes most of the dissolved oxygen (Breitburg et al. 1999).

Chesapeake Bay is a highly productive estuary (Nixon 1988) in which biological activity increases during the spring and peaks in summer (Baird and Ulanowicz 1989). The Bay serves as a nursery area for a number of fish species, including striped bass (*Morone saxatilis*), Atlantic croaker (*Micropogonias undulates*), Atlantic menhaden (*Brevoortia tyrannus*), weakfish (*Cynoscion regalis*), and spot (*Leiostomus xanthurus*) (Jung 2002). Ichthyoplankton surveys of Chesapeake Bay by the Trophic Interactions in Estuarine Systems (TIES) Program (http://www.chesapeake.org/ties/ichplk/ties.html) showed that the larvae of many of these fish were primarily concentrated in the lower Bay and secondarily in the upper Bay region. The zooplankton prey of young fish in Chesapeake Bay during summer is dominated by the calanoid copepod, *Acartia tonsa* (Baird and Ulanowicz 1989). Young fish in the Bay experience significant competition for food from ctenophores and sea nettles (Purcell and Arai 2001). Ctenophores and sea nettles also are major predators on the eggs and larvae of fish. Ctenophores have the potential to eat fish eggs at rates of 10 to 65% d^{-1} (Monteleone and Duguay 1988), and fish larvae at rates of 20 to 40% d^{-1} (Cowan and Houde 1992, 1993). Sea nettles may consume eggs and larvae at rates of 20 to 40% d^{-1} (Cowan and Houde 1992, 1993). The major piscivores in the Bay during summer are bluefish, weakfish, summer flounder and striped bass, which feed

primarily on bay anchovy and menhaden (Baird and Ulanowicz 1989, Hartman and Brandt 1995).

Bay anchovy are one of the most abundant fish species in Chesapeake Bay (Baird and Ulanowicz 1989, Jung 2002), and are an important trophic link between the zooplankton and the piscivores (Baird and Ulanowicz 1989, Luo and Musick 1991). Adult anchovies spawn serially throughout Chesapeake Bay between May and September, with a spawning peak in July (Zastrow et al. 1991). During the summer, their eggs typically make up more than 80% of the total number of fish eggs caught, while larval bay anchovy make up more than 75% of all larval fish captured in Chesapeake Bay icthyoplankton tows (Olney 1983, TIES Program 2003). Larval bay anchovies are primarily thought to consume rotifers, tintinnids, copepod nauplii and copepodites (Detwyler and Houde 1970), while adult bay anchovies mainly consume calanoid copepods (Sheridan 1978). Bay anchovy are a major predator of zooplankton in Chesapeake Bay; potentially consuming 70-90% of the zooplankton consumed by all planktivorous fishes (Baird and Ulanowicz 1989, Houde et al. 1989, Luo and Brandt 1993).

METHODS

Habitat quality for larval bay anchovy (*Anchoa mitchilli*) in Chesapeake Bay was quantified using an individual-based model applied to spatially-detailed field data. One-day simulations were performed to estimate larval growth and mortality rates for the surface and bottom layers at 46 stations in June 1993 and at 48 stations in July 1993. The field data of Rilling and Houde (1999) were used to estimate model inputs of water temperature, zooplankton densities, and the densities and lengths of bay anchovy larvae, ctenophores, and sea nettles. Larval anchovy growth was simulated using a bioenergetics model based on larval encounters and captures of zooplankton. Larval anchovy mortality was simulated based on a model of larval encounters with individual ctenophore and sea nettle predators. The first set of simulations used field data to estimate key model inputs. Layer-specific growth and mortality rates predicted by model simulations for stations were examined for spatial patterns, and were aggregated into regional estimates and compared with similar results obtained from Rilling and Houde's (1999) otolith analysis. A second set of simulations using standardized cohorts of bay anchovy larvae (i.e., uniform lengths and densities rather than the field-based measurements) was used to predict growth potential and mortality rates throughout Chesapeake Bay. Finally, a third set of simulations evaluated the influence of six factors (temperature, sea nettle size, ctenophore length, predator (sea nettle and ctenophore) density, larval length, and zooplankton densities) on the spatial pattern of predicted larval growth and mortality rates.

Collection Methods

The field data used in model simulations were from two cruises that were conducted in June and July of 1993 (see Rilling 1996, Rilling and Houde 1999 for a complete description of the field sampling program). During each cruise, the environmental variables of temperature,

salinity, and dissolved oxygen, and the biological variables of zooplankton density (rotifers and tintinnids, nauplii, copepodites, and adult copepods), and larval fish, ctenophore, and sea nettle sizes and densities were measured at each layer and station sampled. The stations were located on 15 transects spaced at 10 nautical-mile intervals from the head of the Bay (39° 25′N) to near the Bay mouth (37° 05′N) (Figure 1). For his analysis, Rilling (1996) divided Chesapeake Bay into three regions (upper Bay, mid Bay and lower Bay). The upper Bay region was designated as transects 1-5 (39° 25′ N to 38° 45′ N), the mid Bay region as transects 6-10 (38° 45′ N to 37° 55′ N) and the lower Bay region as transects 11-15 (37° 55′ N to 37° 05′ N). These same regional definitions were used in this study.

Environmental variables and zooplankton densities were determined at multiple depths throughout the water column, while larval and predator sizes and densities were determined for the surface and bottom layers. Environmental variables were measured using CTD casts from within 1 m of the surface to within 1 m of the bottom. Zooplankton densities were estimated using 10 liter Niskin bottles placed at 3 to 4 designated depths at each station. Due to time constraints, only the zooplankton samples collected at odd-numbered transects were enumerated. Larval and gelatinous predator (ctenophores and sea nettles) densities were estimated by using two, 2-minute tows at each station with an opening-closing 60-cm bongo net. The first tow sampled the bottom layer from within 1 m of the bottom to the pycnocline (or mid-depth if no pycnocline was present). The second tow sampled the surface layer from the pycnocline to the surface of the water column. Sizes of individuals were measured for samples, or sub-samples, of larvae and gelatinous predators collected by the 2-minute tows. Measured temperatures, zooplankton densities, and the densities and sizes of bay anchovy larvae, ctenophores and sea nettles from the two cruises are summarized in Table 1.

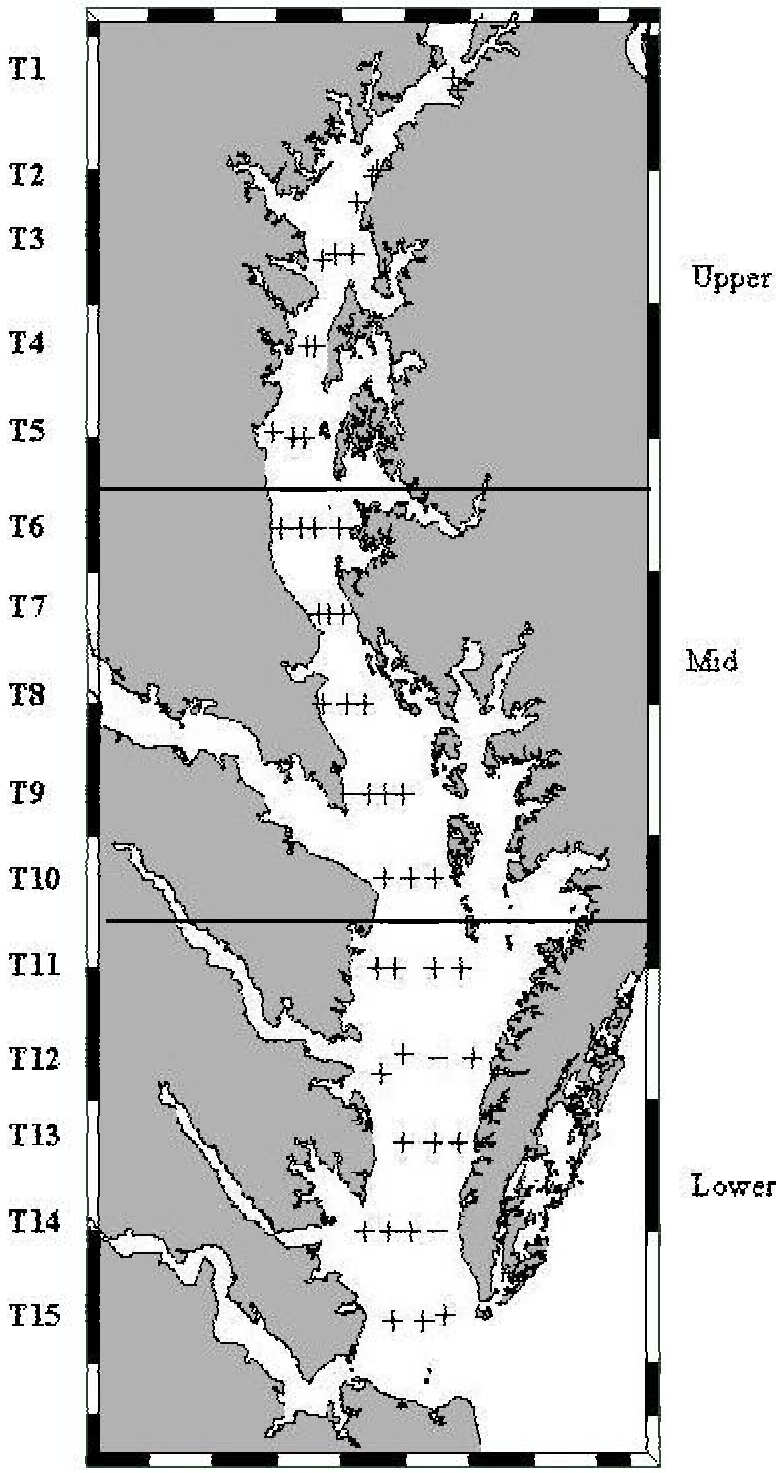

Figure 1: Transect and station locations for environmental and biological sampling by Rilling (1996) in the Chesapeake Bay during June and July 1993. The three regions along the N-S axis (upper, mid, and lower) are also shown.

Table 1: The mean, minimum, and maximum values of the biological and environmental variables measured during field sampling in June and July of 1993. No sea nettles were recorded in June. The data are from Rilling (1996).

Observation	June			July		
	Mean	Min	Max	Mean	Min	Max
Temperature (ºC)	23.19	16.20	26.80	25.91	23.00	28.8
Nauplii (# l^{-1})	42.56	0.60	404.17	116.73	1.20	556.70
Copepodite (# l^{-1})	11.34	0.20	85.00	18.18	0.00	94.20
Adult Copepod (# l^{-1})	2.94	0.00	27.50	9.89	0.00	53.33
Bay Anchovy Larvae (# m^{-3})	2.55	0.00	69.25	22.29	0.00	178.14
Ctenophores (# m^{-3})	15.93	0.00	133.36	3.20	0.00	40.44
Sea Nettle (# m^{-3})	-	-	-	0.03	0.00	0.22
Larval Length (mm)	4.20	1.59	15.87	3.80	1.00	28.03
Ctenophore Length (mm)	26.68	5.00	90.00	37.52	5.00	95.00
Sea Nettle Bell Diameter (mm)	-	-	-	84.28	20.00	185.00

Rilling and Houde (1999) estimated instantaneous weight-specific bay anchovy growth rates for each of the upper, mid, and lower Bay regions using an otolith-based method. Sagittal otoliths from representative samples of larvae within each region were examined in order to determine the age (d) of individual larva. Each larva included in the otolith analysis was measured to the nearest 0.1 mm with an ocular micrometer mounted in a stereomicroscope. The number of increments on each sagittal otolith was counted twice by a single reader (Rilling) using a compound light microscope at 600 to 1000x magnification, and the mean of the two counts plus two days was accepted as the estimated age of the larva. Bay anchovy larval lengths (L_L, mm) were converted to dry weights (W, μg) using a weight-length relationship:

$$W = 0.1550L^{3.5307} \qquad \text{Eq. 1}$$

Rate of growth in weight was then estimated from an exponential regression model, fitted by regressing $\log_e$-transformed dry weights on age for each region using the model:

$$W_t = W_0 e^{Gt} \qquad \text{Eq. 2}$$

where W_t = dry weight (μg) at age t (d); W_0 = dry weight (μg) at hatch (the back transformed

y-intercept of the W_t versus t linear regression); G = weight-specific growth coefficient (d^{-1}), and t = age (d).

Regional instantaneous bay anchovy larval mortality rates were estimated by Rilling and Houde (1999) using an exponential model of decline in abundance with respect to age:

$$N_t = N_0 e^{-Mt} \quad \text{Eq. 3}$$

where N_t = the abundance (number m^{-2}) at age t (d); N_0 = estimated initial abundance (the back transformed y-intercept of the ln N_t versus t regression; number m^{-2}); M = instantaneous mortality coefficient (d^{-1}), and t = age (d). The otolith analysis was used by Rilling and Houde (1999) to develop an age-length key for each month and region. The age-length key was used to convert length frequencies to age frequencies. Equation 3 was then applied to compute mortality rates from the abundance versus age data for each month and region.

Rilling and Houde (1999) used the ratio of instantaneous mortality rate (M) to instantaneous weight specific growth rate (G) to determine the stage-specific or "physiological" mortality rate (M/G) of larval anchovy. The stage-specific mortality rate is the mortality per unit of growth (Houde 1997). M/G ratios can be used to infer habitat quality. When M is greater than G, M/G is greater than 1 and cohort biomass is decreasing. When M is less than G, M/G is less than 1 and cohort biomass is increasing (Houde 1997).

Model Overview

I modified a previously developed individual-based model (Cowan et al. 1996; Breitburg et al. 1999; Breitburg et al. 2003), and used the model to simulate the growth and predation mortality of larval bay anchovy in Chesapeake Bay for the surface and bottom layer at each of the 46 stations in June and the 48 stations in July (Figure 1). The growth portion of the original model simply assigned growth rates to individual larvae. I replaced the original simple growth

model with a more detailed growth model that simulated the growth of larval bay anchovy based on their size, water temperature, and encounters with zooplankton. The new growth model was borrowed from Rose et al. (1999). The predation portion of the model has been modified from its original formulation to include ctenophores as predators and to make predator capture success dependent on the sizes both of the predator and the bay anchovy larva. To simulate the growth and mortality of the larvae, each individual larval bay anchovy in the model loops through a series of steps each day (Figure 2). The individual steps are described in detail below.

Model Dimensions and Initial Conditions

All simulations were single day simulations in a single, well-mixed box with a volume of 2000 m^3. Separate simulations were performed for each layer at each station. At the start of each simulation, water temperature and the initial densities of bay anchovy larvae, ctenophores, sea nettles, and zooplankton prey (rotifers and tintinnids, copepodites, nauplii and adult copepods) were set to the values observed during field sampling for each layer at each station. Field densities of zooplankton were used directly in the model. Field densities of larvae, ctenophores and sea nettles were multiplied by 2,000 m^3 to obtain the number of individuals that started each simulation. Initial sizes were then assigned to the individual larvae (L_L), ctenophores (L_C), and sea nettles (L_{SN}) by randomly generating sizes from empirical size distributions formed from the field data. The empirical distributions were formed by first arranging the measured sizes of individuals in rank order, and then using linear interpolation between measured sizes to form a continuous probability distribution. The desired number of initial sizes were then randomly generated from the probability distributions. The initial dry-weight of each larva (W, mg dry wt.)

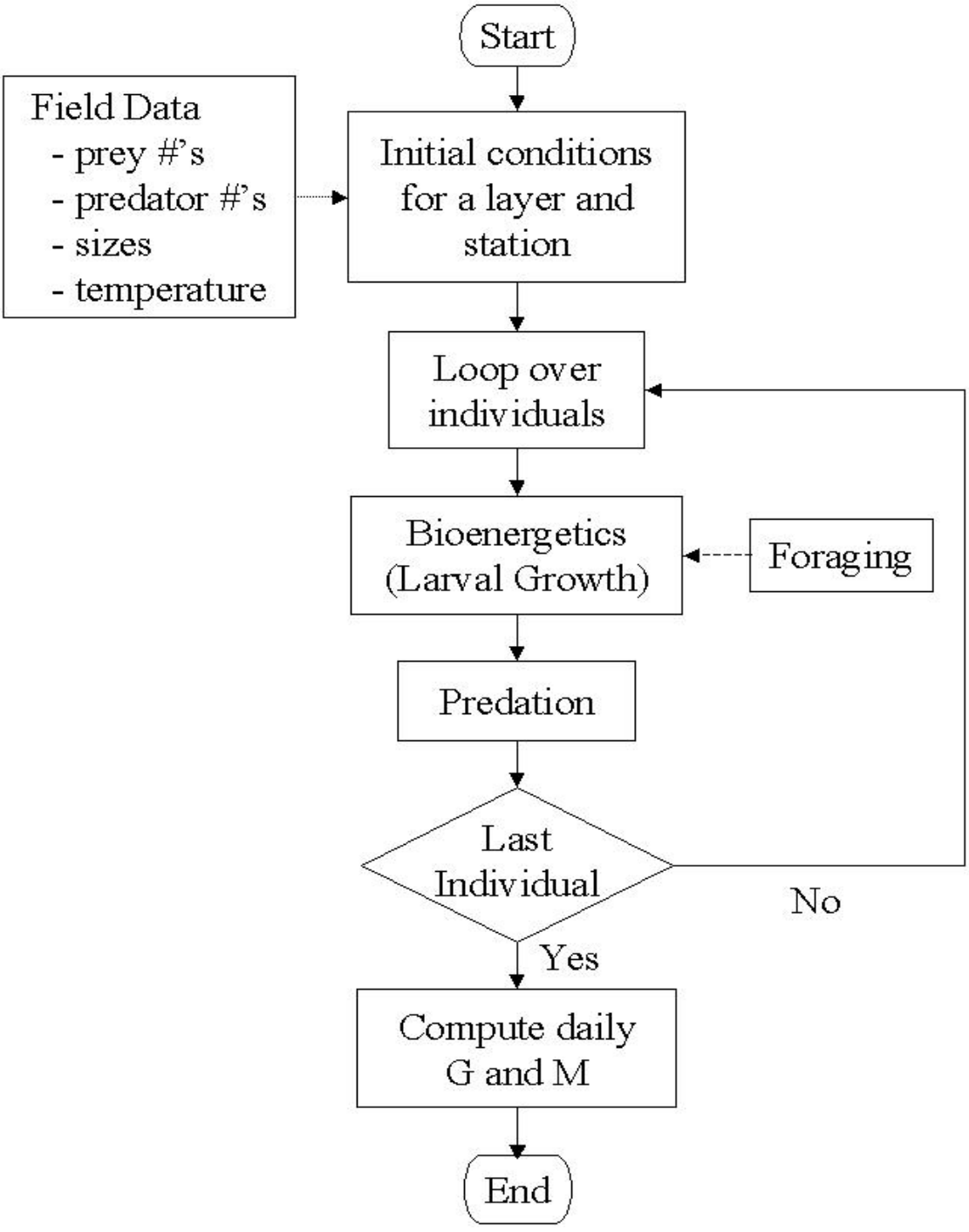

Figure 2: Flow diagram showing the major steps in the individual-based larval model. The dotted line indicates the input of field data into the model while the dashed line indicates the input of data on individual larval bay anchovy predation rates on zooplankton prey to the bioenergetics component of the model.

was determined from its generated initial length using a length-to-weight relationship for bay anchovy (Tucker 1989):

$$L_L = \begin{cases} 51.2W^{0.594} \text{ if W} \le 0.015 \text{ mg (4.3 mm)} \\ 12.4W^{0.254} \text{ if W} > 0.015 \text{ mg} \end{cases} \qquad \text{Eq. 4}$$

Two modifications were made to the field data used in model simulations. Zooplankton were enumerated in the field surveys at odd numbered transects only. For model simulations, zooplankton densities for stations on even numbered transect lines were estimated as the mean of the zooplankton densities at the two closest stations on adjacent transects. The second modification was made to reported densities of rotifers and tintinnids. The densities of rotifers and tintinnids observed during field sampling appeared to be low compared to previous reports (Rose et al. 1999). Densities of rotifers and tintinnids were adjusted upwards for simulations by multiplying their observed densities by 10, setting the adjusted densities of rotifers and tintinnids to a magnitude approximately equal to those reported in Rose et al. (1999). An additional 100 individuals liter^{-1} were added to the adjusted density in order to eliminate zero counts of rotifers and tintinnids. The Appendix shows the values of all model inputs for each layer and station for June and July, as estimated from the field data.

Bioenergetics

Each day the growth in weight of each feeding larva was computed using a difference form of a bioenergetics equation as described in Rose et al. (1999):

$$W_t = W_{t-1} + (pC_{\max} A - R_{tot}) \cdot 1 \text{ day} \qquad \text{Eq. 5}$$

where W_t = new weight of the larvae (mg dry wt.); W_{t-1} = weight of the larvae at the start of the day (mg dry wt.); p = proportion of C_{max} realized and was calculated as $p = C_r/C_{max}$ where C_r was the realized consumption determined in the foraging subroutine (mg dry wt. d^{-1}); C_{max} =

maximum dry-weight consumption as a function of weight and temperature (mg dry wt. d^{-1}); A = utilization efficiency, the fraction of consumption available for growth and metabolism as a function of body weight and consumption; and R_{tot} = total dry-weight metabolic rate (mg dry wt. d^{-1}).

Maximum Consumption, C_{max}, was calculated by using the equation:

$$C_{\max} = \begin{cases} 47.37W^{1.732}F(T) & \text{for W} < 0.022 \text{ mg (= 4.7mm)} \\ 1.1019W^{0.727}F(T) & \text{for W} \geq 0.022 \text{ mg} \end{cases} \qquad \text{Eq. 6}$$

where F(T) = temperature adjustment to C_{max} for warm-water species (Kitchell et al. 1977) with parameters T_0, T_m, and Θ. T_0 was the optimum temperature for larval bay anchovy, 28.0 °C; T_m was the maximum temperature at which larval bay anchovy feed, 37.0 °C; and Θ = 2.2 approximates the Q_{10} relationship for temperatures below optimal for bay anchovy larvae.

Utilization efficiency was computed dependent upon the ratio of realized consumption to maximum consumption:

$$A = \begin{cases} \dfrac{\min(0.7W^{0.15},0.7)}{0.83} & \text{if } \dfrac{C_r}{C_{\max}} < 0.83 \\ \dfrac{\min(0.7W^{0.15},0.7)}{C_r / C_{\max}} & \text{if } 0.83 < \dfrac{C_r}{C_{\max}} < 2.0 \end{cases} \qquad \text{Eq. 7}$$

Utilization efficiency is assumed to be low when consumption is very high, and to increase as realized consumption becomes a smaller fraction of maximum consumption.

Total dry-weight metabolic rate was determined using the equation:

$$R_{tot} = \left[R_r + (ACT - 1)R_r FF\right]\delta \qquad \text{Eq. 8}$$

where R_r = routine metabolism and was determined as a function of larval weight and a Q_{10} temperature relationship; ACT = activity multiplier and was assumed to be 2.0 for the larval stage; FF = fraction of the day during which metabolism was active, 13 of 24 hours; and δ is an

adjustment to slow the rate of weight loss when C_r is less than the consumption required to maintain a larva's weight (see Rose et al. 1999). In equation 8, active metabolism is a multiplier of routine metabolism and is assumed to occur during daylight hours.

Foraging

The realized consumption of zooplankton prey (mg d^{-1}), C_r, was determined each day for each larva using the method of Rose et al. (1999). Larvae fed on four types of zooplankton prey: rotifers and tintinnids, nauplii, copepodites, and adult copepods. The number of each prey type encountered by a larva was determined stochastically using the mean encounter rate (e_i^M) for the *i*th prey type:

$$e_i^M = S_i \cdot PD_i \qquad \text{Eq. 9}$$

where

$$S_i = \frac{\pi}{2}(RD_i F_{RD})^2 \left[a_{ss} L_L FF \frac{3600\text{s}}{\text{day}} \right] \frac{10^{-6}\ \text{liters}}{\text{mm}^3} \qquad \text{Eq. 10}$$

S_i = the volume searched by the larva for the *i*th prey type, determined as half the volume of a cylinder with radius equal to the reactive distance of the larvae and height equal to the distance swum during daylight hours; PD_i = the observed prey density (number l^{-1}); RD_i = reactive distance of the larvae as a function of prey height and angle of acuity of the larva; F_{RD} = a reduction in reactive distance due to turbidity; a_{ss} = larval fish swimming speed; and FF = fraction of the day spent swimming (13 of 24 hours a day). Reactive distance of the larva increases with larval size and with longer prey items (Rose et al. 1999).

The realized number of encounters (e_i^R) between each individual larva and each zooplankton prey type was determined using the equation:

$$e_i^R = e_i^M \cdot F(x) \qquad \text{Eq. 11}$$

where F(x) was a multiplier designed to simulate the effects of spatial patchiness of zooplankton prey. Rose et al. (1999) estimated cumulative distribution functions for each zooplankton type by fitting non-linear functions to monthly net samples (44 μm mesh) from 1985 to 1989 at two stations in the mesohaline Chesapeake Bay off Calvert Cliffs (Figure 3). In model simulations, a uniform random number between 0 and 1 is generated for each larva encountering each zooplankton group and used as the x-axis value to obtain a multiplier of the mean density.

Bay anchovy larvae do not attack every prey individual that they encounter (Rose et al. 1999) nor do they capture every prey item that they attack. To compute an estimate of how many of the encountered prey they subsequently successfully attacked and captured, the following equation was used:

$$B_i = e_i^R \cdot \mathrm{P(Attack)} \cdot CAP_i \qquad \text{Eq. 12}$$

where B_i = the number of prey type *i* encountered, attacked, and captured by a larvae; P(Attack) was a non-linear function of anchovy length that gives the probability that a larva attacked a prey item (Figure 4); and CAP_i = probability of a larvae capturing an individual of prey type *i*. Capture success was calculated based on larval length for each of the zooplankton prey types:

$$\mathrm{CAP}_i = \begin{cases} 0.114L_L + 0.057 & \text{for tintinnids and rotifers} \\ 0.115L_L - 0.23 & \text{for nauplii} \\ 0.115L_L - 0.46 & \text{for copepodites} \\ 0.140L_L - 1.95 & \text{for adult copepods} \end{cases} \qquad \text{Eq.13}$$

CAP_i was limited to the interval of 0 to 0.9.

The number of zooplankton prey of each type actually eaten was determined from the numbers of prey encountered, attacked, and captured using an optimal foraging algorithm that is described in detail in Rose et al. (1999). This algorithm determines the order of preference for the prey types "eaten" by ranking the expected gains in energy that the larva would expect to

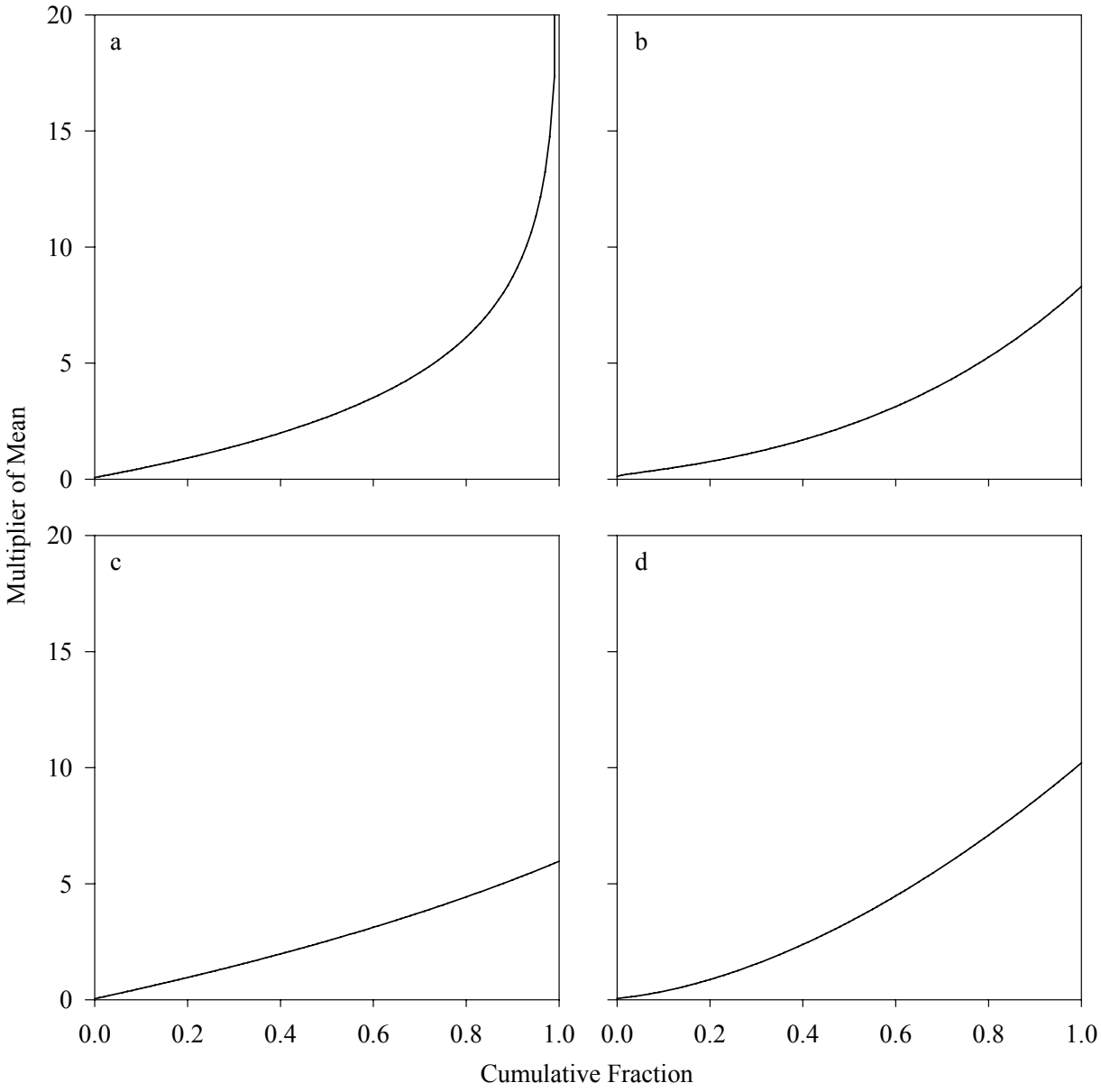

Figure 3: Cumulative distribution functions (CDFs) of rotifers and tintinnids, nauplii, copepodites, and adult copepods relating the cumulative fraction of field samples with prey concentrations less than some value (expressed as a multiplier of the mean). The CDFs are from Rose et al. (1999). (a) Rotifers and tintinnids, (b) Nauplii, (c) Copepodites, (d) Adult copepods.

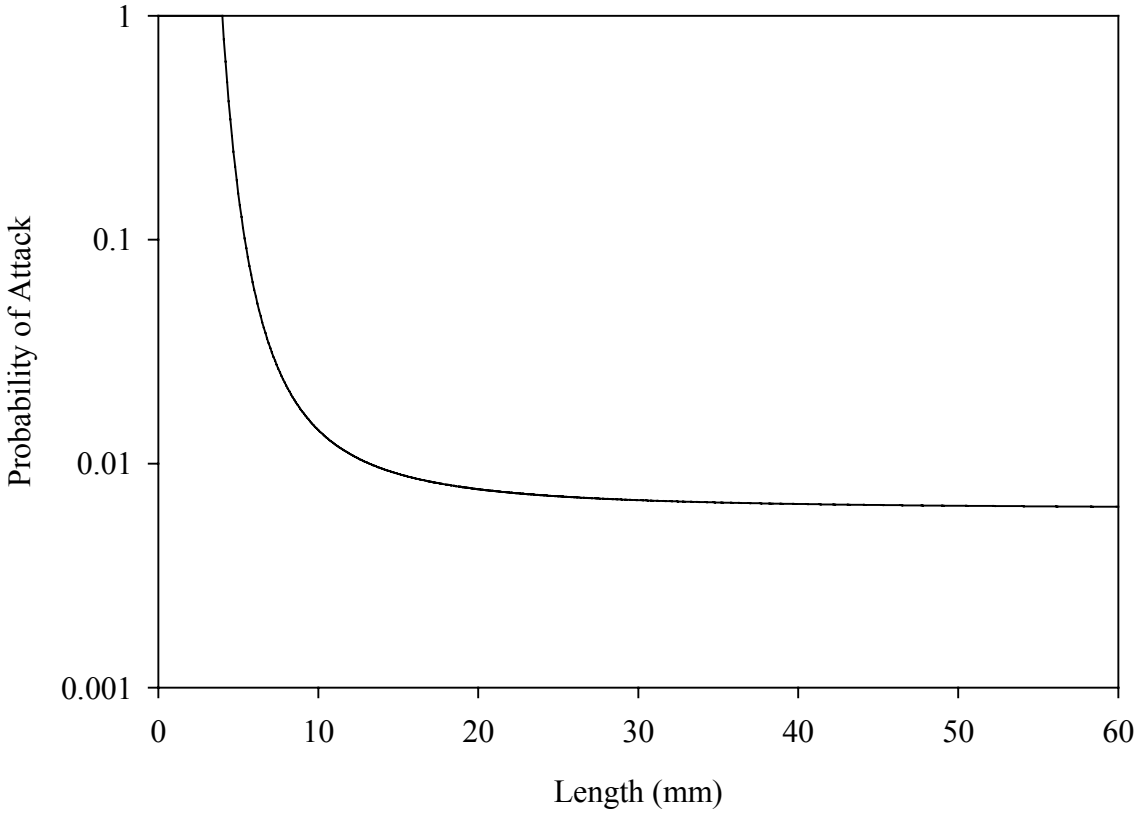

Figure 4: Probability that a bay anchovy larvae will attack a prey item that it has encountered. The probability of attack value for an anchovy of a given length is used for all four zooplankton prey types.

receive if it consumed each prey type. The expected gain in energy is calculated using the equation:

$$\text{Gain in Energy} = PW_i \times CAP_i \qquad \text{Eq. 14}$$

where PW_i = the weight of the prey item (mg) (Table 2). The prey type receiving the highest ranking was added to the larva's diet first. Additional prey types were added to the diet in the order that they were ranked until the consumption rate index with the added prey type *i* (Q_i, mg s^{-1}) decreased compared to the index with prey types 1 through i-1 (Q_{i-1}). The consumption rate index was:

$$Q_i = \frac{\sum_{k=1}^{i} PW_k B_k T_D}{1 + \sum_{k=1}^{i} B_k T_D} \quad \text{Eq. 15}$$

where k = the rank of the prey type; PW_k = dry weight (mg) per individual of the prey type k (Table 2); B_k = number of individuals of prey type k encountered, attacked, and captured; and T_D = the inverse of the approximate number of seconds during daylight hours (2.3×10^{-5}). Prey types were consumed in the order they were ranked until either all zooplankton captured were consumed or consumption exceeded twice the larva's maximum consumption. The consumption realized by the larva then was calculated as:

$$C_r = \sum_{i=1}^{n'} B_i PW_i \quad \text{Eq. 16}$$

where i = 1 to n' is the number and order in which prey types are evaluated; B_i = number of prey type i eaten (encountered, attacked, captured, and selected); and PW_i = weight per individual of prey type i (mg).

Table 2: Weights of zooplankton prey types used in model simulations (Rose et al. 1999).

Prey type	Dry weight (mg)
Tintinnids and rotifers	0.00016
Nauplii	0.00152
Copepodites	0.0033
Copepod adults	0.011

Predation

Whether each individual larva was encountered and eaten by a predator was determined each day using the method of Cowan et al. (1996), which assumed that predators do not satiate when feeding on larvae. The mean number of encounters during a day $(\overline{E})$ between each individual larva and each individual predator (ctenophore, sea nettle) was determined using the Gerritsen-Strickler formulation (Gerritsen and Strickler, 1977), modified to account for the

non-negligible size of larval bay anchovy (Bailey and Batty, 1983). The mean number of encounters was determined using the equation:

$$\overline{E} = \pi (R_L + R_P)^2 \cdot C \cdot (10^{-9} / V) \qquad \text{Eq. 17}$$

where

$$C = \frac{D_L^2 + 3D_P^2}{3D_P} \quad \text{if } D_P > D_L$$
$$C = \frac{D_P^2 + 3D_L^2}{3D_L} \quad \text{if } D_P < D_L \qquad \text{Eq. 18}$$

where R_L = encounter radius of the larva (mm); R_P = encounter radius of the predator (mm); C = foraging rate of the predator (mm s^{-1}); V = volume modeled (m^3); D_L = distance swum in a day by the larva (mm); and D_P = distance swum in a day by the predator (mm). $\overline{E}$ is the mean number of times in a day that the encounter volume of a larva enters the encounter volume of a predator. Bay anchovy larvae and predator encounter radii (R_L and R_P respectively) and distance swum in a day (D_L and D_P), adapted from Cowan and Houde (1992), are given in Table 3.

The actual number of encounters between a larva and a predator was generated as a random deviate from a Poisson distribution with mean equal to $\overline{E}$. The number of encounters that actually resulted in the larva being eaten was determined from a binomial distribution, with the number of actual encounters used as the number of trials, and the predator's capture success for that larva as the probability of success for each trial. This process was repeated daily for each larva and individual predators. If at least one encounter resulted in a successful capture, the larvae was 'eaten' and was removed from the simulation.

The probability that a predator will capture a bay anchovy larvae was modified from previous versions of the model to include the effect of predator length on capture success (Table 3). Larvae that are large in size relative to their predators (~30-60% of their length) may be

invulnerable or less vulnerable to predation (Fuiman 1994). Relatively large larvae are better at escaping (Pepin et al. 1987) and require more handling time than smaller larvae (Werner 1974; Luecke et al. 1990). The original capture success relationship, which depended only upon larval fish length, was expanded to also include the effects of predator length. In the expanded relationship, capture success of predators preying upon larvae decreases with increasing ratio of larva size to predator size. The expanded relationship was derived by refitting the original capture success equation (Cowan and Houde 1992) to the same laboratory data but including the measured predator lengths in the relationship.

Simulations

Three sets of model simulations were performed. The first set of simulations used the field data for temperature, zooplankton, and sizes and densities of larvae, ctenophores, and sea nettles to predict the instantaneous growth and mortality rates of larval bay anchovy for each layer at each station in the Chesapeake Bay during June and July of 1993. The second set of simulations standardized the larval bay anchovy cohort simulated at each site, setting the size range of larval bay anchovy to 4.0 to 5.0 mm and the initial number of larvae to 50,000, so that instantaneous growth and mortality rates could be predicted for each site in the Bay independent of the field-measured larval densities and whether larvae were collected at a station or not. Standardizing the sizes and densities of anchovy removes any confounding effects of larval sizes and densities on predicted growth and mortality rates, thus allowing for differences in growth and mortality rates among stations to be attributed to differences in prey and predator abundances. The third set of simulations evaluated the importance of six factors in causing the observed spatial patterns in predicted larval growth and mortality rates. The six factors examined

Table 3: Encounter radii and distances swum from Cowan and Houde (1992) in a day for larval bay anchovy, ctenophores, and sea nettles, and capture probability relationships of ctenophores and sea nettles eating bay anchovy larvae modified from Cowan and Houde (1992).

Parameter	Larval Bay Anchovy	Ctenophore	Sea Nettle
Encounter Radius (mm)	$\frac{2 \cdot L_L}{\pi^2}$	$0.33 \cdot L_C$	$0.5 \cdot L_{SN}$
Distance Swum (mm)	$1.5L_L \cdot 46800$	$0.025 \cdot L_C \cdot 86400$	$1.2 + 0.04 \cdot L_{SN} \cdot 86400$
Realized Capture Probability	N/A	$0.813 - 4.416\frac{L_L}{L_C}$	$0.505 + 4.653\frac{L_L}{L_{SN}} - 66.215\left(\frac{L_L}{L_{SN}}\right)^2 + 155.377\left(\frac{L_L}{L_{SN}}\right)^3$

were temperature, sea nettle size, ctenophore length, predator (sea nettle and ctenophore) density, larval length, and zooplankton densities.

For all simulations, predicted instantaneous growth and mortality rates were determined for each layer (surface and bottom) and station. The instantaneous growth rate (G) was calculated using the equation:

$$G = \ln\left(\frac{\overline{W_1}}{\overline{W_0}}\right) \qquad \text{Eq. 19}$$

where $\overline{W_1}$ = the mean weight of the surviving larvae at the end of the one day simulation; and $\overline{W_0}$ = the mean initial weight of the larvae at the beginning of the simulation. The instantaneous mortality rate (M) was calculated using the equation:

$$M = -\ln\left(\frac{N_1}{N_0}\right) \qquad \text{Eq. 20}$$

where N_1 = the number of larvae surviving the one day simulation; and N_0 = the initial number of larvae in the simulation.

Field-Based Simulations

The first set of simulations used all of the field data and predicted the instantaneous growth and mortality rates of larval bay anchovy in each layer at each station during June and July of 1993. Initial conditions for each simulation used the zooplankton densities, the sizes and densities of larvae and predators, and the temperature observed during field sampling in a layer at each station.

Model predictions of growth and mortality rates were compared to the values reported by Rilling and Houde (1999) and to growth and mortality rates values reported for bay anchovy in the literature. In making comparisons to the rates reported by Rilling and Houde (1999), I used the standard errors that they reported for instantaneous weight-specific growth rates and the

standard error of the regression coefficient for instantaneous mortality rates to develop confidence intervals for Rilling and Houde's (1999) rate estimates. Rigorous validation of model predictions using an independent data set is not possible. Similarity between model predicted rates and reported rates provides some corroborative evidence that model simulations are realistic. Predicted growth rates in weight (d^{-1}) were also expressed as growth in length (mm d^{-1}) to permit comparison to literature values.

Predicted growth and mortality rates were aggregated into three regions along the north to south (N-S) axis and three regions across the west to east (W-E) axis of the Bay. Instantaneous growth and mortality rates predicted for each layer at each station were averaged to obtain a single value for each station by weighting each layer's rates by its initial abundance of larvae (number m^{-3} × thickness of the layer, in m). The weighted averages for stations then were averaged for each region, weighting by the larval abundances at each station. Weighted standard errors (S.E.) of the growth and mortality rates were calculated from the multiple stations values in each region using the same weights (larval abundance) as were used in computing the weighted average. Single estimates of the M/G ratios were computed using the average growth and mortality rates for each region. Standard errors for the M/G ratios for each region were calculated using the equation:

$$\text{S.E.} = \sqrt{\frac{\text{Var}(M/G)}{n}} \quad \text{Eq. 21}$$

where

$$\text{Var}\,(M/G) = \frac{1}{\bar{x}_G^{\,2}}\left(\text{Var}(x_G)\cdot\frac{\bar{x}_M^{\,2}}{\bar{x}_G^{\,2}} + \text{Var}(x_M) - 2r\cdot\sqrt{\text{Var}(x_G)}\cdot\sqrt{\text{Var}(x_M)}\cdot\frac{\bar{x}_M}{\bar{x}_G}\right) \quad \text{Eq. 22}$$

where Var (x_G or x_M) = weighted variance of growth or mortality rates for a region obtained as the variance of station-specific values in the region weighted by the larval abundance at each

station, $\bar{x}_G$ = the mean growth rate, $\bar{x}_M$ = the mean mortality rate, and r = the correlation coefficient between station-specific estimates of growth or mortality rates (Rice 1995).

Regions along the N-S axis were described previously in the methods (shown in Figure 1). Stations were assigned to three regions along the W-E axis as follows:

1.) For transects with only two stations, both stations were classified as being in the central-Bay region.

2.) For transects with three or four stations:

   a. the western-most station was classified as being in the western-edge region

   b. the eastern-most station was classified as being in the eastern-edge region

   c. the station or stations located between the western most station and the eastern most station were classified as being in the central-Bay region.

Production of larval bay anchovy after a 20 day period was forecasted for the three N-S regions and the three W-E regions for the field-based simulations. For each layer at each site, the number of larvae surviving a 20 day period was determined using equation 3, where t = 20 days, M = the instantaneous mortality rate predicted by the one-day model simulations, and N_t = the initial number of larvae in the layer. The number of survivors at each layer and station was then summed over all stations within a region, and the percentage of survivors originating from each region was then determined.

Standardized Larvae Simulations

The second set of simulations was designed to minimize the effect of initial larval length on predicted bay anchovy growth and mortality rates. The second set of simulations repeated the field-based simulations, but used the same larval lengths and densities for all layers and stations. Examination of the results of the field-based simulations indicated that the initial lengths of

larvae were correlated with the instantaneous weight-specific growth rates of larvae (June: $r = -0.712$, $p<0.0001$; July: $r = 0.281$, $p=0.0088$), and initial larval lengths in the field data were correlated with stations along the N-S axis. In June, relatively longer larvae were collected in the mid region of the Bay, with smaller larvae collected in the upper and lower Bay regions (Appendix Figure 4). In July, relatively longer larvae were collected in the upper Bay, while smaller larvae were collected in the mid and lower Bay regions. Also, there were some stations that had no larvae collected, and these stations were therefore not included in the field-based simulations. To eliminate any confounding effects of initial larval size and density on predicted growth and mortality rates, the initial number of larvae was set to 50,000 individuals and their lengths were generated from a normal distribution with mean = 4.5 mm and s.d. = 0.5 (minimum = 4.0, maximum = 5.0 mm). The value of 50,000 is arbitrary as growth and mortality are density-independent in the model. The minimum and maximum lengths were selected because most larval lengths observed in the field sampling were between 4.0 and 5.0 mm. The standardized larval simulations permit direct comparison of prey and predator effects on larval growth and mortality rates. The same comparisons that were made for the field-based simulations (predicted growth and mortality rates, M/G ratios, and larval production) were performed for the standardized larval simulations.

Factor Influence

The third set of simulations evaluated the influence of six factors (temperature, sea nettle size, ctenophore length, predator (sea nettle and ctenophore) density, larval length, and zooplankton densities) on the spatial patterns of bay anchovy growth and mortality. I only simulated the month of July because both ctenophores and sea nettles were present in July, and July generally is the month of peak bay anchovy larval abundance in the Bay (Zastrow et al.

1991; Rilling and Houde 1999). Each factor's influence on the spatial pattern of predicted bay anchovy growth and mortality rates was evaluated separately. To evaluate a factor, simulations were conducted for each layer at each station sampled during July. With the exception of the factor being evaluated, all of the initial conditions for the model were set to their bay-wide (unweighted) mean values measured in July. The initial condition for the factor being evaluated was set to the value observed during field sampling at the layer and station being simulated. At the end of each simulation, the instantaneous growth and mortality rates was predicted. This process was repeated for each of the six factors being evaluated.

The influence of each factor on the spatial patterns of predicted bay anchovy growth and mortality was examined using Pearson correlation. The predicted values of the growth or mortality rates for each factor simulation were paired with the growth or mortality values for the same layer and station from the field-based simulation. Correlation coefficients were then calculated between the paired growth or mortality values. High correlation would imply that the factor that was varied accounted for much of the spatial variation in growth or mortality predicted in the field-based simulations.

RESULTS

Field-Based Simulations: Layer- and Station-Specific Predictions

June

During the month of June, mortality generally increased as one moved down bay (Figure 5). On transects 1 through 4, mortality rates were zero or near zero and there was little variability in mortality rates. Mortality rates at stations on transects 5 through 11 averaged 0.15 d^{-1}, and were more variable and generally higher than the rates on the first four transects. The highest mortality rates were predicted on transects 12 through 15, where mortality rates averaged 0.37 d^{-1} but had a range of 0 to 1.64 d^{-1}. Surface and bottom layer mortality rates were similar on individual transects and throughout the Bay (open versus closed circles in Figure 5), with median rates of 0.09 d^{-1} in the surface and 0.07 d^{-1} in the bottom layer (Table 4).

Growth rates were highly variable across Chesapeake Bay during June, with generally positive growth rates in the upper Bay, generally negative growth rates in the mid Bay, and an even split between positive and negative growth rates in the lower Bay (Figure 6). Growth on transect 1 was only slightly positive, with an average growth rate of 0.04 d^{-1}. On transects 2 through 6 growth rates were generally high (average growth = 0.23 d^{-1}) and variable, with the exception of one site on transect 6 where larvae on average had negative growth rates. Growth was poor on transects 7 through 12 with an average growth rate of -0.03 d^{-1}, and only 2 sites with larvae on average, experiencing positive growth in weight. Transects 13, 14, and 15 had variable growth rates with just more than half the sites having a growth rate of approximately 0.18 d^{-1}, while the remainder of the sites had negative growth rates. During June, fifteen sites were predicted to have negative growth rates. Surface layer and bottom layer growth rates generally

overlapped both along transects (open versus closed circles in Figure 6) and across the Bay (Table 5).

July

July mortality rates (Figure 7) were higher than June mortality rates (Figure 5) in the upper and mid Bay region, but were lower than the June mortality rates in the lower Bay region. Mortality rates on transects 2 through 11 were generally variable and were high compared to June (Figure 7). On transect 1 and transects 12 through 15, mortality rates were at or near zero and were not variable. Mortality rate values did not differ systematically with water column layer on any transect (open versus closed circles in Figure 7) or Bay-wide (Table 4).

The overall spatial pattern of growth rates during July (Figure 8) was similar to that observed during June (Figure 6), but the reduction in growth rates predicted for June in the mid Bay region was less apparent in July due to a general increase in growth rates throughout the Bay. For July, the number of sites with negative growth rates declined to only 6 (Figure 8). Bay anchovy growth was much faster along transect 1 in July compared to the rates observed during June; however one site on transect 1 had negative growth during July. Growth rates for the surface and bottom layers along all transects (open versus closed circles in Figure 8) and across the Bay (Table 5) were generally similar during July.

Table 4: The predicted weighted mean, median, and range (minimum to maximum), of larval bay anchovy instantaneous mortality rates (d^{-1}) for the surface and bottom layers for June and July for the field-based simulations.

Parameter	June		July	
	Surface	Bottom	Surface	Bottom
Mean (weighted)	0.0614	0.120	0.0257	0.0158
Median	0.0947	0.0679	0.120	0.0345
Range	0 – 1.644	0 - 0.0782	0 – 0.702	0 - 0.696

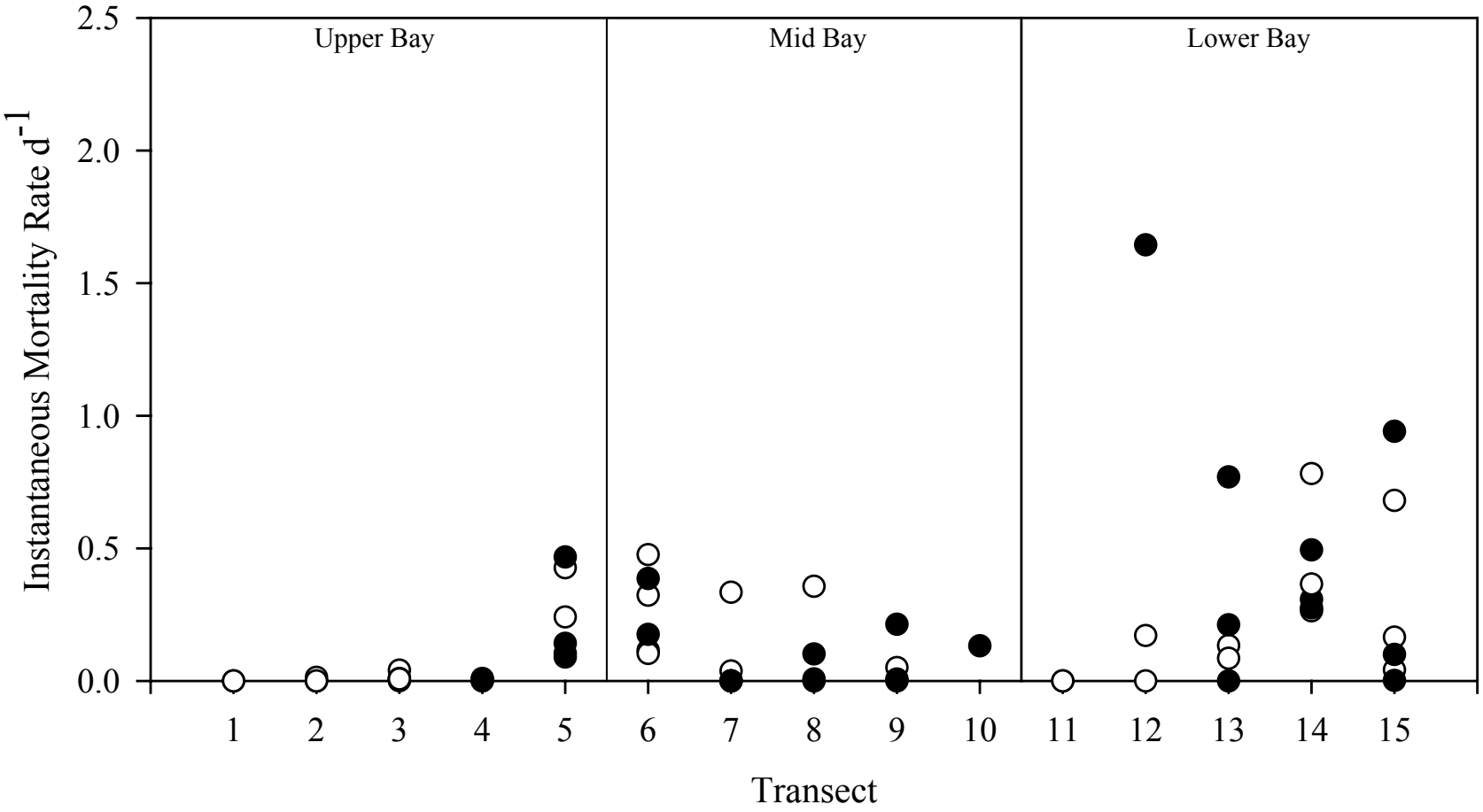

Figure 5: Predicted instantaneous mortality rates for June by transect and layer for the field-based simulations. Closed circles indicate the instantaneous mortality rates at surface-layer stations while open circles indicate instantaneous mortality rates at bottom-layer stations.

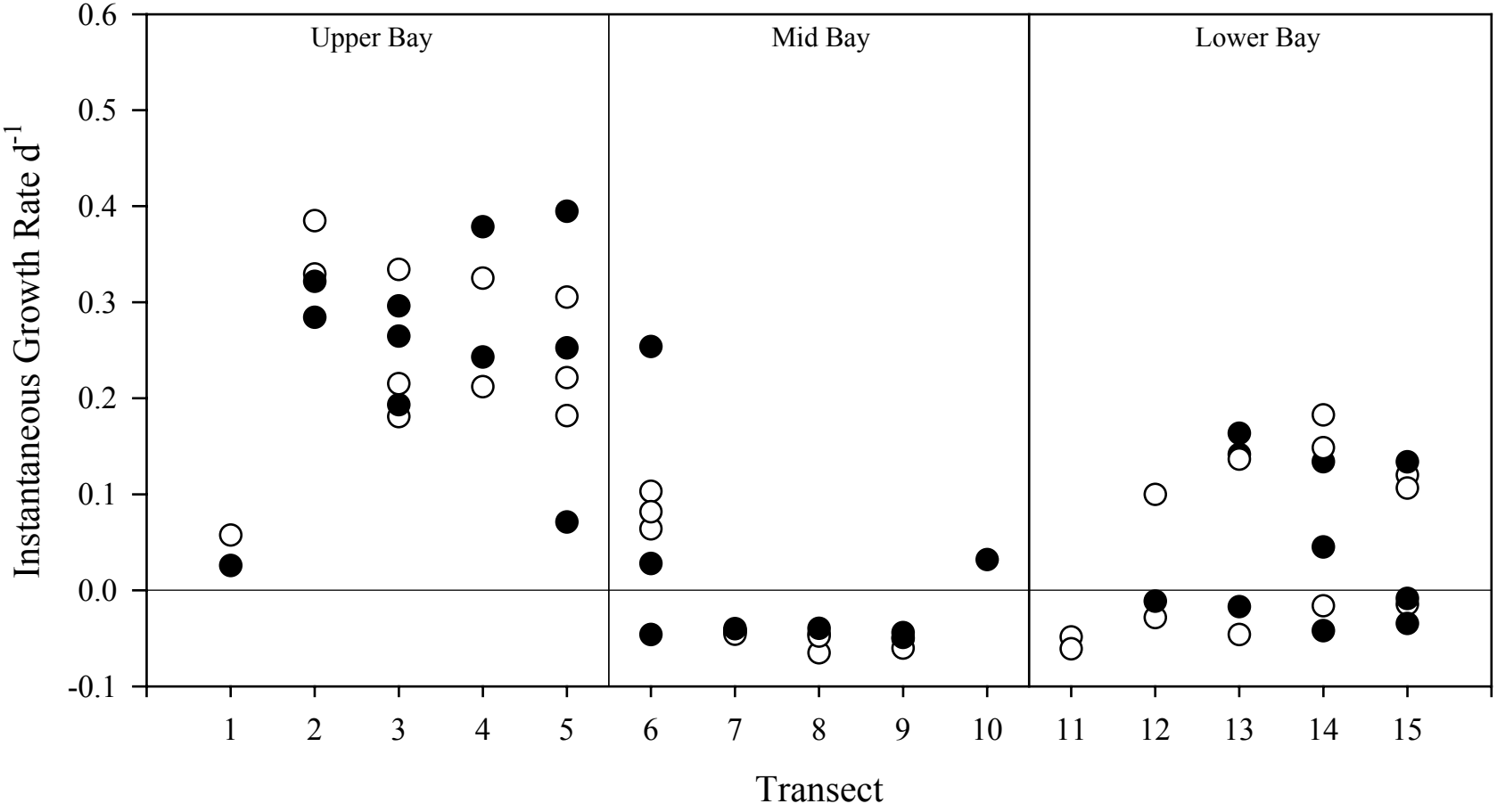

Figure 6: Predicted instantaneous weight-specific growth rates for June by transect and layer for the field-based simulation. Closed circles indicate the instantaneous weight-specific growth rates at surface-layer stations while open circles indicate weight-specific growth rates at bottom-layer stations.

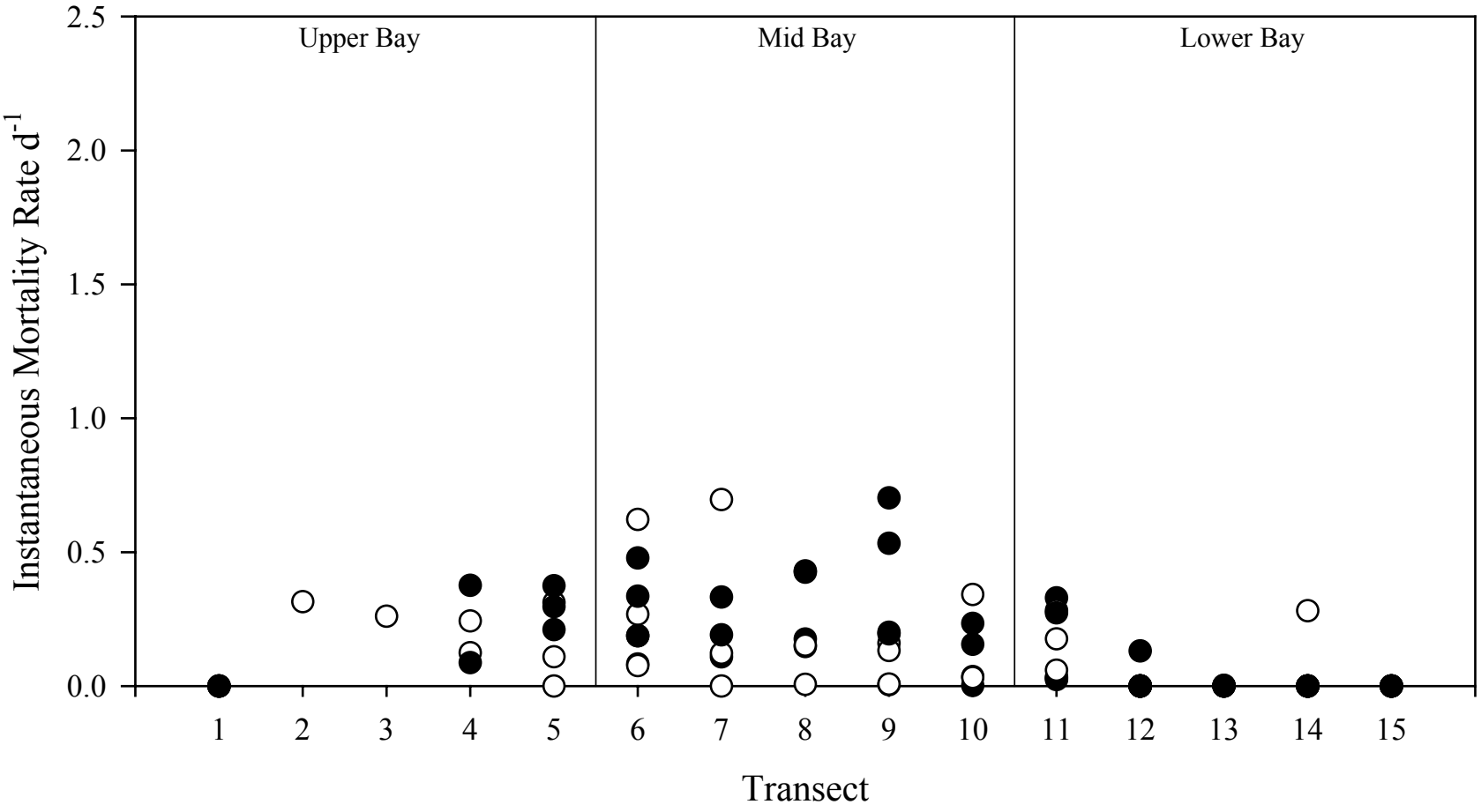

Figure 7: Predicted instantaneous mortality rates for July by transect and layer for the field-based simulation. Closed circles indicate the instantaneous mortality rates at surface-layer stations while open circles indicate instantaneous mortality rates at bottom-layer stations.

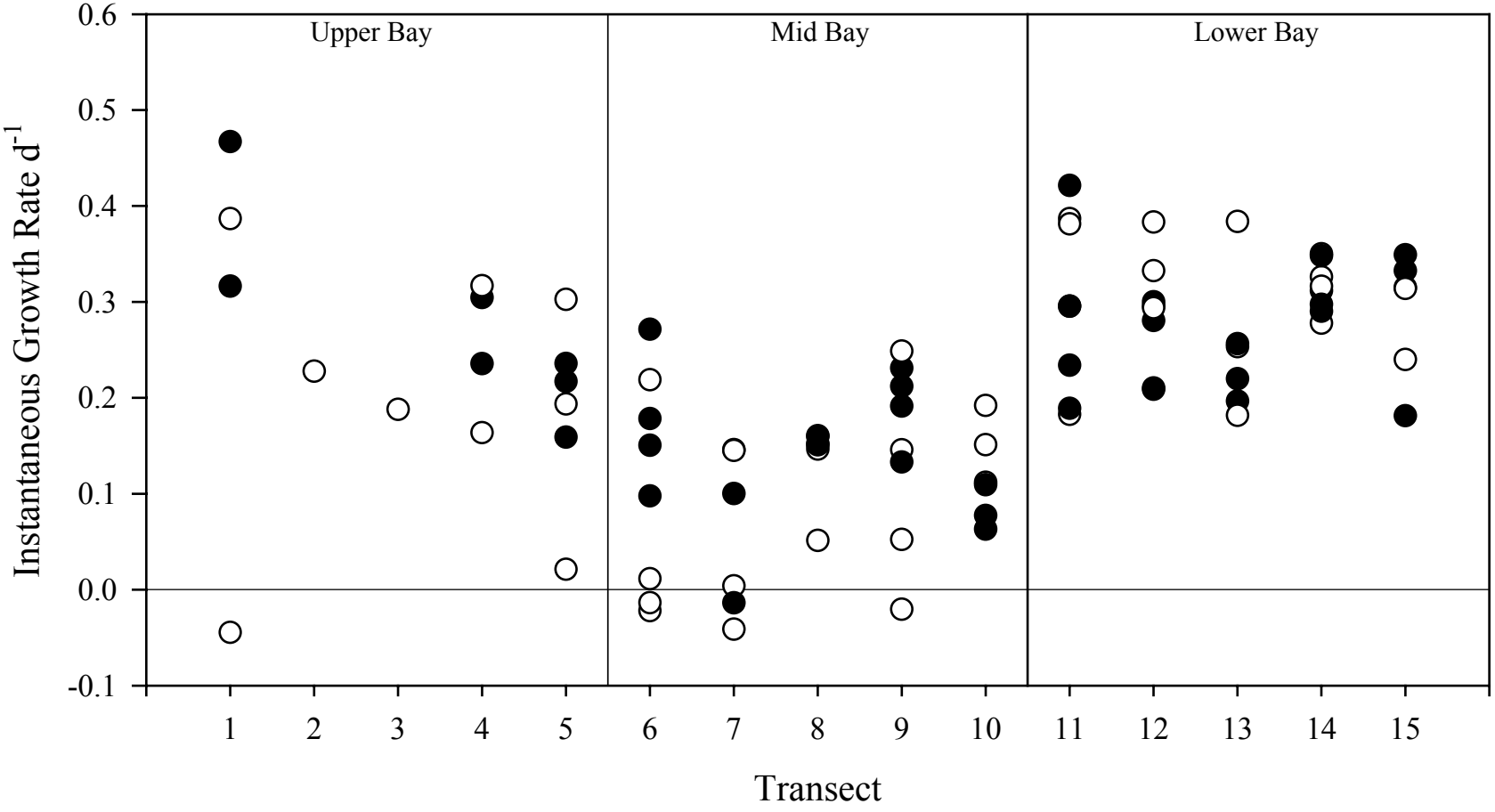

Figure 8: Predicted instantaneous weight-specific growth rates for July by transect and layer for the field-based simulation. Closed circles indicate the instantaneous weight-specific growth rates at surface sites while open circles indicate instantaneous weight-specific growth rates at bottom sites.

Table 5: The predicted weighted mean, median, and range (minimum to maximum), of larval bay anchovy instantaneous weight-specific growth rates (d^{-1}) in the surface and bottom layers for June and July for the field-based simulations.

Parameter	June		July	
	Surface	Bottom	Surface	Bottom
Mean (weighted)	0.205	0.224	0.273	0.297
Median	0.0385	0.101	0.273	0.297
Range	-0.0491 – 0.395	-0.0652 – 0.385	-0.0139 – 0.467	-0.0446 – 0.387

Corroboration

For the majority of model runs, mortality rates (Table 4) and growth rates (Table 5) from the field-based simulations for both June and July were within the range of instantaneous mortality rates (Table 6; 0.08 – 4.24 d^{-1}) and daily growth rates (Table 7; 0.25 – 0.93 mm d^{-1}) reported in the literature. Instantaneous mortality rates from the June simulations (Figure 5) were within the range of literature values (Table 6) for 33 of the 64 simulations, while rates from the July simulations (Figure 7) were within the range of literature values for 43 of the 86 simulations (Table 6). Daily growth-in-length rates, rather than instantaneous weight-specific growth rates, were used for comparison to the growth rates predicted by the simulations as daily growth in length rates were reported much more frequently in the literature. Growth rates from the field-based simulations were within the range of values reported in the literature for 23 of 64 simulations during June (Figure 6; Table 7) and 68 of 86 simulations during July (Figure 8; Table 7).

Field-Based Simulations: North to South Regional Patterns and Comparison to Field Results

June

For the month of June, field-based simulations predicted higher bay anchovy mortality rates in the mid (0.21 d^{-1}) and lower (0.19 d^{-1}) Bay regions, while Rilling and Houde (1999) estimated higher larval mortality rates in the upper (0.48 d^{-1}) and lower (0.54 d^{-1}) regions of the

Table 6: Instantaneous larval bay anchovy mortality rates, larval sizes and ages, study location, and study details.

Source	Mortality (M, d^{-1})	Larval Size/Age	Location	Details
Leak and Houde (1987)	0.30 – 0.45	hatch – 14 days	Biscayne Bay, FL	lab study
Cowan and Houde (1990)	0.08 – 0.23	hatch – 14.8 mm	mesocosms in Chesapeake Bay	no large predators
Castro and Cowen (1991)	1.19 – 4.02	eggs – 2 days	Great South Bay	field estimates
	0.18 – 0.48	3 days – 15 days		
Dorsey (1993)	0.41 – 4.24	yolk-sac larvae	Chesapeake Bay (yolk-sac larvae)	field estimates
MacGregor (1994)	0.23 – 1.20		Chesapeake Bay	
Rilling and Houde (1999)	0.14 – 0.54	hatch – 28 days	Chesapeake Bay (regional rates)	field estimates

Table 7: Daily larval bay anchovy growth in length and instantaneous weight-specific growth rates, larval sizes and ages, study location, and study details.

Source	Growth ($mm\ d^{-1}$)	Growth (d^{-1})	Larval Size/Age	Location	Details
Saksena and Houde (1972)	0.48 – 0.54	-	hatch - ~ 19 mm	Lab	20 liter aquaria, food study
Detwyler and Houde (1970)	0.70	-	average after 4 dph	Lab	75 liter aquaria
Gallagher et al. (1983)	0.59 – 0.93	-	-	Patuxent River, MD	-
Fives et al. (1986)	0.25	-	1 – 12 mm	Newport River Estuary, NC	10 – 115
	0.31	-	13 – 24 mm	Newport River Estuary, NC	liter aquaria
Leak and Houde (1987)	0.43 – 0.56	0.23 – 0.30	4.5 – 12.5 mm	Biscayne Bay, FL	field estimates
Cowan and Houde (1990)	0.39 – 0.61	0.17 – 0.24	hatch – 14.8 mm	Chesapeake Bay	mesocosms
Castro and Cowen (1991)	0.52 – 0.59	-	2 – 15 mm	Great South Bay	field estimates
Rilling and Houde (1999)	0.53 – 0.78	0.25 – 0.40	hatch – 28 days	Chesapeake Bay	regional rates
Jordan et al. (2000)	0.39 – 0.88	-	-	Hudson River Estuary	-

Bay (Figure 9a). The regional mortality rates for the upper and lower Bay estimated by Rilling and Houde (1999) were 3-5 times greater than the mortality rates predicted here using the field-based simulations. For the mid Bay region however, both estimates of the larval bay anchovy instantaneous mortality rate were approximately 0.21 d^{-1}.

Based upon the field-based simulations, bay anchovy larvae growth rates in the upper Bay region (0.25 d^{-1}) during June were predicted to be at least twice as fast as the larval growth rates in the mid (0.043 d^{-1}) and lower (0.11d^{-1}) Bay (Figure 9b). This was contrary to the finding of Rilling and Houde (1999), who did not observe a strong trend in June growth rates along the N-S axis (0.28 d^{-1} in the upper Bay; 0.25 d^{-1} in the lower Bay). Larval growth rates for June predicted by the field-based simulations were generally half the magnitude of the growth rates estimated by Rilling and Houde (1999).

Along the N-S axis of the Bay, simulated cohorts of bay anchovy larvae were predicted to increase their biomass in the upper Bay (M/G = 0.28), and lose biomass in the mid (M/G = 5) and lower (M/G = 1.69) Bay regions (Figure 9c). Rilling and Houde (1999) found that the mid Bay region (M/G = 0.87) had the highest production of bay anchovy larval biomass, while cohorts in the upper (M/G = 1.72) and lower Bay (M/G = 2.17) lost biomass. The M/G ratio predicted for the mid Bay region from the field-based simulations was much higher than any other region's M/G ratio, suggesting the mid Bay may have been a particularly poor habitat for bay anchovy.

July

For the month of July, field-based simulations predicted that the highest larval bay anchovy mortality rates would be in the upper (0.23 d^{-1}) and mid (0.20 d^{-1}) Bay, while Rilling and Houde (1999) estimated that the highest mortality rates were in the lower Bay (Figure 9d). Regional mortality rates from the field-based simulations and from Rilling and Houde (1999)

were similar in magnitude for the upper and mid Bay regions, but were quite different for the lower Bay. In the lower Bay, Rilling and Houde (1999) estimated a mortality rate of 0.34 d^{-1}, while the field-based simulations predicted almost no mortality (0.009 d^{-1}). Both the field-based simulations and Rilling and Houde's (1999) estimated that July mortality rates were generally lower than the June rates (Figure 9a versus Figure 9d).

Growth rates predicted for July by the field-based simulation were highest in the lower Bay and lowest in the mid Bay, while Rilling and Houde (1999) estimated growth rates that decreased moving from the upper Bay (0.40 d^{-1}) to the lower Bay (0.28 d^{-1}) (Figure 9e). Predicted growth rates were lower than the growth rates estimated by Rilling and Houde (1999) for the upper and mid Bay, but similar to the estimated growth rates in the lower Bay. Growth rates in July were generally higher than the growth rates during June along the N-S axis of the Bay (Figure 9b versus Figure 9e).

Rilling and Houde's (1999) estimated M/G ratios and the ratios predicted from the field-based simulations both increased moving from the upper Bay to the mid Bay, but in the lower Bay the field-based simulations predicted M/G ratio declined while Rilling and Houde's (1999) M/G ratio increased (Figure 9f). The predicted M/G ratios were higher than Rilling and Houde's (1999) in the upper and mid Bay, but the predicted ratio was lower than Rilling and Houde's (1999) in the lower Bay. M/G ratios for the month of July were generally lower than the M/G ratios for the month of June (Figure 9c versus 9f).

Standardized Larvae Simulations: Layer- and Station-Specific Predictions and Comparison to Field-Based Simulations

June

Instantaneous mortality rates predicted for the June standardized larvae simulations (Table 8, Figure 10) were generally higher than the mortality rates predicted for the June

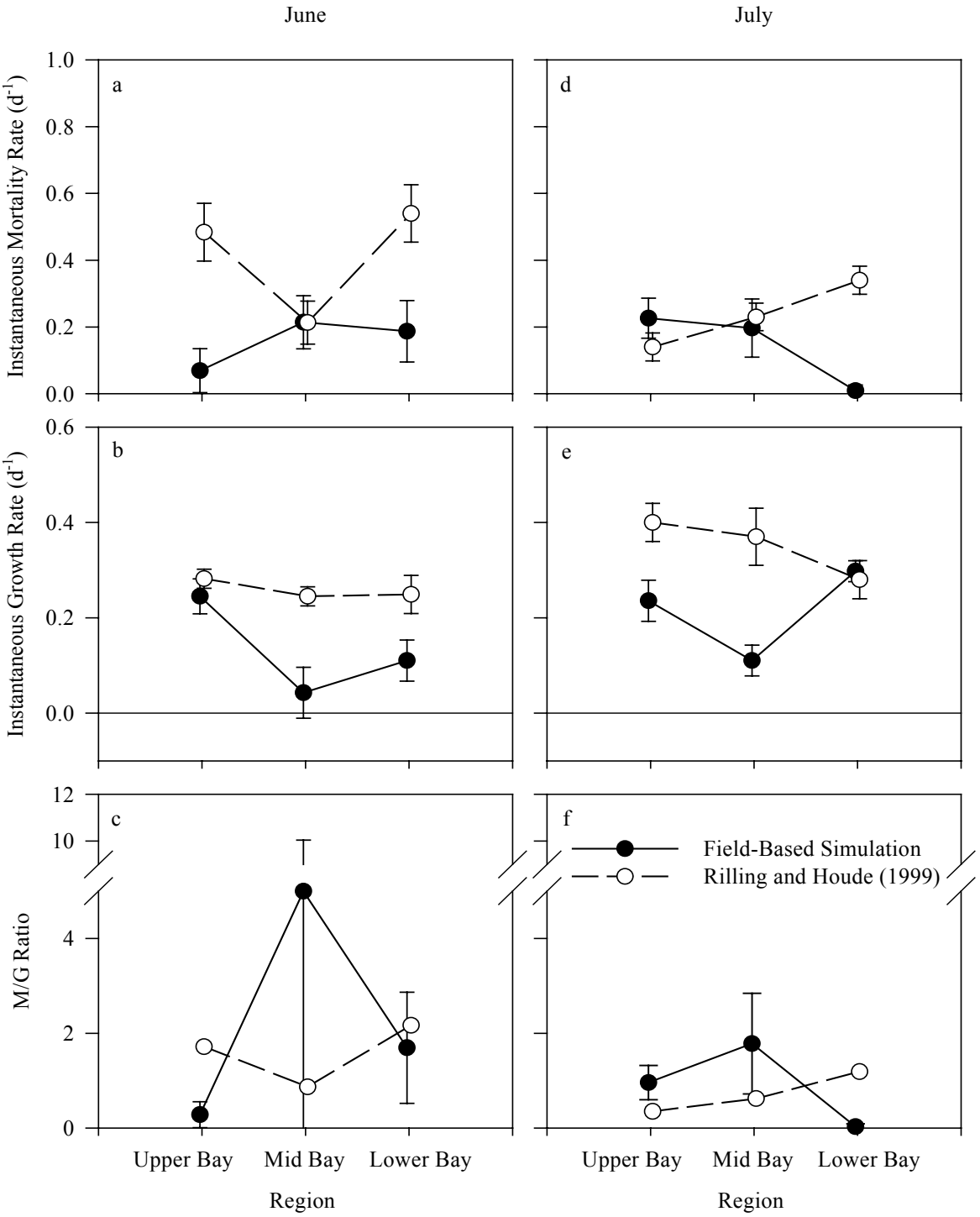

Figure 9: North to south axis regional instantaneous mortality rates (± 2 SE), weight-specific growth rates (± 2 SE), and M/G ratios (± 2 SE) for larval bay anchovy for June and July. Results are shown for the field-based simulations and from Rilling and Houde (1999). (a) Mortality rate in June, (b) Growth rate in June, (c) M/G ratio in June, (d) Mortality rate in July, (e) Growth rate in July, (f) M/G ratio in July.

field-based simulations (Table 4, Figure 5), and showed the same general spatial pattern of increasing mortality rates from the upper to lower Bay. There was little variation in predicted mortality rates along transects 1 through 4, with all sites having mortality rates near zero (Figure 10). Mortality rates on transects 5 through 15 were generally higher and more variable than the mortality rates on the first four transects. As was the case for the field-based simulations, the highest mortality rates for the standardized larvae simulations were found on transects 12 through 15. Surface and bottom layer mortality rates did not vary consistently with water column layer along both individual transects (closed versus open circles in Figure 10) and across the entire Bay (Table 8).

Instantaneous weight-specific growth rates predicted for the June standardized larvae simulations (Table 9, Figure 11) were generally higher than the growth rates predicted for the field-based simulations, and exhibited the same general spatial patterns (Table 5, Figure 6). Growth was generally high and somewhat variable on transects 1 through 6 and on transects 10 through 15. Transects 7, 8, and 9 had lower growth rates than the other transects (Figure 11), but the rates were still much higher than the rates predicted for the same transects for the field-based simulations (Figure 6). Growth rates in the surface and bottom layers were generally interspersed (Table 9), but bottom layer growth rates may have had a tendency of being slower than the surface layer growth rates (closed versus open circles in Figure 11), particularly towards the northern end of the Bay.

July

Instantaneous mortality rates predicted for the July standardized larvae simulations (Table 8, Figure 12) were slightly higher than the mortality rates for the July field-based simulations (Table 4 and Figure 7), and also exhibited the same overall spatial pattern (Figure

12). Mortality rates were at, or near zero, on transects 1, 13, and 15, and mortality rates were generally high and variable on all other transects. Surface layer and bottom layer mortality rates were interspersed on both individual transect lines (Figure 12) and Bay-wide (Table 8).

The spatial pattern of instantaneous weight-specific growth rates predicted for the standardized larvae simulations (Figure 13) was quite different from the spatial pattern predicted for the field-based simulations (Figure 8). Whereas the field-based simulations predicted growth rates that showed a minimum in the mid-Bay (Figure 8), the standardized larvae simulations showed generally higher growth rates (0.50 – 0.55 d^{-1}) uniformly throughout the Bay (Figure 13). Additionally, along transects 5-13, predicted growth rates at a number of sites in the bottom layer of the water column were much slower (growth rates of about 0.05 to 0.25 d^{-1}) than the rates predicted in the surface layer sites (~0.52 d^{-1}). On a Bay-wide basis, the mean growth rates for the surface (0.504 d^{-1}) and bottom (0.395 d^{-1}) layers were more similar (Table 9).

Table 8: The predicted weighted mean, median, and range (minimum to maximum), of larval bay anchovy instantaneous mortality rates (d^{-1}) for the surface and bottom layers for June and July for the standardized larvae simulations.

Parameter	June		July	
	Surface	Bottom	Surface	Bottom
Mean (weighted)	0.389	0.333	0.213	0.135
Median	0.195	0.229	0.121	0.058
Range	0 – 2.428	0 – 1.176	0 – 0.791	0 – 0.831

Table 9: The predicted weighted mean, median, and range (minimum to maximum), of larval bay anchovy instantaneous weight-specific growth rates (d^{-1}) in the surface and bottom layers for June and July for the standardized larvae simulations.

Parameter	June		July	
	Surface	Bottom	Surface	Bottom
Mean (weighted)	0.242	0.242	0.504	0.395
Median	0.228	0.239	0.518	0.491
Range	-0.0267 – 0.541	0.0391 – 0.526	0.342 – 0.553	0.0371 – 0.556

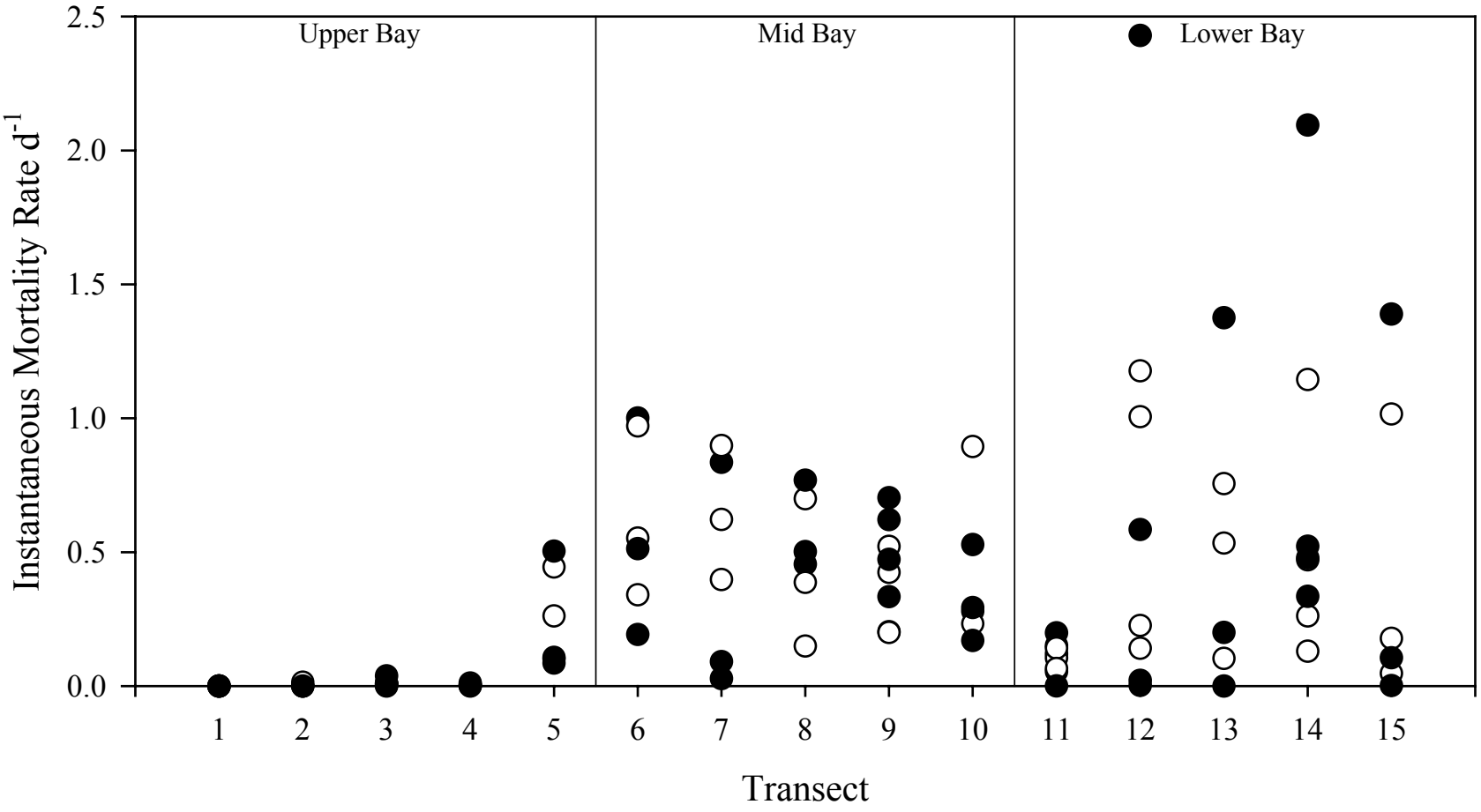

Figure 10: Predicted instantaneous mortality rates for June by transect and layer for the standardized larvae simulation. Closed circles indicate the instantaneous mortality rates at surface-layer stations while open circles indicate instantaneous mortality rates at bottom-layer stations.

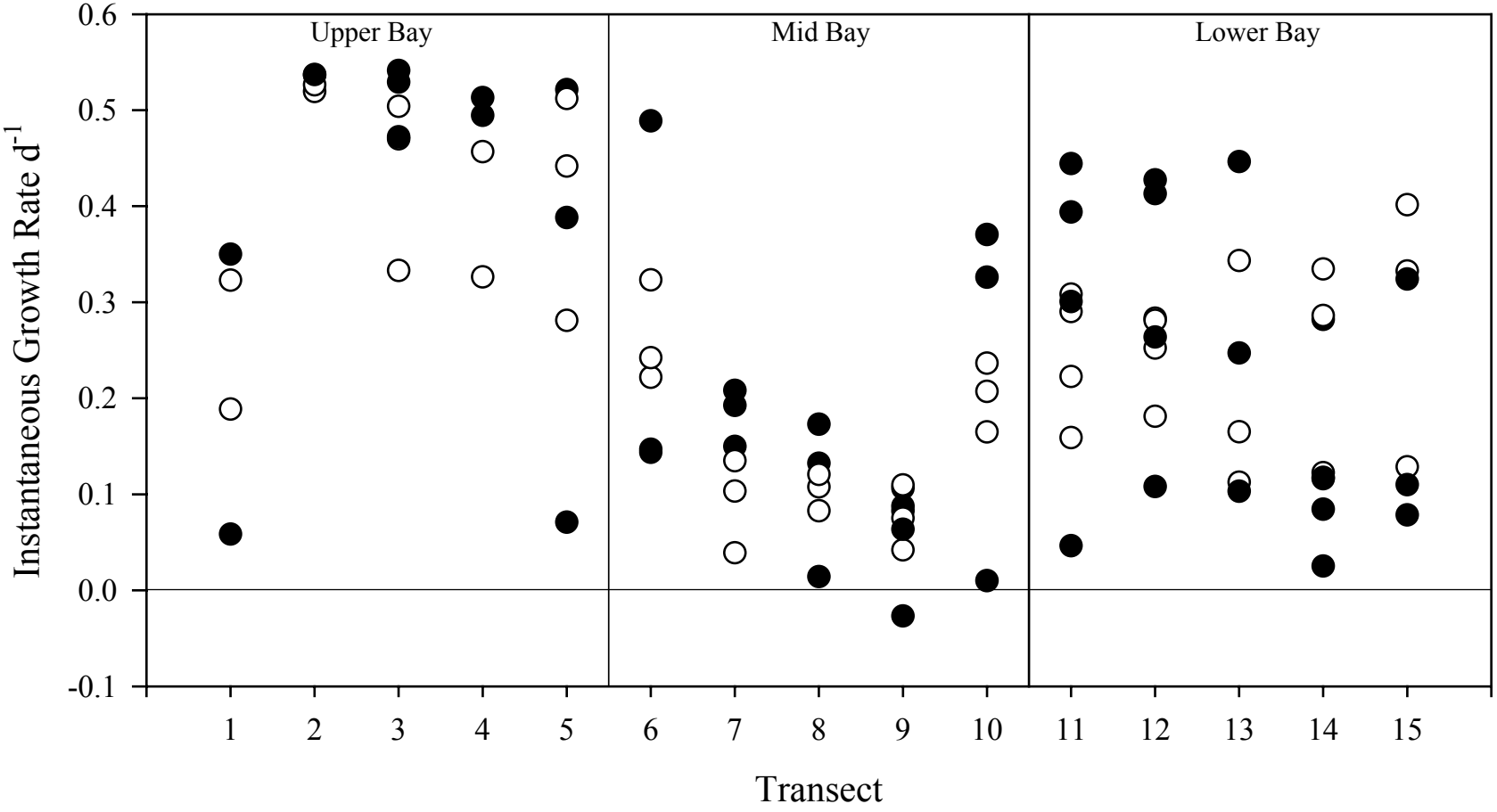

Figure 11: Predicted instantaneous weight-specific growth rates for June by transect and layer for the standardized larvae simulation. Closed circles indicate the instantaneous weight-specific growth rates at surface-layer stations while open circles indicate instantaneous weight-specific growth rates at bottom-layer stations.

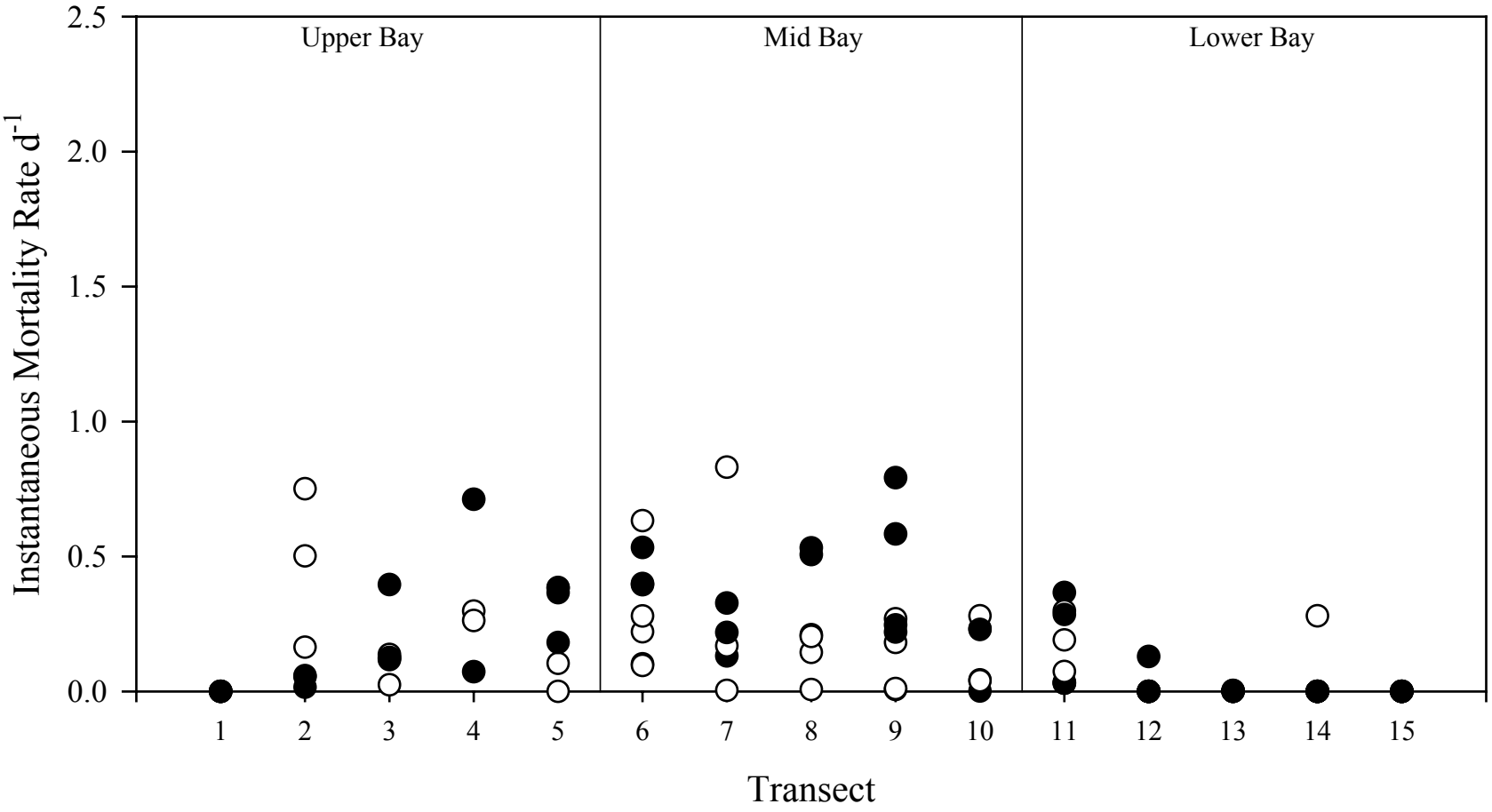

Figure 12: Predicted instantaneous mortality rates for July by transect and layer for the standardized larvae simulation. Closed circles indicate the instantaneous mortality rates at surface-layer stations while open circles indicate instantaneous mortality rates at bottom-layer stations.

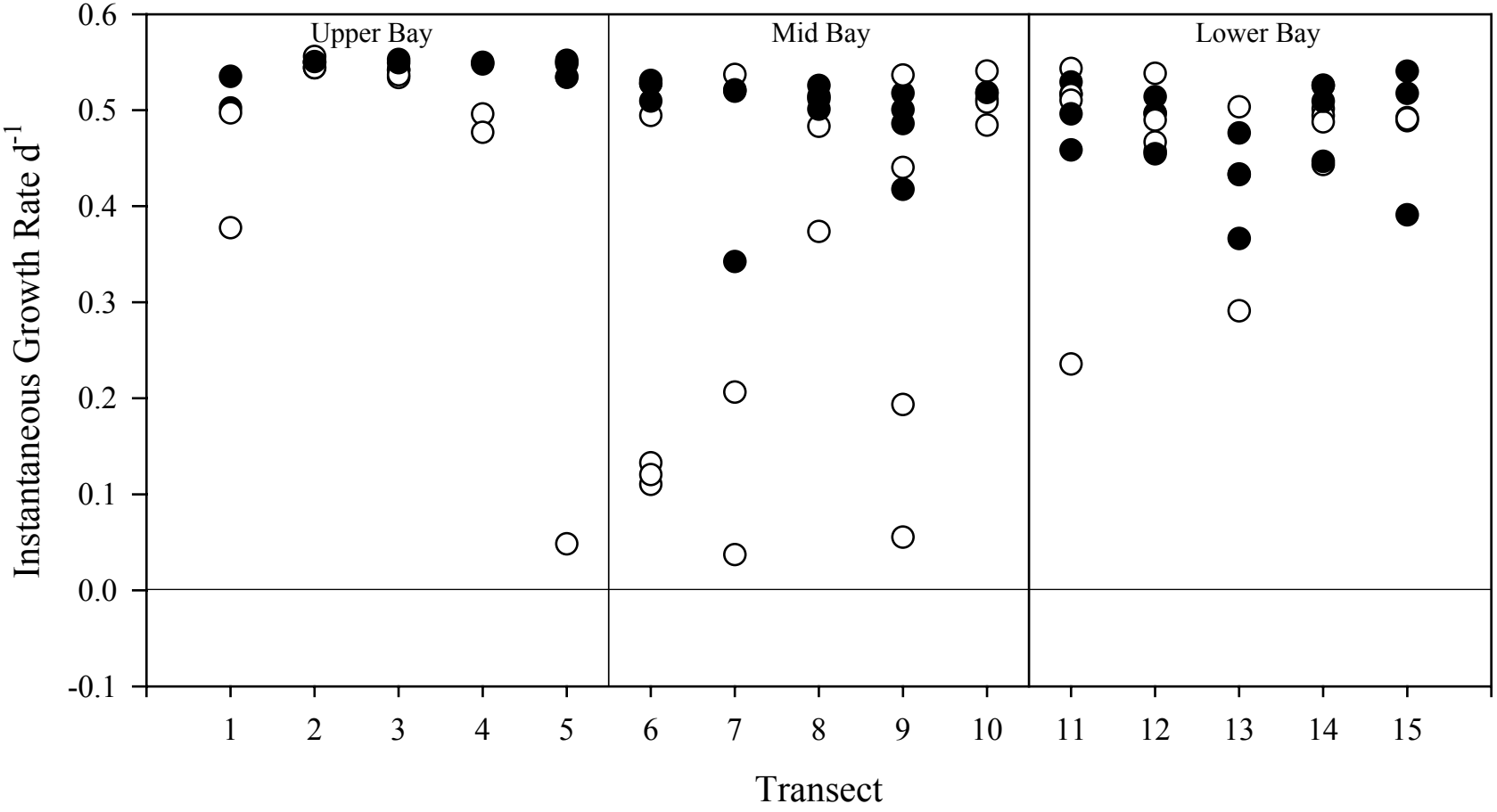

Figure 13: Predicted instantaneous weight-specific growth rates for July by transect and layer for the standardized larvae simulation. Closed circles indicate the instantaneous weight-specific growth rates at surface-layer stations while open circles indicate instantaneous weight-specific growth rates at bottom-layer stations.

Standardized Larvae Simulations: North to South Regional Patterns and Comparison to Field-Based Simulations

June

Larval bay anchovy mortality rates predicted by the standardized larvae and field-based simulations showed the same general spatial pattern, with the highest mortality rates for both simulations located in the mid and lower Bay regions, and the lowest mortality rates located in the upper Bay region (Figure 14a). However, the mortality rates predicted by the standardized larvae simulations in the mid and lower Bay regions (~0.46 d^{-1}) were more than twice the mortality rates predicted by the field-based simulations (~0.20 d^{-1}). In the upper Bay region, the predicted mortality rates for the two sets of simulations were similar in magnitude, with the standardized larvae simulations having a predicted mortality rate of 0.069 d^{-1} and the field-based simulations having a predicted mortality rate of 0.056 d^{-1}.

Growth rates predicted by the standardized larvae and field-based simulations also had similar spatial patterns, with the upper Bay region having the highest growth rates and the mid Bay region having the lowest growth rates (Figure 14b). Growth rates predicted by the standardized larvae simulations were generally 0.13 d^{-1} faster than the growth rates predicted by the field-based simulations. Predicted growth rates in the standardized larvae simulations for the lower Bay region (0.24 d^{-1}) were intermediate to the rates predicted for the mid Bay (0.15 d^{-1}) and for the upper Bay (0.38 d^{-1}).

Predictions of larval bay anchovy biomass production using M/G ratios for both sets of simulations found that the upper Bay region (M/G = 0.15) had the lowest M/G ratio (i.e., highest biomass production), while the mid Bay region (M/G = 3.39) had the highest M/G ratio (i.e., lowest biomass production) (Figure 14c). The predicted M/G ratio in the lower Bay region was greater than one for both sets of simulations indicating that, according to the field-based and

standardized larvae simulations, larval bay anchovy cohorts would lose biomass in lower Bay region. M/G ratios predicted by the field-based and standardized larvae were similar in the upper and lower Bay, but field-based simulations predicted a higher M/G ratio than the standardized larvae simulations for the mid Bay region.

July

For July, the highest mortality rates predicted by the standardized larvae simulations were in the mid Bay (0.26 d^{-1}) closely followed by the mortality rates in the upper Bay (0.20 d^{-1}), while the field-based simulations predicted the highest mortality rates were in the upper Bay region (0.23 d^{-1}) closely followed by the mid Bay region (0.20 d^{-1}) (Figure 14d). Both sets of simulations predicted that the lower Bay region would have substantially lower mortality rates than the other two regions. The magnitudes of the predicted mortality rates were closer for the two sets of simulations in July then they were in June (Figure 14a versus Figure 14d), but for two of the three regions, the standardized larvae simulations (Figure 14d) predicted higher mortality rates than the field-based simulations.

Regional growth rates predicted by the field-based and the standardized larvae simulations both indicated that the mid Bay region had the slowest growth rates and that the upper and lower Bay regions had the fastest growth rates, but the predictions were not consistent on the magnitude of these differences (Figure 14e). Differences in the regional growth rates predicted by the standardized larvae simulations were small in magnitude, with the slowest growth rate being 0.41 d^{-1} in the mid Bay region and the fastest growth rate being 0.49 d^{-1} in the upper Bay. Predicted growth rates were much more variable for the field based simulations, with the slowest growth rate being 0.11 d^{-1} in the mid Bay and the fastest growth rate being 0.30 d^{-1} in the lower Bay.

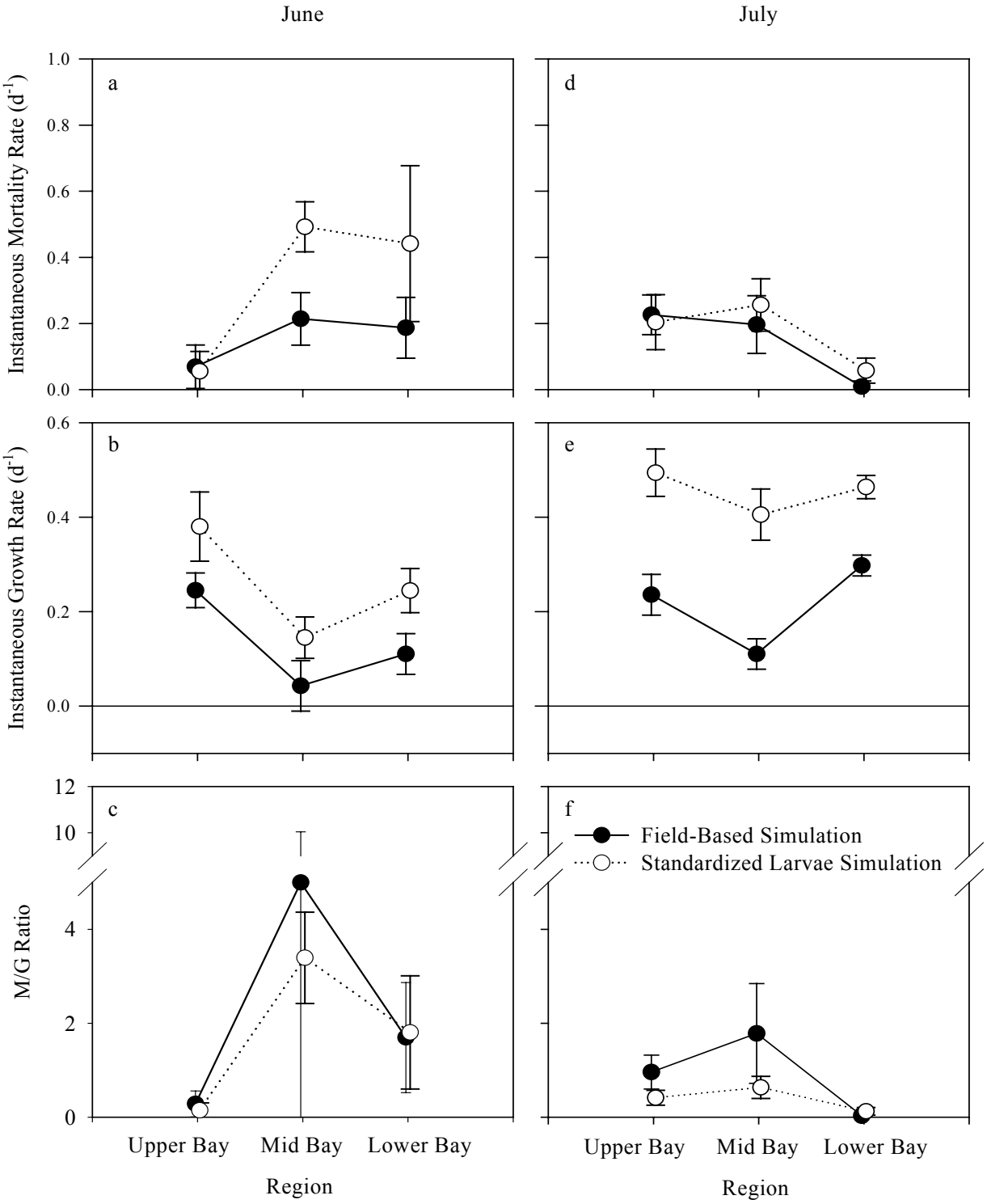

Figure 14: North to south axis regional instantaneous mortality rates (± 2 SE), weight-specific growth rates (± 2 SE), and M/G ratios (± 2 SE) for larval bay anchovy for June and July. Results are shown for the field-based simulations and the standardized larvae simulations. (a) Mortality rate in June. (b) Growth rate in June, (c) M/G ratio in June, (d) Mortality rate in July, (e) Growth rate in July, (f) M/G ratio in July.

Predicted spatial patterns of larval bay anchovy production based on M/G ratios were similar for the field-based and standardized larvae simulations, with the mid Bay region predicted to have the highest ratio and the lower Bay region predicted to the have the lowest ratio (Figure 14f). The standardized larvae simulations predicted M/G ratios that were less than 0.65 for all three regions of the Chesapeake Bay, suggesting that the larvae were gaining biomass throughout the Bay during July. Field-based simulations predicted M/G ratios of 0.96 in the upper Bay and 1.78 in the mid Bay, suggesting that larvae in these regions were either marginally increasing their biomass or more likely losing biomass. In the lower Bay region, the M/G ratio predicted by the field-based simulations was 0.03 indicating that larvae in that region were strongly increasing their biomass.

Field-Based and Standardized Larvae Simulations: West to East Regional Patterns

June

Regional instantaneous mortality rates for both the field-based simulations and the standardized larvae simulations decreased moving from the western edge of the Bay to the eastern edge of the Bay (W-E), though there was little difference in the predicted mortality rates from the field-based simulations between the central Bay and the eastern edge regions (Figure 15a). Regional mortality rates were approximately 0.2 d^{-1} higher for the standardized larvae simulations compared to rates predicted in the field-based simulations.

Regional growth rates along the W-E axis of the Bay were nearly constant across stations for both sets of simulations (Figure 15b). Growth rates from the field-based simulations ranged from 0.19 to 0.24 d^{-1}, and the growth rates from the standardized larvae simulations ranged closely about 0.25 d^{-1}.

Predicted M/G ratios decreased moving from the western edge of the Bay (M/G = 2.02) to the eastern edge of the Bay (M/G = 0.98) for the standardized larvae simulations, while the M/G ratio was highest in the western edge (M/G = 1.35) for the field-based simulation (Figure 15c). Standardized larvae simulations suggested that bay anchovy larvae populations would lose biomass in the western and central regions (M/G ratios were greater than 1) and maintain biomass in the eastern edge region (M/G ratio = 0.98). For the field-based simulations, bay anchovy larvae populations along the western edge of the Bay were predicted to lose biomass, while larvae in the central Bay and eastern edge were expected to gain biomass.

July

Predicted mortality rates from the standardized larvae length simulations were generally higher than those from the field-based simulations (Figure 15d). Predicted larval mortality rates in the standardized larvae simulations decreased moving from the western edge (0.27 d^{-1}) of the Bay to the eastern edge (0.12 d^{-1}), while predicted mortality rates in the field-based simulations did not show a clear pattern. Mortality rates were generally lower in July than in June for both sets of simulations (Figure 15a versus Figure 15d).

Predicted growth rates along the W-E axis of the Bay were higher for the standardized larvae simulations than for the field-based simulations, but neither set of simulations predicted a strong cross-Bay pattern in growth rate (Figure 15e). Growth rates predicted for the standardized larvae simulations were 0.43 to 0.48 d^{-1}, while the field-based simulations predicted mean regional growth rates ranging from 0.31 d^{-1} along the western edge to 0.25 d^{-1} along the eastern edge. July regional growth rates were generally higher than the growth rates predicted for June for both sets of simulations (Figure 15b versus Figure 15e).

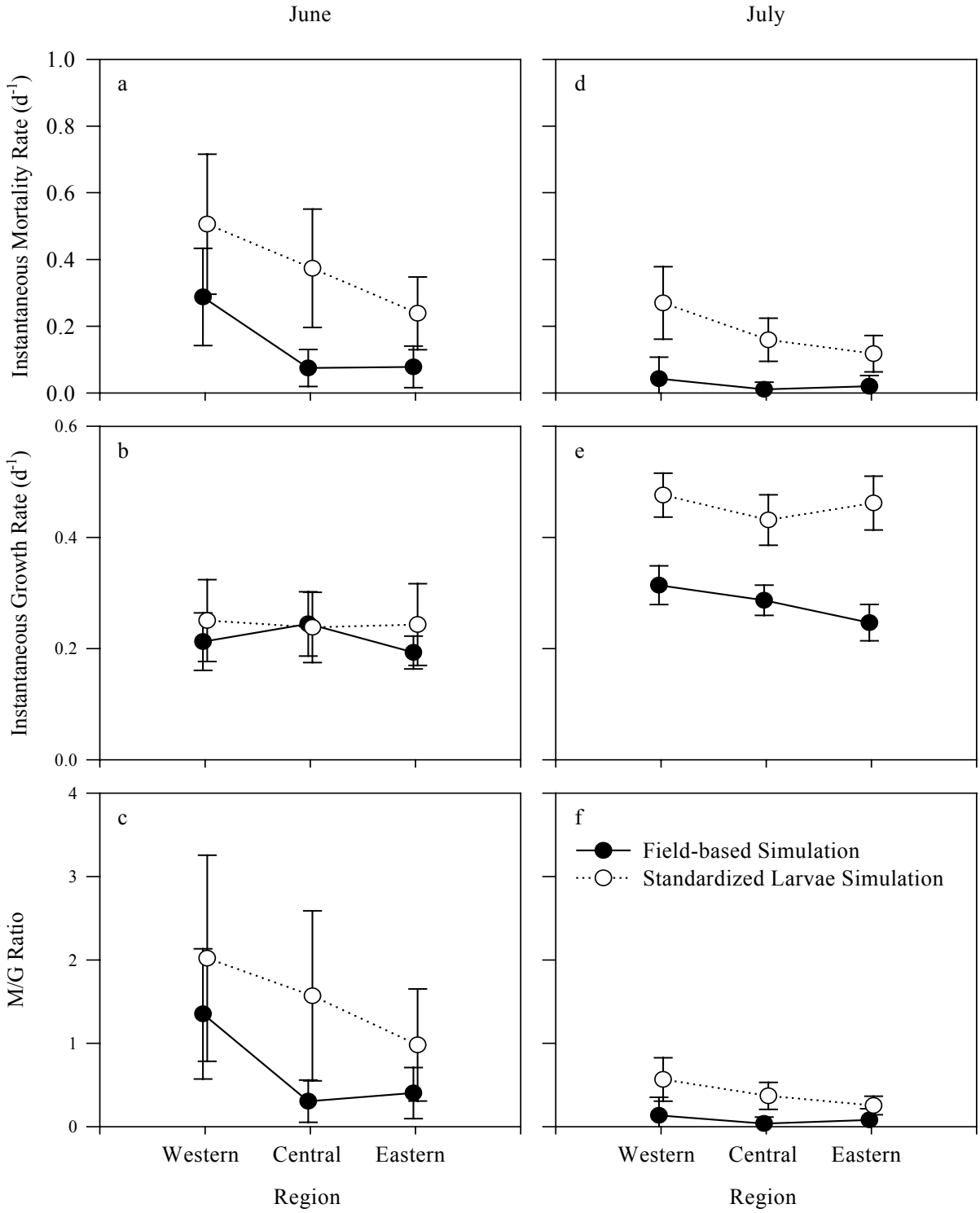

Figure 15: West to east axis regional instantaneous mortality rates (± 2 SE), weight-specific growth rates (± 2 SE), and M/G ratios (± 2 SE) for larval bay anchovy for June and July. Results are shown for the field-based and standardized larvae simulations. (a) Mortality rate in June, (b) Growth rate in June, (c) M/G ratio in June, (d) Mortality rate in July, (e) Growth rate in July, (f) M/G ratio in July.

During July, all three regions for both sets of simulations were predicted to have low M/G ratios, which indicate larval bay anchovy populations were increasing in biomass (Figure 15f). The field-based simulations had lower M/G ratios than the standardized larvae simulations. Predicted M/G ratios for the field-based simulations were somewhat constant across the Bay, but the standardized larvae simulations predicted decreasing M/G ratios going from the western edge of the Bay (M/G =0.57) to the eastern edge of the Bay (M/G = 0.25). M/G ratios were lower in July then they were in June in both sets of simulations (Figure 15c versus Figure 15f).

Larval Sources

June

Field-based simulations for June predicted that along the N-S axis of Chesapeake Bay 90.6% of all larvae surviving 20 days into the future came from the upper Bay region (Table 10). The mid Bay region contributed only 0.7% of the survivors and the lower Bay region contributed the remaining 8.6%. The upper Bay was the only region to increase its relative share of the bay anchovy larvae population over its share based upon initial larval abundances (85.4 to 90.6%). In general, the percent of surviving larvae from each region was consistent with the percentages of initial larvae found at each region.

For the standardized larvae simulations, the upper Bay region was again the highest producer of larval bay anchovies and the only region to increase its relative share of the Bay-wide bay anchovy larvae population (26.1% of the initial larvae to 69.9% of survivors) (Table 11). The mid Bay region once again contributed the smallest percentage of survivors (3.7%) despite having 34.8% of the initial larvae, while the lower Bay region contributed the remaining 26.4% of the survivors.

Along the W-E axis of Chesapeake Bay, the field-based simulations predicted that the percentage of survivors in each region increased moving from the western edge of the Bay (3.8%) to the eastern edge (55.2%) (Table 10). The eastern edge region and the central Bay region both slightly increased their relative share of the Bay-wide population of larvae surviving 20 days (37.7 to 40.9% and 51.6 to 55.2%, Table 10).

Standardizing the bay anchovy larvae populations resulted in the central Bay region having the highest percentage of all survivors (64.3%), followed by the eastern edge region (23.7%), and then the western edge (12%) (Table 11). The only region predicted by the standardized simulations to increase its relative share of the Bay-wide population of bay anchovy larvae was the central Bay region (47.8 to 64.3%, Table 11).

Table 10: The initial percentage of all larvae and the predicted percentage of all larvae surviving 20 days into the future for each N-S and W-E region during June and July for the field-based simulations. The 20-day predictions are based on extrapolating the one-day predictions of mortality rate from the field-based simulations at each layer and station.

	Initial Larvae (%)	Survivors (%)		Initial Larvae (%)	Survivors (%)
June Field					
Upper Bay	85.4	90.6	Western Edge	10.7	3.8
Mid Bay	1.5	0.7	Central Bay	37.7	40.9
Lower Bay	13.1	8.6	Eastern Edge	51.6	55.2
July Field					
Upper Bay	0.3	0.03	Western Edge	24.9	22.5
Mid Bay	5.2	1.8	Central Bay	55.2	58.0
Lower Bay	94.6	98.2	Eastern Edge	19.9	19.5

July

During the month of July, larval production was predicted to be concentrated in the lower Bay region by both the field-based simulations (98.2% of all survivors, Table 10) and the standardized larvae simulations (67.0% of all survivors, Table 11). Field-based simulations predicted that the few survivors not produced in the lower Bay region were produced primarily

Table 11: The initial percentage of all larvae and the predicted percentage of all larvae surviving 20 days into the future for each N-S and W-E region for June and July for the standardized larvae simulations. The 20-day predictions are based on extrapolating the one-day predictions of mortality rate from the standardized larvae simulations at each layer and station.

	Initial Larvae (%)	Survivors (%)		Initial Larvae (%)	Survivors (%)
June Standardized					
Upper Bay	26.1	69.9	Western Edge	26.1	12.0
Mid Bay	34.8	3.7	Central Bay	47.8	64.3
Lower Bay	39.1	26.4	Eastern Edge	26.1	23.7
July Standardized					
Upper Bay	27.1	18.7	Western Edge	27.1	17.2
Mid Bay	35.4	14.3	Central Bay	45.8	51.5
Lower Bay	37.5	67.0	Eastern Edge	27.1	31.3

in the mid Bay region (1.8% of all survivors), while the remaining 0.03% of survivors came from the upper Bay (Table 10). Standardized larvae simulations suggested that the production in the upper and mid Bay regions was more evenly split with 18.7% of the production of surviving bay anchovy larvae occurring in the upper Bay and the remaining 14.3 % of the surviving bay anchovy originating in the mid Bay. The field-based and standardized larvae simulations both predicted that the lower Bay region would be the only region to increase it's relative share of the Bay-wide bay anchovy population (94.6 to 98.2% for the field-based and 37.5 to 67.0% for the standardized larvae), while the upper and mid Bay regions were both predicted to lose some of their population share.

Along the W-E axis of the Bay, the central Bay region was predicted to produce most of the survivors by both the field-based (58.0% of all survivors, Table 10) and the standardized larvae (51.5% of all survivors, Table 11) simulations. The field-based simulations predicted that the western edge and eastern edge regions would produce similar numbers of survivors (22.5% and 19.5%, Table 10), while standardized larvae simulations predicted that the eastern edge region would produce nearly double the percentage of survivors produced along the western

edge of the Bay (31.3% versus 17.2%, Table 11). The central Bay region was the only region predicted by the field-based simulations to increase its relative share of the Bay-wide larvae population (55.2 to 58.1%, Table 10). The standardized larvae simulations predicted that both the central Bay and the eastern edge regions would slightly increase their relative shares of the surviving bay anchovy larvae (central Bay: 45.8 to 51.5% of all survivors; eastern edge: 27.1 to 31.3%) (Table 11).

Factor Influence on Spatial Patterns

Mortality

The single most important factor affecting the spatial pattern of larval bay anchovy mortality rates predicted under the field-based simulations was the number of predators, which explained 48.7% of the variability in the spatial pattern (Figure 16). Larval length was the second most important factor, but it explained only 8.0% of the variation in spatial pattern, which may indicate that it is of minimal importance. The four remaining factors each explained less than 3% of the variability in spatial pattern and were deemed to be insignificant.

Growth

Larval length and zooplankton density were the two factors found to influence the spatial pattern of larval growth rates, explaining 56.0% and 36.0% of the variability respectively (Figure 16). The four remaining factors each explained less than 2.5% of the variability in spatial pattern and were deemed to be insignificant.

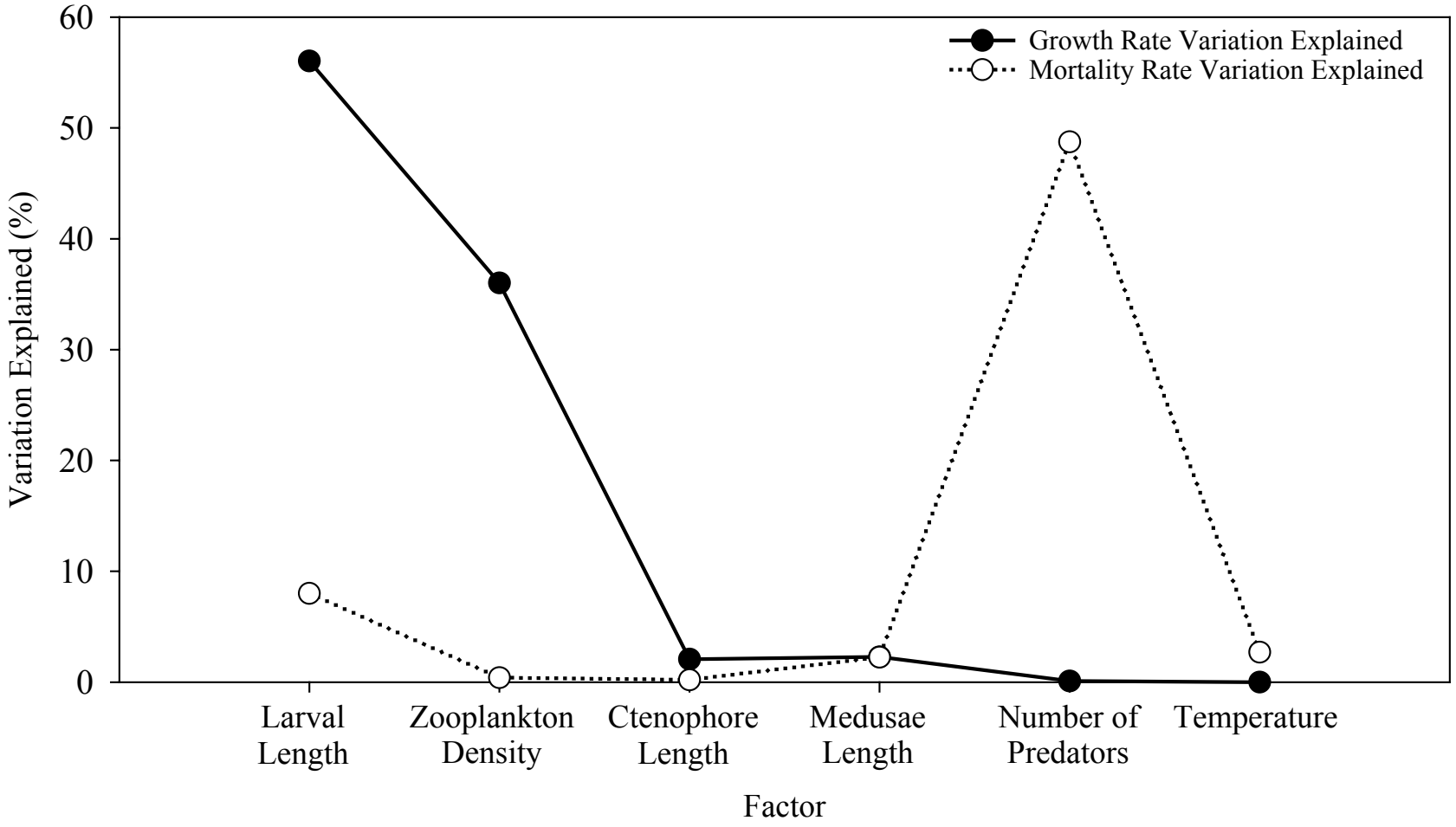

Figure 16: Percentage of the variation in July instantaneous growth and mortality rates predicted by the field-based simulations explained by the six factors: larval length, zooplankton density, ctenophore length, medusae length, number of predators, and temperature.

DISCUSSION

With fish populations at low levels worldwide and anthropogenic stressors increasing, quantifying habitat quality for fish is critical for effective fisheries management (National Research Council 1999). The Sustainable Fisheries Act requires that essential fish habitat (EFH), "those waters and substrates necessary to fish for spawning, breeding, feeding or growth to maturity", be defined and requires managers "to promote and protect essential fish habitat" (Schmitten 1999). Quantifying habitat quality is especially important for larval fish that inhabit estuaries because estuaries are a common nursery area for many species and because estuaries are subject to a multitude of human related stressors such as eutrophication, contaminant loading, and loss of physical habitat (National Research Council 1999).

A commonly used method for determining mortality and growth rates of larval fish is to aggregate individuals into spatial regions based upon their location of capture and to compute growth and mortality rates from otoliths by region (e.g. Nixon and Jones 1997, Rilling and Houde 1999, Bailey and Heath 2001, Comyns et al. 2002). This approach looks backward in time and uses the recent past history of individuals to infer growth and mortality rates. I used individual-based simulation modeling to compute instantaneous growth and mortality of larvae over the next day based upon the conditions (temperature, density of zooplankton, and the densities and size of gelatinous predators and larvae collected during field sampling) at the time and location of capture. My approach avoids the necessity of aggregating individuals at multiple stations into broad geographic regions in order to obtain estimates of mortality and growth rates, and reduces the reliance of these estimates on past history. It is important to also recognize that the initial conditions from the field data used in model simulations are not completely

independent of past conditions as they are the end result of growth and mortality rates experienced by those larvae that resulted in their survival and size at the time of capture.

Rigorous validation of the model is not possible as a completely independent data set is not available, but there are several model to data comparisons that can provide corroborative evidence of model realism. Mortality rates of larval bay anchovy predicted by the field-based simulations at individual stations were generally within the range of mortality rates reported in the literature. The highest predicted mortality rate at an individual site (1.64 day^{-1}) was much lower than the highest reported mortality rate (4.24 day^{-1}) for yolk-sac larvae in Chesapeake Bay reported by Dorsey et al. (1996). The lowest predicted mortality rates (zero mortality) were lower than the lowest reported rate of 0.08 day^{-1} (Cowan and Houde 1990). Low predicted larval bay anchovy mortality rates were a result of larvae only being able to "die" in simulations if they were "eaten" by a ctenophore or a sea nettle. Houde et al. (1994) reported that, in a study using mesocosms, bay anchovy larvae had a mortality rate of 0.16 day^{-1} in control mesocosms that did not contain obvious predators. If there were no gelatinous predators collected at a site during field collections, the model predicts no mortality, as the model does not consider other predators or other mortality sources.

Predicted growth rates of larval bay anchovy at individual sites were frequently within the range of rates reported in the literature, but there were a number of instances where growth rates were outside of the reported ranges. Predicted growth rates that were faster than the rates reported in the literature were likely the result of the simulations lasting a single day. Rilling and Houde's (1999) otolith-based estimates of larval growth rates were estimates of the average growth rate of all the larvae in a region, over the time span of their ages (June: ~2 – 17 days post-hatch; July: ~2 – 32 days post-hatch). A second reason for slow predicted growth rates was that

field-based simulations could predict negative growth rates which are generally not recorded in field-based estimation methods.

Layer and Month Effects

Larval bay anchovy growth and mortality rates predicted for the surface and bottom layers during both June and July by the field-based and standardized larvae simulations showed no consistent differences between layers. Model predictions of no consistent differences in predicted mortality rates for the surface and bottom layers during June (open versus closed circles on Figure 5 and Figure 10) were likely due to a lack of difference in the densities (Rilling 1996; Appendix Figure A2) and sizes (Appendix Figure A5) of ctenophores between the two layers. During July, Rilling (1996) found that predator densities were significantly higher above the pycnocline (surface layer) than below it (see also Appendix Figures A2 and A3). The finding of little or no difference in the predicted mortality rates of larvae in the two layers during July (open versus closed circles on Figure 7 and Figure 12) was likely due to the initially low numbers of larvae (Appendix Figure A1) in the regions with the highest ctenophore densities (Appendix Figure A2) and sea nettle (Appendix Figure A3) densities.

Regional estimates were weighted by larval abundances at stations. Predicted larval growth rates showed little or no difference in growth rates between layers (Figures 6, 8, 11 and 13). Zooplankton biomass and larval lengths, the two most important factors for larval growth rates (Figure 16), also show no consistent pattern of differences between the surface and bottom layers. Despite predicting no consistent difference in growth and mortality rates in the surface and bottom layers during June and July, it is possible that there were actual differences in the growth and mortality rates in the two layers due to the potential direct and indirect effects of

hypoxia and anoxia on the growth and mortality rates of larvae (Breitburg et al. 1999), but these effects were not included in the model simulations.

Changes in regional larval bay anchovy mortality rates between June and July were not consistent across regions along the N-S or the W-E axes for the field-based simulations (Figure 9a versus Figure 9d), the standardized larvae simulations (Figure 14a versus 14d; Figure 15a versus 15d), or for Rilling and Houde's (1999) field data (Figure 9a versus 9d). In some regions, mortality rates increased between June and July, while in other regions the mortality rates decreased. This was likely due to changes in the spatial patterns of predator densities between June and July (Appendix Figures A2 and A3).

Larval bay anchovy growth rates were found to generally increase between June and July by Rilling and Houde (1999) (Figure 9a versus 9d), and also by the field-based and standardized larvae simulations along both the N-S (Figure 9a versus 9d; Figure 14a versus 14d) and W-E (Figure 15a versus 15d) axes of Chesapeake Bay. The primary cause for predicted growth rates in July being faster than the predicted growth rates in June was likely the increased zooplankton biomass during July (Appendix Figure A7). Larval length was not thought to be a major factor in the increase in growth rates between June and July, as growth rates generally increased in both the field-based and standardized larvae simulations.

Rilling and Houde (1999) and the two sets of simulations predicted that the regional M/G ratios for larval bay anchovy generally decreased between June and July. Decreases in M/G ratios were primarily driven by the general increase in growth rates between June and July (Figure 9b versus 9e; Figure 14a versus 14e; Figure 15a versus 15e). In the case where the M/G ratios increased between June and July in the field-based and standardized larvae simulations (June upper Bay, Figure 9c versus 9f; Figure 14c versus 14f), the regional growth rates were

relatively unchanged between June and July but the regional mortality rates increased substantially due to an increase in regional predator densities (Appendix Figures A2 and A3).

Habitat Quality

Predictions of habitat quality made by Rilling and Houde (1999) were somewhat counterintuitive. The regions that were predicted to be best (lowest M/G ratio) for larval bay anchovy production, the mid Bay region during June and the upper Bay region during July, were the regions that had the lowest abundances of larval bay anchovy (Figure 17). The lower Bay region, which was predicted to be the worst habitat for larval bay anchovy during both months, had only marginally higher abundance of larvae than the best region in June (mid Bay) and had the highest abundance of larvae of any region during July. Additionally, the regions that were predicted to be best for larval anchovy had among the highest densities of gelatinous predators, while the regions that were predicted to be worst for larval bay anchovy had lower abundances of gelatinous predators (Appendix Figures A2 and A3). Zooplankton biomass did not appear to have a significant effect on the growth rates of larval bay anchovy reported by Rilling and Houde (1999), as their estimated growth rates did not appear to differ significantly among regions in either month (Figure 9b and Figure 9e).

In contrast, the predictions of habitat quality made by the field-based simulations were more consistent with the biological conditions in the regions. Regions that were predicted by the field-based simulations to have the best habitat (upper Bay during June and lower Bay during July) also had the highest abundances of larval bay anchovy. Furthermore, regions that were predicted to have the worst habitat (mid Bay region during both June and July) generally had the lowest abundances of larval bay anchovy (Figure 17). Model predictions of M/G ratios did not use larval abundances. As expected, model predictions of M/G were consistent with the field

measured zooplankton biomass and predator densities as these were used as inputs to the model. In both months, the regions that were predicted to be the best for larval bay anchovy production by the field-based simulations had the lowest abundances of gelatinous predators (Appendix Figures A2 and A3), and somewhat abundant zooplankton biomass (Appendix Figure A7). The mid Bay region, which was predicted to be the worst region for larval bay anchovy production during June and July, had the highest abundances of gelatinous predators and the lowest zooplankton biomass of the three regions for both months.

It was somewhat surprising to discover that there was not one case where Rilling and Houde's (1999) estimated M/G ratios and the M/G ratios predicted by the field-based simulations were in agreement as to a region having either the lowest M/G ratio or the highest M/G ratio. In fact, there were two cases where the two methods predicted the exact opposite. The first case was in June, where Rilling and Houde (1999) predicted that the mid Bay region would have the lowest M/G ratio but the field-based simulations predicted that the mid Bay region would have the highest M/G ratio (Figure 9c). The second case was in July, where the field-based simulations predicted that the lower Bay region would have the lowest M/G ratio but Rilling and Houde (1999) predicted that the lower Bay region would have the highest M/G ratio (Figure 9d).

Two potentially interacting causes for low egg densities and subsequent low densities of bay anchovy larvae in the mid Bay region during June are low zooplankton densities and high ctenophore abundances. Peebles et al. (1996) suggested that bay anchovy may use income breeding, spawning soon after energy for egg production becomes available, as a mechanism to minimize the mismatch between food availability and their larvae. The low or negative growth rates predicted by the field-based simulation along most transects in the mid Bay region

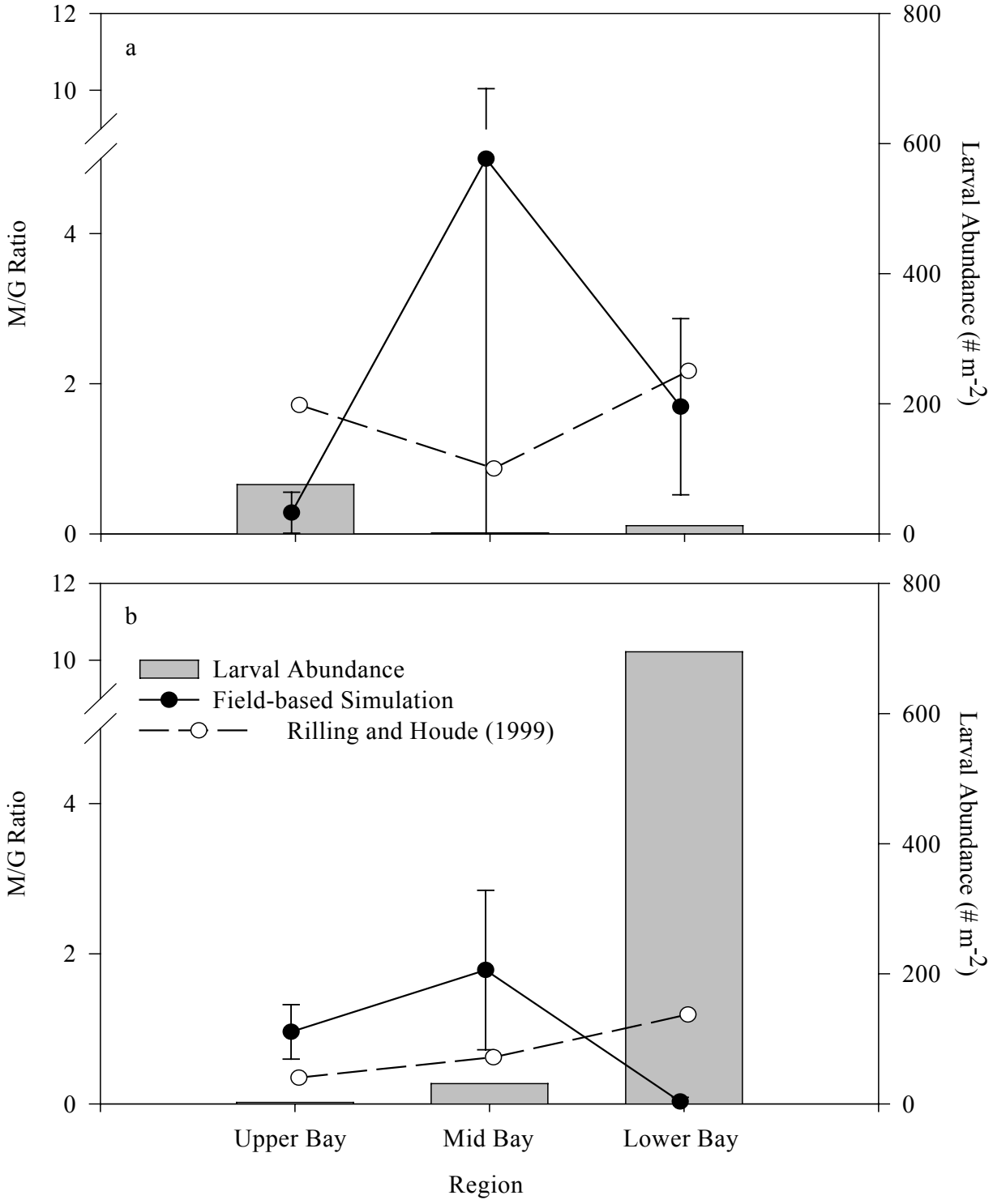

Figure 17: Comparison of M/G ratios predicted from the field-based simulations and estimated by Rilling and Houde (1999) with the abundances of larval bay anchovy observed in the upper, mid, and lower Bay regions of Chesapeake Bay during June and July of 1993. Larval abundances are from Rilling and Houde (1999). (a) June, (b) July.

(Figure 6) clearly indicate that there was a mismatch between zooplankton and larvae in the region. Because of the poor growth conditions in the region, adult bay anchovy may have either spawned smaller batches of eggs in the region or simple not spawned at all due to a lack of energy for egg production. High densities of ctenophores may have caused reduced densities of bay anchovy eggs and larvae in the mid Bay region by lowering the fecundities of adult bay anchovy through competition for copepod prey (Peebles et al. 1996) and by direct predation on bay anchovy eggs and larvae (Purcell and Arai 2001).

The high mortality rate that Rilling and Houde (1999) estimated in the lower Bay region in July (Figure 9d) could be due to the effects of fish predators on bay anchovy or due to up-estuary migration. One finding of the TIES program is that larval and juvenile fish that feed on larval bay anchovy are relatively abundant in the mid Bay region (TIES 2003). Rilling and Houde (1999), citing the findings of MacGregor and Houde (1996), suggested that the mortality rates that they found in the lower Bay region may have been over-estimated due to the up-estuary migration of late larval and early juvenile stage anchovy larvae. A later study by North (2002) suggested that bay anchovy larvae in the lower Bay region could potentially be advected either up-estuary or down-estuary depending on their depth resulting in the larvae being transported to either the mid Bay region or out of Chesapeake Bay.

Standardized larvae simulations, which were used to eliminate the confounding regional effects of larval lengths, and to allow for the prediction of growth and mortality rates where larvae were not captured during collections, confirmed the general spatial trends of M/G ratios predicted by the field based-simulations (Figure 14c and 14f). Regions that were predicted to be the best or worst (low or high M/G ratios) by the field-based simulations were the same regions that were predicted to be the best or worst region by the standardized larvae simulations.

However, magnitudes of the growth and mortality rates were substantially different between the two sets of simulations. Those differences were likely due to the differences in larval lengths between the field-based (Appendix Figure 4) and standardized larvae simulations. Small larvae (~4.5 mm) that were used for all standardized larvae simulations, were less proficient feeders and relied more on the smaller zooplankton prey types, and were also more vulnerable to predation (Pepin 1993).

There are a number of potential reasons for the differences in the predicted M/G ratios between the field-based simulations and Rilling and Houde's (1999) analysis. Predictions of mortality by the field-based simulations only accounted for the mortality due to predation by gelatinous predators. In the field, bay anchovy larvae may be eaten by both planktonic predators (Hunter 1981, Heath 1992, Houde et al. 1994) and fish predators, such as small Atlantic croakers (Cowan, personal communication) and juvenile Atlantic silversides, *Menidia menidia* (Castro and Cowen 1999). Additionally, a number of studies have suggested that first feeding larval fish may suffer high mortality due to starvation (Houde 1974, Heath 1992), whereas starvation was not possible in one-day simulations. Predicted differences in growth rates among stations and regions in the field-based simulations, which were based on measured zooplankton densities, may not be realistic. The individual-based model imposed cumulative distribution functions (CDF) that were designed to address spatial patchiness of zooplankton, but were based on a different data set than the zooplankton collections used here and the CDFs were imposed uniformly throughout the Bay. Further, the densities of rotifers and tintinnids were adjusted upwards in simulations to allow small larvae some prey. Measurement of the densities of tintinnids and rotifers in the field is difficult, and the adjusted densities used in model

simulations may not be representative of the actual densities of rotifers and tintinnids at individual stations.

There are also potential problems in comparing M/G ratios predicted by the field-based simulation with Rilling and Houde's (1999) estimated M/G ratios due to differences in time scales and the effects of large-scale physical and biological processes. Because of the estimation procedures involved with otolith-based analyses, estimated growth and mortality rates may have been more representative of the conditions experienced by the larvae over the previous weeks or reflective of conditions at another station or even region. Environmental conditions at a location can change rapidly, especially at the small spatial and temporal scales experienced by fish larvae. Rilling (1996) pointed out that mortality rates of larvae during July might have been underestimated in the mid Bay region and overestimated in the lower Bay region due to up-Bay transport of larvae. Kimura et al. (2000) suggested that up-Bay transport of late larval and early juvenile stage bay anchovy occurs in Chesapeake Bay. Growth rate predictions may be affected by seasonal changes in the location of spawning adult bay anchovy or by the transport of late larval and early juvenile stage bay anchovy. During June, the highest abundances of eggs and larvae were located in the upper Bay region, while in July the highest abundances were in the lower Bay region. Assuming that the number of eggs produced is closely correlated with the number of spawners, this pattern of egg production indicates that the bay anchovy spawning stock is migrating down the estuary over the period of June to July, as has been suggested by Jung (2002). The presence of large larvae in the upper and mid Bay regions may cause the predicted growth rates to be higher than they would be otherwise. Finally, the regression models used to estimate growth and mortality rates assume that growth and mortality are constant over time (Everhart and Youngs 1981). The validity of this assumption was questioned by Rilling

(1996) who found that 5-10 day old larvae died at rates (June 0.718 d^{-1}; July 0.443 d^{-1}) that were nearly double the rates of 11-15 day old larvae (June 0.405 d^{-1}; July 0.254 d^{-1}).

The differences in the abundances of eggs (Rilling 1996) and larvae (Appendix Figure 1) among regions overwhelmed the field-based simulation's predicted differences in habitat quality among regions. During both June and July and along both the N-S axis and the E-W axis, the rank-order of each region in terms of initial larval abundance and the forecasted number of survivors produced by a region 20 days in the future were identical. Regions with the greater percent of initial larvae also yielded the greater percent of survivors. However, when the standardized larvae simulations were used, habitat quality did have an affect on the regional contributions to survivors. In the standardized larvae simulations, all three regions (N-S and E-W) started with roughly equivalent abundances of larvae. Standardized larvae simulations for June predicted that the upper Bay had the highest habitat quality (M/G = 0.15). Over a period of 20 days, the upper Bay region went from having the smallest proportion of initial larvae (26.1%) to producing the majority of the survivors (69.9%) (Table 11). During July, the lower Bay region was predicted by the standardized larvae simulations to have the best habitat quality (M/G = 0.12). Initially, the lower Bay had approximately the same number of larvae as the mid Bay region (37.5% versus 35.4% of the initial number of larvae) and a 10% higher share of the initial number of larvae than the upper Bay (27.1% of the initial number of larvae). After 20 days, the lower Bay region was projected to produce 67% of the surviving larvae. Thus, if egg production was spread uniformly throughout Chesapeake Bay, habitat quality could have an important effect on the regional production of larvae, and perhaps on recruitment.

West to East Axis of Chesapeake Bay

Along the west to east axis of Chesapeake Bay, field-based simulations predicted that the western edge of the Bay would have the highest M/G ratios for both June and July, making it the worst habitat for larval bay anchovy (Figure 15c and 15f). In contrast, the central region and the eastern edge of Chesapeake Bay were both predicted to have relatively low M/G ratios during both June and July. Regional mortality rates of larval bay anchovy appeared to be the primary cause of the high M/G ratios along the western edge of the Bay, as the western edge region had the highest mortality rates during both June (0.29 day^{-1}) and July (0.042 day^{-1}, Figure 15a and 15d). It is not clear why mortality was highest along the western edge of the Bay, as during both months the highest abundances of gelatinous predators were found in the central Bay region. Growth rates of larval bay anchovy appeared to be relatively consistent across the west to east axis of Chesapeake Bay during both June and July, and therefore did not appear to be the cause of the high M/G ratios along the western edge of the Bay. In partial agreement with the high M/G ratios, the highest abundances of eggs and larvae were never found in the western edge region. Abundances of eggs were lowest in the western edge region and highest in the eastern edge region during both months (Rilling 1996), while the abundances of larvae were highest in the eastern edge region during June and in the central bay region during July.

Factors Affecting Spatial Patterns

The spatial variation of larval bay anchovy growth rates appeared to be primarily influenced by larval length (56.0% of the variability) and zooplankton density (36.0% of the variability), while mortality rates were influenced by the number of predators (48.7% of the variability) (Figure 16). Larval length influenced predicted larval growth rates in model simulations through its effects on larval foraging capabilities and bioenergetics. Many of the

growth related processes in the model were formulated to depend on larval length or weight, with skills improving with larval size. As larvae grow in size, their sensory capabilities increase, their ability to capture prey items improves, and the sizes of the prey items that they can capture increases (Detwyler and Houde 1970, Blaxter 1986). However, increasing larval length also increases the baseline metabolic rate of larvae, requiring larvae to consume ever-greater amounts of food in order to sustain themselves.

The second most important factor affecting the spatial variation in predicted growth rates was zooplankton density. Zooplankton density has a major influence on larval growth rates because consumption drives larval bay anchovy growth. The more zooplankton a larva consumes, the more energy it has to grow. Thus regions with high densities of zooplankton prey also are likely to be regions with high larval growth rates, while areas with lower densities of zooplankton would likely have slower growth (Saksena and Houde 1972). It was somewhat surprising that temperature had such a small influence on larval growth rates, as a number of studies have suggested that temperature has a major impact on larval growth rates (Houde 1977, Houde 1989). Possible explanations for the lack of importance of temperature is that the model does not sufficiently include temperature effects, that temperature during the summer months does not vary enough to cause major differences in larval growth, or that the effects of temperature are also included implicitly through zooplankton densities (Peebles et al. 1996).

The finding that the number of gelatinous predators was influential on the spatial pattern of predicted larval bay anchovy mortality was expected. Increasing the number of predators in simulations increased the probability that a larva would be eaten by a predator. Interestingly, predator size was not important in determining the spatial variation in predicted larval mortality rates, despite some clear patterns in ctenophore lengths within the Bay (Appendix Figure 5).

Future Directions

Several additional studies could improve the individual-based modeling approach to quantifying the habitat quality of larval fish. The primary question that needs to be addressed is how do larval bay anchovy die? In the present study, modeled larval bay anchovies could only die by being eaten by ctenophores or sea nettles. Other important predators on larval bay anchovies, such as young fish, could have been included in simulations if information was available on fish predator densities and how fish predators fed on larval bay anchovies. Information on larval bay anchovy predators other than ctenophores and sea nettles is somewhat sparse due to the difficulty of studying larval fish mortality in the field (Hunter 1981, Heath 1992). A cursory examination of this complicated situation indicates that there is large, undocumented source of morality on larval bay anchovy. Cowan and Houde (1990) estimated larval anchovy mortality rates of 10 to 15% day^{-1} in mesocosms that excluded large predators, indicating that small planktonic predators may be causing some of the mortality of larval bay anchovy (Houde et al. 1984). For the invertebrate predators, more information on how predation changes with changes in the ratio of predator size to larva size is needed (Pepin 1993, Fuiman 1994). The relationship used in the model was estimated from laboratory experiments that were not designed to examine the effects of prey to predator size on predator capture success. One can also examine the growth and mortality models and find many other areas that would benefit by additional empirical data.

Future field studies should focus on improving estimates of zooplankton and predator densities, and sampling larvae and predators with finer vertical resolution. In my analyses, the numbers of rotifers and tintinnids had to be arbitrarily adjusted in order to obtain reasonable prey densities, thus allowing reasonable bay anchovy growth rates. Additionally, at a number of

sampling sites no copepods and copepodites were recorded, resulting in an estimated density of zero liter^{-1}, which was unrealistic for the 2000 m^3 water column that I simulated. Sampling the gelatinous predators and bay anchovy larvae at more than surface and bottom layers locations would improve the estimates of layer and station abundances and permit model simulations of a stratified water column (all layers simultaneously), rather than simulating the surface and bottom layers separately. Additionally, this model would allow for the inclusion in simulations of the effects of dissolved oxygen on growth and mortality rates via vertical movement of larvae and predators in response to oxygen conditions in the layers (Breitburg et al. 1999).

I used an individual-based modeling approach to predict instantaneous larval fish growth and mortality rates based on local environmental conditions. The approach used in this study was different from the approaches typically used in individual-based and spatially-explicit bioenergetics modeling studies. Rather than running simulations for several time-steps in order to reduce the effect of initial conditions on model predictions, this study used single time-step simulations, as I was interested in the effects of initial conditions on growth and mortality rates. Unlike many previous applications of bioenergetics modeling to quantify habitat quality (Brandt and Kirsch 1993, Luo and Brandt 1993, Logerwell et al. 2001, Tyler and Brandt 2001), I compared predicted regional growth rates from the simulations with the estimated growth rates based on field data and I predicted mortality rates in addition to the usual growth rates. My approach also differed from the otolith-based approach by using a model to attempt to truly generate growth and mortality rates reflective of the immediate conditions. Despite the use of common field data, the results of my analyses in terms of the habitat quality of different regions of the Bay differed from the conclusions of Rilling and Houde (1999). These differences deserve further examination and investigation.

LITERATURE CITED

Bailey, K. M. and Batty, R. S. 1983. A laboratory study of predation by *Aurelia aurita* on larval herring (*Clupea harengus*): experimental observations compared with model predictions. Marine Biology. 72: 295-301.

Bailey, M. C., and Heath, M.R. 2001. Spatial variability in the growth rate of blue whiting (*Micromesistius poutassou*) larvae at the shelf edge west of the UK. Fishery Research. 50: 73-87

Baird, D. and Ulanowicz, R. E. 1989. The seasonal dynamics of the Chesapeake Bay ecosystem. Ecological Monographs. 59(4): 329-364.

Blaxter, J. H. S. 1986. Development of sense organs and behaviour of teleost larvae with special reference to feeding and predator avoidance. Transactions of the American Fisheries Society. 115: 98-114.

Brandt, S. B. and Kirsch, J. 1993. Spatially explicit models of striped bass growth potential in Chesapeake Bay. Transactions of the American Fisheries Society. 122: 845-869.

Breitburg, D. L., Adamack, A., Rose, K. A., Kolesar, S. E., Decker, M. B., Purcell, J. E., and Cowan, J. H. Jr. 2003. The pattern and influence of low dissolved oxygen in the Patuxent River, a seasonally hypoxic estuary. Estuaries. 26: 280-297.

Breitburg, D. L., Rose, K. A., and Cowan, J. H. Jr. 1999. Linking water quality to larval survival: predation mortality of fish larvae in an oxygen-stratified water column. Marine Ecology Progress Series. 178: 39-54.

Carter, H. H., and Pritchard, D. W. 1988. Oceanography of Chesapeake Bay. In: Kjerfve, B. (ed.) Hydrodynamics of estuaries: Volume II estuarine case studies. CRC Press, Boca Raton, p. 1-16.

Castro, L. R. and Cowen, R. K. 1991. Environmental factors affecting the early life history of bay anchovy *Anchoa mitchilli* in Great South Bay, New York. Marine Ecology Progress Series. 76: 235-247.

Chesapeake Bay Program: America's premier watershed restoration partnership. Chesapeake Bay Program. May 30, 2002. <http://www.chesapeakebay.net> .

Comyns, B. H., Shaw, R. F., and Lyczkowski-Shultz, J. 2002. Small-scale spatial and temporal variability in growth and mortality of fish larvae in the subtropical northcentral Gulf of Mexico: implications for assessing recruitment success. Fishery Bulletin. 101: 10-21.

Cowan, J. H. Jr., and Houde, E. D. 1990. Growth and survival of bay anchovy *Anchoa mitchilli* larvae in mesocosm enclosures. Marine Ecology Progress Series. 68: 47-57

Cowan, J. H. Jr., and Houde, E. D. 1992. Size-dependent predation on marine fish larvae by ctenophores, scyphomedusae and planktivorous fish. Fisheries Oceanography 1: 113-126.

Cowan, J. H. Jr., and Houde, E. D. 1993. Relative predation potentials of scyphomedusae, ctenophores and planktivorous fish on ichthyoplankton in Chesapeake Bay. Marine Ecology Progress Series. 95: 55-65.

Cowan, J. H. Jr., Houde, E. D., and Rose, K. A. 1996. Size-dependent vulnerability of marine fish larvae to predation: an individual-based numerical experiment. ICES Journal of Marine Science. 53: 23-37.

Day, J. W. Jr., Hall, C. A. S., Kemp, W. M. and Yáñez-Arancibia, A. 1989. Estuarine Ecology. John Wiley & Sons, Inc. New York.

Detwyler, R. and Houde, E. D. 1970. Food selection by laboratory-reared larvae of scaled sardine *Harengula pensacolae* (Pisces, Clupeidae) and the bay anchovy *Anchoa mitchilli* (Pisces, Engraulidae). Marine Biology 7: 214-222.

Dorsey, S. E. 1993. Daily variability in mortality of bay anchovy, *Anchoa mitchilli* eggs and yolk-sac larvae in Chesapeake Bay, USA. MS. Thesis. Univ. of Maryland, College Park. MD 109pp.

Dorsey, S. E., Houde, E. D. and Gamble, J. C. 1996. Cohort abundances and daily variability in mortality of eggs and yolk-sac larvae of bay anchovy, *Anchoa mitchilli*, in Chesapeake Bay. Fishery Bulletin. 94: 257-267.

Everhart, W. H. and Youngs, W. D. 1981. Principles of fishery science 2nd edition. Comstock Publishing Associates. Ithaca pg. 349

Fives, J. M., Warlen, S. M. and Hoss, D. E. 1986. Aging and growth of larval bay anchovy, *Anchoa mitchilli*, from the Newport River Estuary, North Carolina. Estuaries. 9: 362-367.

Fuiman, L. A. 1994. The interplay of ontogeny and scaling in the interactions of fish larvae and their predators. Journal of Fish Biology. 45(A): 55-79.

Gallagher, R. P., Hirschfield, M. F., and Perry, E. S. 1983. Age, growth, and mortality estimates for larval bay anchovy *Anchoa mitchilli* in the Patuxent River. Benedict Estuarine Research Laboratory publication, Division of Environmental Research; Academy of Natural Sciences of Philadelphia, Philadelphia. PA, 34p.

Gerritsen, J. and Strickler J. R. 1977. Encounter probabilities and community structure in zooplankton: a mathematical model. Journal of the Fisheries Research Board of Canada. 34: 77-82.

Hartman, K. J. and Brandt, S. B. 1995. Predatory demand and impact of striped bass, bluefish, and weakfish in the Chesapeake Bay: application of bioenergetics models. Canadian Journal of Fisheries and Aquatic Science. 52: 1667-1687.

Heath, M. R. 1992. Field Investigations of the Early Life Stages of Marine Fish. Advances in Marine Biology. 28: 1-173.

Höök, T. O., Rutherford, E. S., Brines, S. J., Mason, D. M., Schwab, D. J. McCormick III, M. J., Fleischer, G. W., and De Sorcie, T. J. 2003. Spatially Explicit Measures of Production of Young Alewives in lake Michigan: Linkage Between Essential Fish Habitat and Recruitment. Estuaries. 26: 21-29.

Houde, E. D. 1974. Effects of temperature and delayed feeding on growth and survival of larvae of three species of subtropical marine fishes. Marine Biology. 26: 271-285.

Houde, E. D. 1977. Food concentration and stocking density effects on survival and growth of laboratory-reared larvae of bay anchovy *Anchoa mitchilli* and lined sole *Achirus lineatus*. Marine Biology. 43: 333-341.

Houde, E. D. 1987. Early life dynamics and recruitment variability. American Fisheries Symposium. 2: 17-29.

Houde, E. D. 1989. Comparative growth, mortality and energetics of marine fish larvae: Temperature and implied latitudinal effects. Fishery Bulletin. 87: 471-495

Houde, E. D. 1997. Patterns and consequences of selective processes in teleost early life histories. *In* Early life history and recruitment in fish populations. Ed. Trippel, E. A. Chapman & Hall, London.

Houde, E. D., Chesney, E. J., Newberger, T. A., Vazquez, A. V., Zastrow, C. E., Morin, L. G., Harvey, H. R., and Gooch, J. W. 1989. Population biology of bay anchovy in Mid-Chesapeake Bay. Ref. No. (UMCEES)-CBL 89-141. Chesapeake Biol. Lab., Solomons, MD

Houde, E. D., Gamble, J. C., Dorsey, S. E., and Cowan, J. H. Jr. 1994. Drifting mesocosms: the influence of gelatinous zooplankton on mortality of bay anchovy, *Anchoa mitchilli*, eggs and yolk-sac larvae. ICES Journal of Marine Science. 51: 383-394.

Houde, E. D., and Rutherford, E. S. 1993. Recent trends in estuarine fisheries: Predictions of fish production and yield. Estuaries. 16(2): 161-176.

Hunter, J. R. 1981. Feeding ecology and predation of marine fish larvae. *In* Marine fish larvae: Morphology, ecology and relations to fisheries. Ed. Lasker, R. University of Washington Press. Seattle, WA. pg. 33-77.

Jordan, R. C., Gospodarek, A. M., Schultz, E. T., Cowen, R. K. and Kamazima, L. 2000. Spatial and temporal growth rate variation of bay anchovy (*Anchoa mitchilli*) larvae in the mid Hudson River Estuary. Estuaries. 23: 683-689.

Jung, S. 2002. Fish community structure and the spatial and temporal variability in recruitment and biomass production in Chesapeake Bay. Ph.D. Dissertation, University of Maryland, College Park.

Keister, J. E., Houde, E. D., and Breitburg, D. L. 2000. Effects of bottom-layer hypoxia on abundances and depth distribution of organisms in Patuxent River, Chesapeake Bay. Marine Ecology Progress Series. 205: 43-59.

Kimura, R., Secor, D. H., Houde, E. D., and Piccoli, P. M. 2000. Up-estuary dispersal of young -of-the-year bay anchovy *Anchoa mitchilli* in the Chesapeake Bay: inferences from microprobe analysis of strontium in otoliths. Marine Ecology Progress Series. 208: 217-227.

Kitchell, J. F., Stewart, D. J., and Weininger, D. 1977. Applications of bioenergetics model to yellow perch (*Perca flavescens*) and walleye (*Stizostedion vitreum vitreum*). Journal of the Fisheries Resource Board of Canada. 34: 1922-1935.

Leak, J. C. and Houde, E. D. 1987. Cohort growth and survival of bay anchovy *Anchoa mitchilli* larvae in Biscayne Bay, Florida. Marine Ecology Progress Series. 7:109-122.

Logerwell, E. A., Lavaniegos, B., and Smith, P. E. 2001. Spatially-explicit bioenergetics of Pacific sardine in the Southern California Bight: are mesoscale eddies areas of exceptional prerecruit production? Progress in Oceanography. 49: 391-406.

Luecke, C. Rice, J. A., Crowder, L. B. Yeo, S. E., and Binkowski, F. P. 1990. Recruitment mechanisms of bloater in Lake Michigan: an analysis of the predatory gauntlet. Canadian Journal of Fisheries and Aquatic Sciences. 47: 524-532.

Luo, J. and Brandt, S. B. 1993. Bay anchovy *Anchoa mitchilli* production and consumption in mid-Chesapeake Bay based on a bioenergetics model and acoustic measures of fish abundance. Marine Ecology Progress Series. 98: 223-236.

Luo, J. and Musick, J. A. 1991. Reproductive biology of the bay anchovy in Chesapeake Bay. Transactions of the American Fisheries Society. 120: 701-710.

MacGregor, J. M. 1994. M. S. Thesis. Temporal and spatial variability in cross-bay distribution and abundance of bay anchovy (*Anchoa mitchilli*) eggs and larvae. University of Maryland. College Park, MD. 138pp

MacGregor, J. M. and Houde, E. D. 1996. Onshore-offshore pattern and variability in distribution and abundance of bay anchovy *Anchoa mitchilli* eggs and larvae in Chesapeake Bay. Marine Ecology Progress Series. 138: 15-25.

Minello, T. J., Able, K. W., Weinstein, M. P. and Hays, C. G. 2003. Salt marshes as nurseries for nekton: testing hypotheses on density, growth and survival through meta-analysis. Marine Ecology Progress Series. 246: 39-59.

Monteleone, D. M. and Duguay, L. E. 1988. Laboratory studies of predation by the ctenophore *Mnemiopsis leidyi* on the early stages in the life history of the bay anchovy, *Anchoa mitchilli*. Journal of Plankton Research. 10: 359-372.

National Research Council. 1999. Sustaining Marine Fisheries. National Academy Press. Washington, D.C. 164.

Nixon, S. W. 1988. Physical energy inputs and the comparative ecology of lake and marine ecosystems. Limnology and Oceanography 33: 1005-1025.

Nixon, S. W., Jones, C. M. 1997. Age and growth of larval and juvenile Atlantic croaker, *Micropogonias undulates*, from the Middle Atlantic Bight and estuarine waters of Virginia. Fishery Bulletin. 95: 773-784.

North, E. W. 2001. Transport and retention of fish early-life stages in Chesapeake Bay: mechanisms and implications for recruitment. Ph.D. Dissertation, University of Maryland, College Park. 306p.

Olney, J. E. 1983. Eggs and early larvae of the bay anchovy, *Anchoa mitchilli*, and the weakfish, *Cynoscion regalis*, in lower Chesapeake Bay with notes on associated ichthyoplankton. Estuaries 6: 20-35.

Paradis, A. R. and Pepin, P. 2001. Modeling changes in the length-frequency distributions of fish larvae using field estimates of predator abundance and size distributions. Fisheries Oceanography. 10(2): 217-234.

Peebles, E. B., Hall, J. R. and Tolley, S. G. 1996. Egg production by the bay anchovy *Anchoa mitchilli* in relation to adult and larval prey fields. Marine Ecology Progress Series. 131: 61-73.

Pepin, P. 1993. An appraisal of the size-dependent mortality hypothesis for larval fish: Comparison of a multispecies study with an empirical review. Can J Fish Aquat Sci. 50: 2166-2174.

Pepin, P. Pearre, S. Jr., and Koslow, J. A. 1987. Predation of larval fish by Atlantic mackerel, *Scomber scombrus*, with a comparison of predation by zooplankton. Canadian Journal of Fisheries and Aquatic Sciences. 44: 2012-2018.

Purcell, J. E. and Arai, M. N. 2001. Interactions of pelagic cnidarians and ctenophores with fish: a review. Hydrobiologia. 451: 27-44.

Rice, J.A. 1995. Mathematical Statistics and Data Analysis. 2nd Edition. Duxbury Press. Belmont, CA

Rice, J. A., Miller, T. J., Rose, K. A., Crowder, L. B., Marschall, E. A., Trebitz, A. S., and DeAngelis, D. L. 1993. Growth rate variation and larval survival: inferences from an individual-based size-dependent predation model. Can J Fish Aquat Sci. 50(1): 133-142.

Rilling, G. C. 1996. Regional and temporal variability in growth, mortality, and age structure of bay anchovy (*Anchoa mitchilli*) eggs and larvae in the Chesapeake Bay. MSc Thesis, University of Maryland, College Park.

Rilling, G. C., and Houde, E. D. 1999. Regional and temporal variability in growth and mortality of bay anchovy, *Anchoa mitchilli*, larvae in Chesapeake Bay. Fish Bull. 97: 555-569.

Roman, M. R., Holliday, D. V. 2001. Temporal and spatial patterns of zooplankton in the Chesapeake Bay turbidity maximum. Marine Ecology Progress Series. 213:215-227.

Rose, K. A., Cowan, J. H. Jr., Clark, M. E., Houde, E. D., and Wang, S. 1999. An individual -based model of bay anchovy population dynamics in the mesohaline region of Chesapeake Bay. Marine Ecology Progress Series. 185: 113-132.

Saksena, V. P. and Houde, E. D. 1972. Effects of food level on the growth and survival of laboratory-reared larvae of bay anchovy (*Anchoa mitchilli* Valenciennes) and scaled sardine (*Harengula pensacolae* Goode and Bean). Journal of Experimental Marine Biology and Ecology. 8: 249-258.

Schmitten, R. A. 1999. Essential fish habitat: Opportunities and challenges for the next millennium. pg. 3-10 *in* L. Benka, editor. Fish habitat: essential fish habitat and rehabilitation. American Fisheries Society, Symposium 22, Bethesda Maryland.

Sheridan, P. F. 1978. Food habits of the bay anchovy, *Anchoa mitchilli*, in Apalachicola Bay, Florida. Northeast Gulf Science. 2: 126-132.

TIES, Chesapeake Bay LMER, Trophic Interactions in Estuarine Systems. July 7, 2003. <http://www.chesapeake.org/ties/>

Tucker, J. W. 1989. Energy utiliation in bay anchovy, *Anchoa mitchilli*, and black sea bass, *Centropristis striata striata*, eggs and larvae. Fishery Bulletin. 87: 279-293.

Tyler, J. A., and Brandt, S. B. 2001. Do spatial models of growth rate potential reflect fish growth in a heterogeneous environment? A comparison of model results. Ecology of Freshwater Fish. 10: 43-56.

Werner, E. E. 1974. The fish size, prey size, handling time relation in several sunfishes and some implications. Journal of the Fisheries Research Board of Canada. 31: 1531-1536.

Zastrow, C. E., Houde, E. D. and Morin, L. G. 1991. Spawning, fecundity, hatch-date frequency and young-of-the-year growth of bay anchovy *Anchoa mitchilli* in mid-Chesapeake Bay. Marine Ecology Progress Series. 73: 161-171.

APPENDIX: VALUES OF MODEL INPUTS FROM RILLING (1996) FIELD SURVEYS

The data shown in the following series of figures originates from the field data collected as a part of the thesis research conducted by Gene C. Rilling at the University of Maryland (Rilling 1996). As was described in the methods, this data has been modified to make it compatible with the requirements of the individual based model. With the exception of sea nettles, which were only collected during July, the following figures show the initial conditions for each simulation during June and July. Figures A1, A2, and A3 show the initial numbers of bay anchovy larvae, ctenophores, and sea nettles in each layer at each site. The densities of larvae (larvae m^{-3}), ctenophores (ctenophores m^{-3}), and sea nettles (sea nettles m^{-3}) collected at each layer of each station was multiplied by 2000 m^3 to obtain the initial numbers of individuals. Figures A4, A5 and A6 show the mean initial sizes of larvae, ctenophores and sea nettles in each layer at each site. Figure A7 shows the dry-weight biomass of zooplankton in each layer at each site. Figure A8 shows the temperature in each layer at each site.

Figure A1: Initial number of larval bay anchovy at each site for the months of June and July. The initial number of larvae is equal to the density of the larvae observed during a 2-minute tow at a site × 2000 m^3. Closed circles indicate initial numbers of larvae at surface-layer stations while open circles indicate initial numbers of larvae at bottom-layer stations.

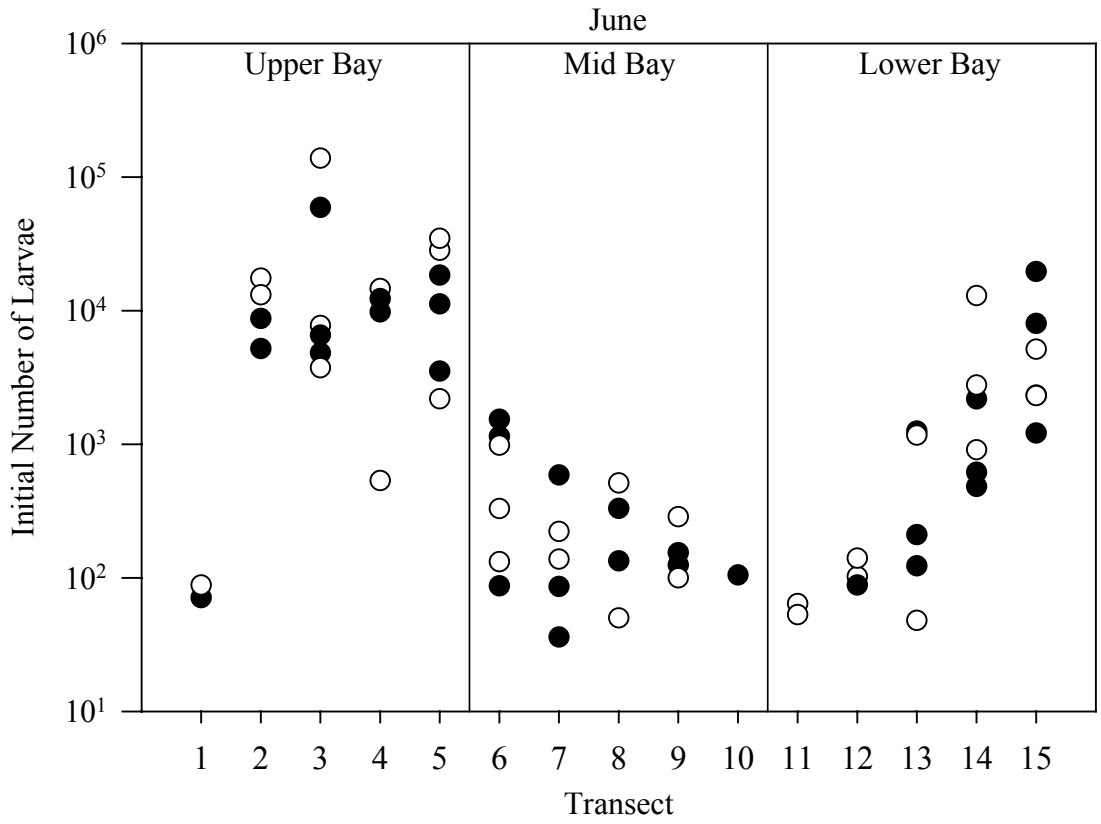
June
Upper Bay
Mid Bay
Lower Bay
Initial Number of Larvae
10^6
10^5
10^4
10^3
10^2
10^1
1 2 3 4 5 6 7 8 9 10 11 12 13 14 15
Transect

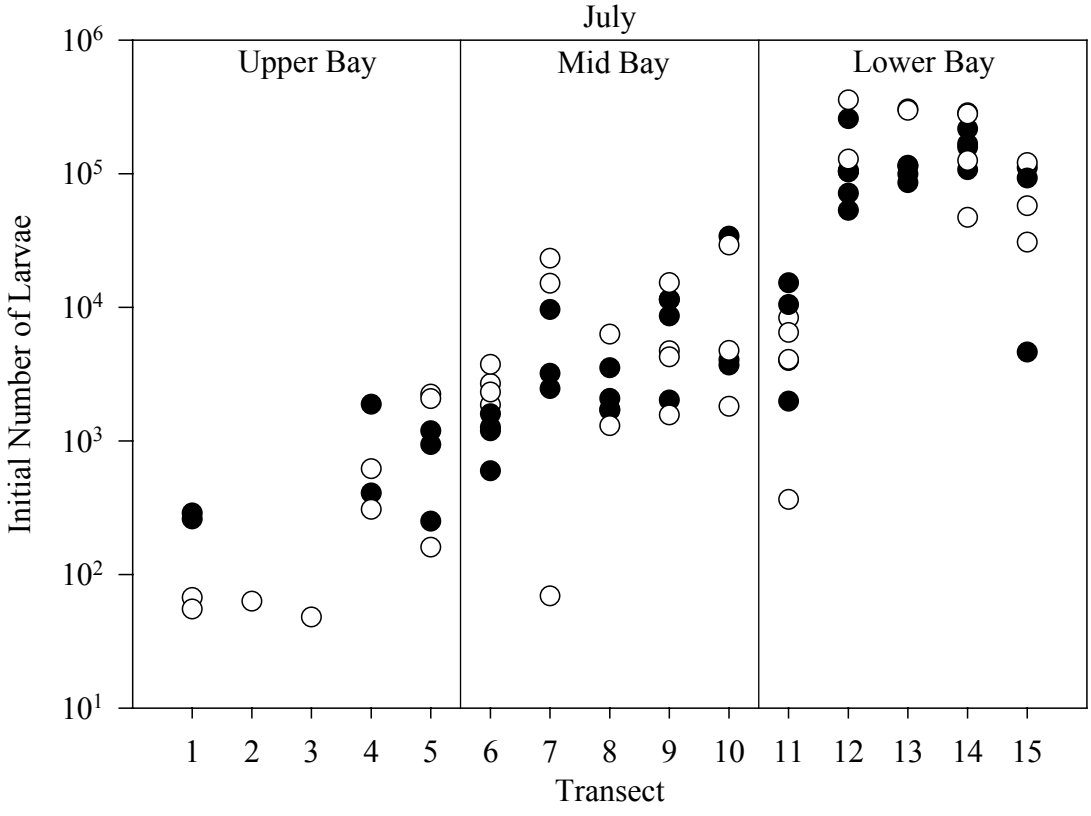
July
Upper Bay
Mid Bay
Lower Bay
Initial Number of Larvae
10^6
10^5
10^4
10^3
10^2
10^1
1 2 3 4 5 6 7 8 9 10 11 12 13 14 15
Transect

Figure A2: Initial number of ctenophores at each site for the months of June and July. The initial number of ctenophores is equal to the density of the ctenophores observed during a 2-minute tow at a site × 2000 m^3. Closed circles indicate initial numbers of ctenophores at surface-layer stations while open circles indicate initial numbers of ctenophores at bottom-layer stations.

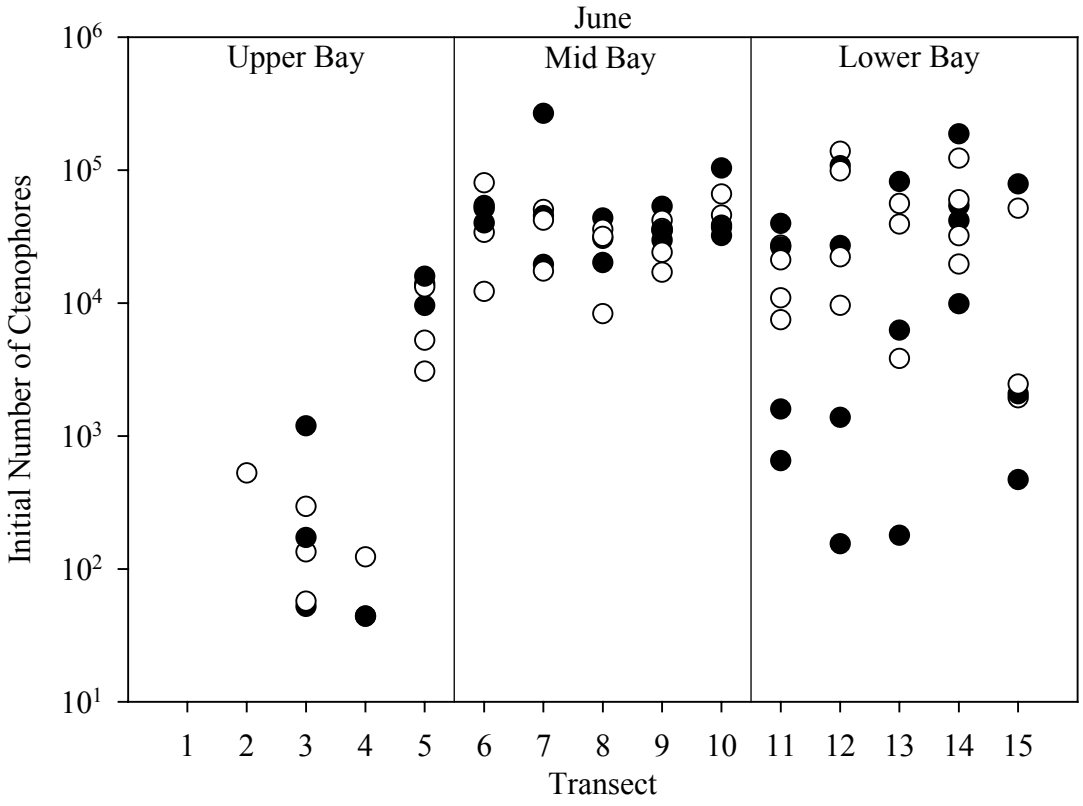
June
Upper Bay
Mid Bay
Lower Bay
Initial Number of Ctenophores
10^6
10^5
10^4
10^3
10^2
10^1
1 2 3 4 5 6 7 8 9 10 11 12 13 14 15
Transect

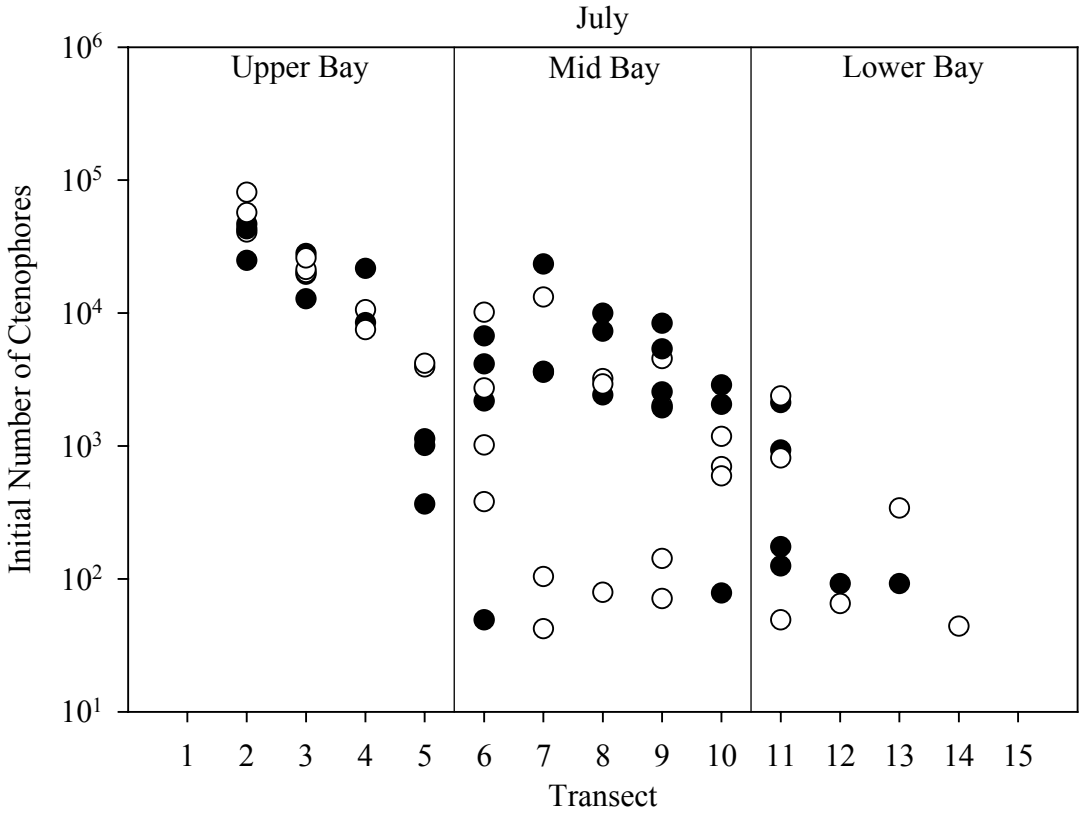
July
Upper Bay
Mid Bay
Lower Bay
Initial Number of Ctenophores
10^6
10^5
10^4
10^3
10^2
10^1
1 2 3 4 5 6 7 8 9 10 11 12 13 14 15
Transect

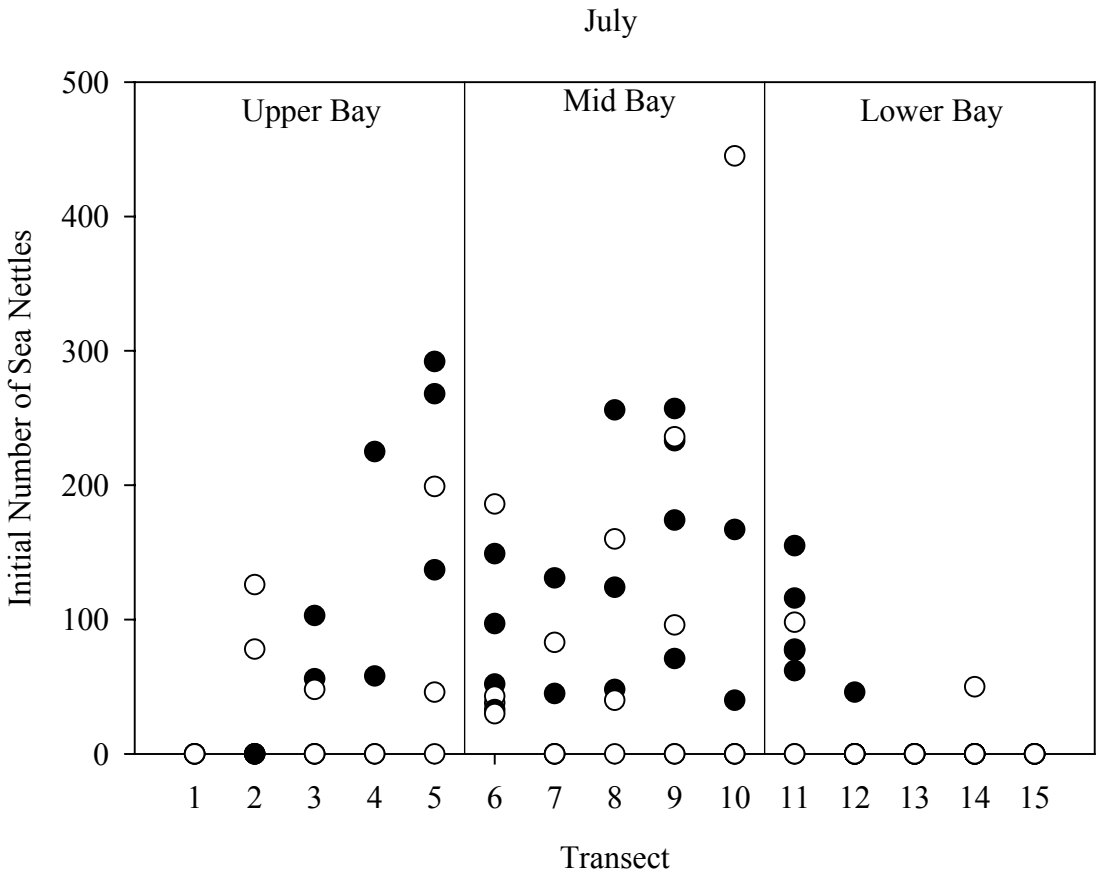

Figure A3: Initial number of sea nettles at each sites for the months of June and July. The initial number of sea nettles is equal to the density of the sea nettles observed during a 2-minute tow at a site × 2000 m^3. Closed circles indicate initial numbers of sea nettles at surface-layer stations while open circles indicate initial numbers of sea nettles at bottom-layer stations.

Figure A4: Mean initial lengths of larval bay anchovy at each site for the months of June and July. Closed circles indicate mean initial lengths of larvae at surface-layer stations while open circles indicate mean initial lengths of larvae at bottom-layer stations.

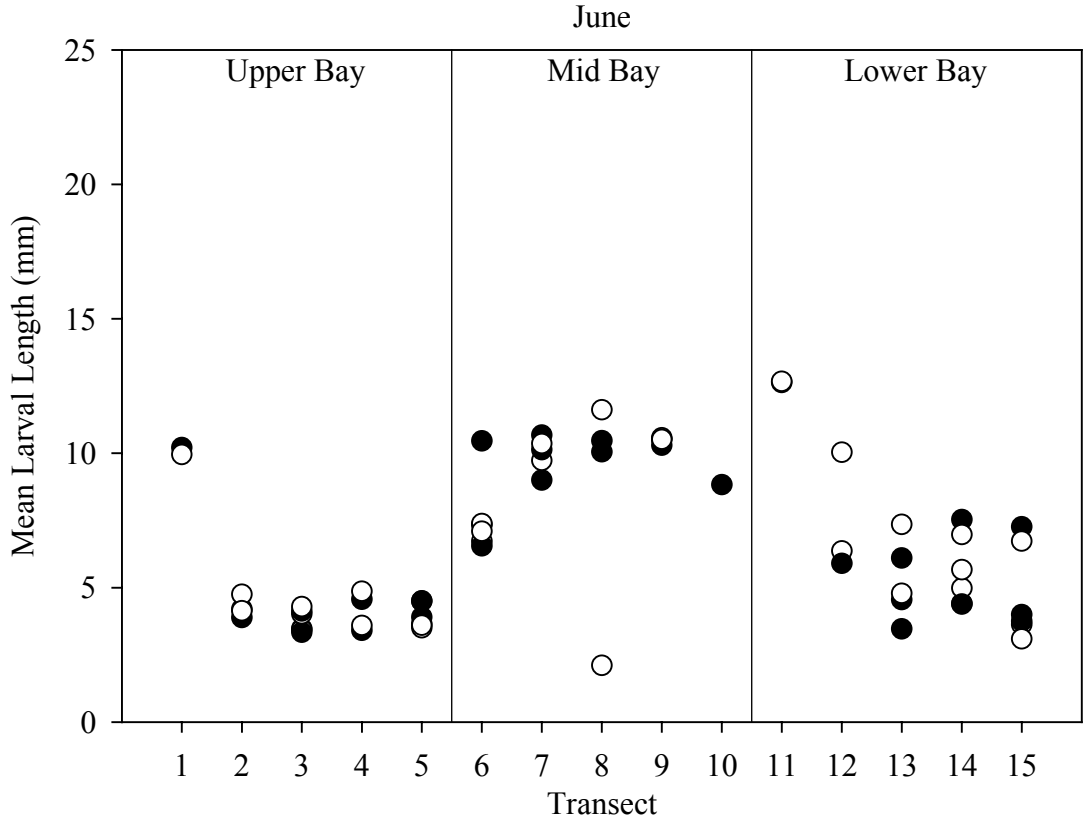
June
Upper Bay
Mid Bay
Lower Bay
Mean Larval Length (mm)
0
5
10
15
20
25
1 2 3 4 5 6 7 8 9 10 11 12 13 14 15
Transcect

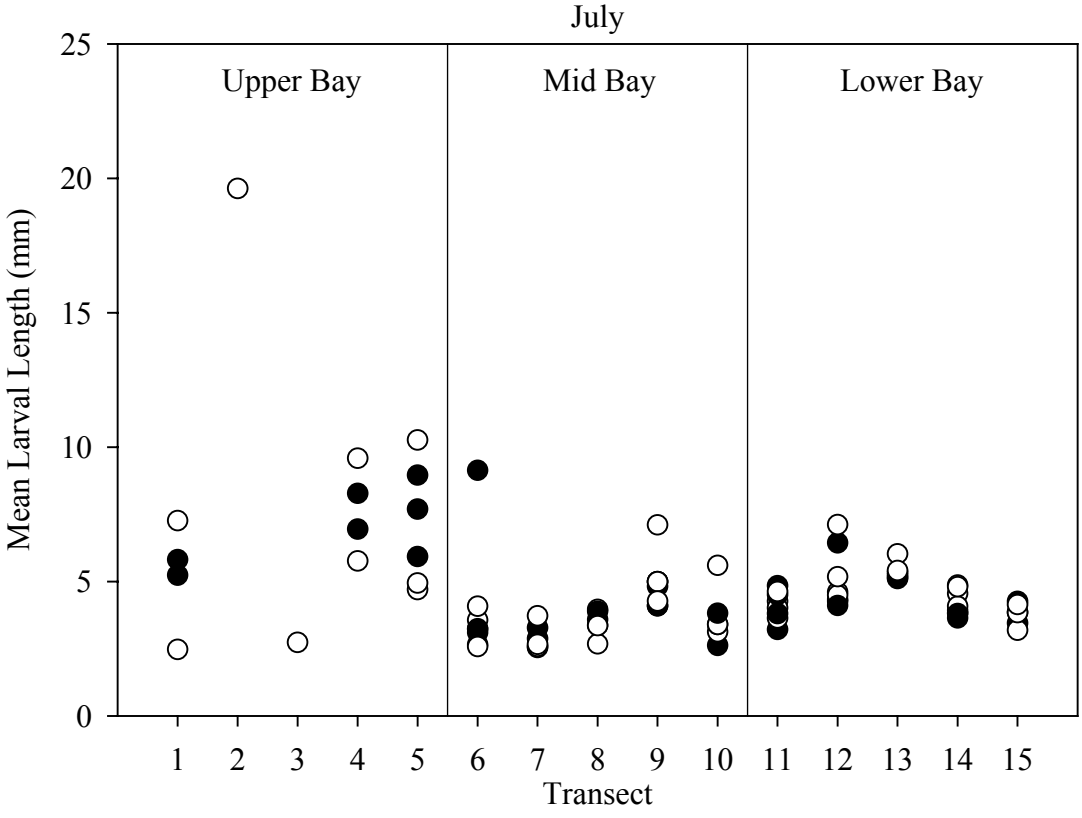
July
Upper Bay
Mid Bay
Lower Bay
Mean Larval Length (mm)
0
5
10
15
20
25
1 2 3 4 5 6 7 8 9 10 11 12 13 14 15
Transect

Figure A5: Mean initial lengths of ctenophores at each site for the months of June and July. Closed circles indicate mean initial lengths of ctenophores at surface-layer stations while open circles indicate mean initial lengths of ctenophores at bottom-layer stations.

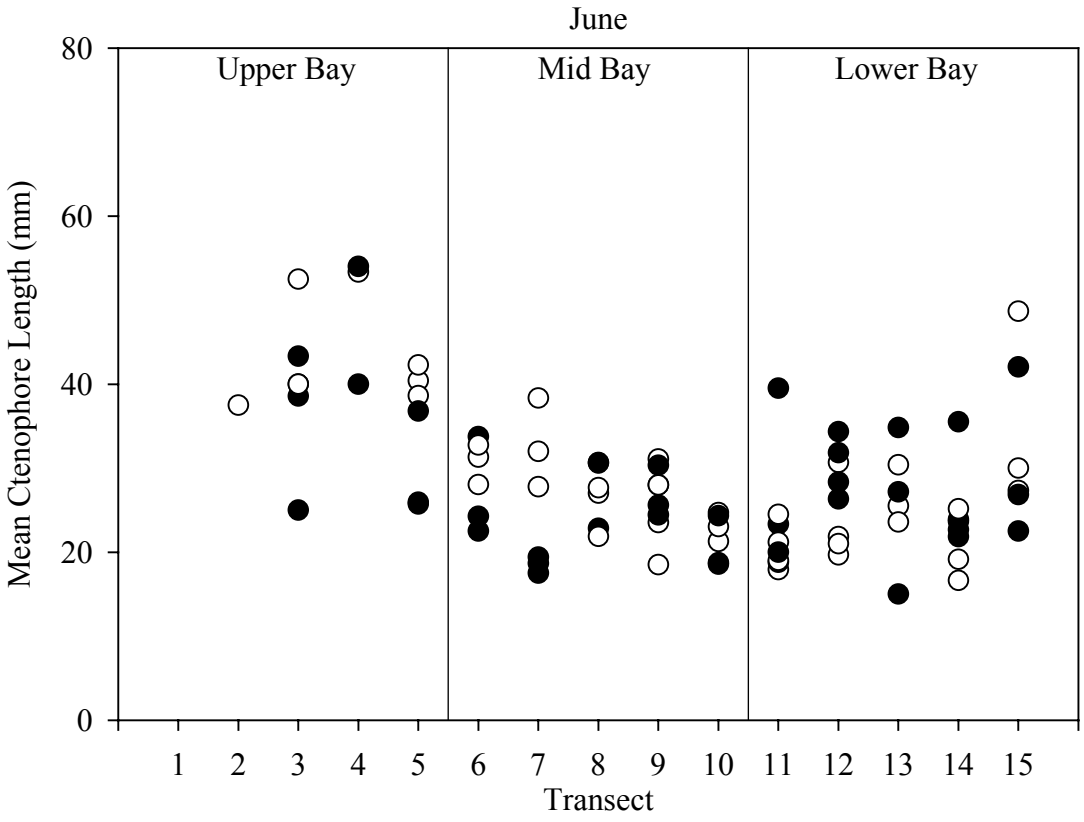
June
Upper Bay
Mid Bay
Lower Bay
Mean Ctenophore Length (mm)
0
20
40
60
80
1 2 3 4 5 6 7 8 9 10 11 12 13 14 15
Transect

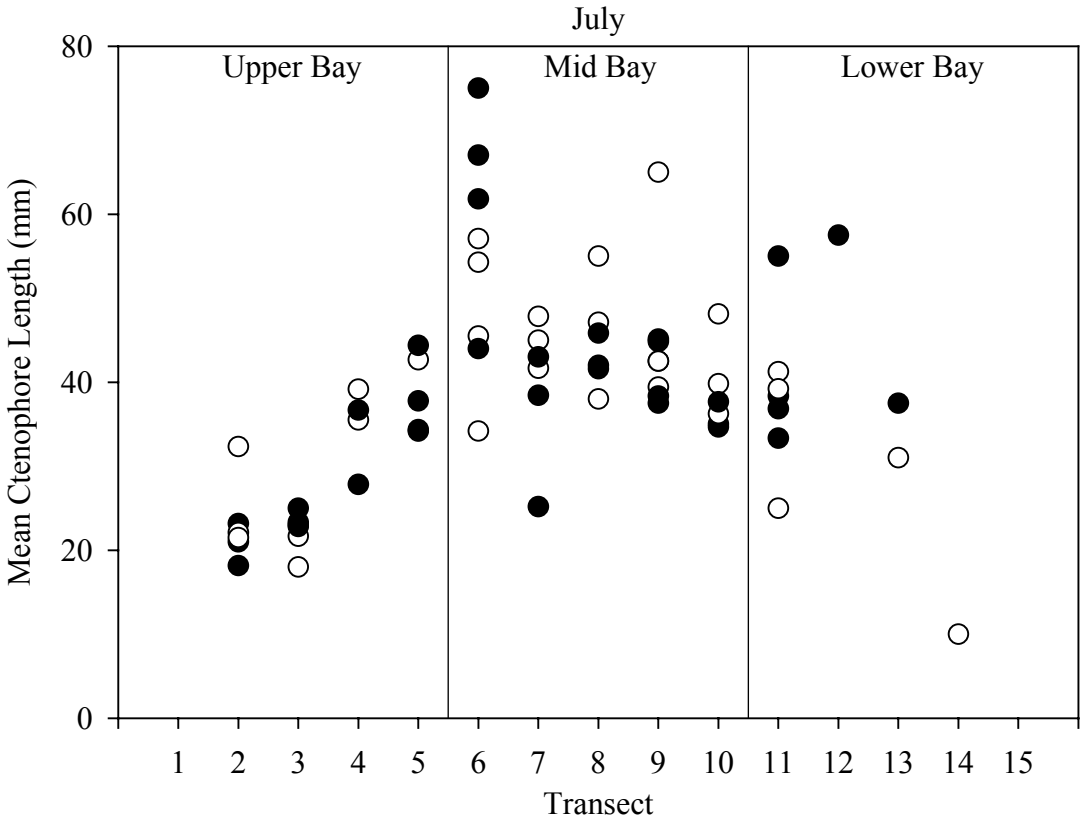
July
Upper Bay
Mid Bay
Lower Bay
Mean Ctenophore Length (mm)
0
20
40
60
80
1 2 3 4 5 6 7 8 9 10 11 12 13 14 15
Transect

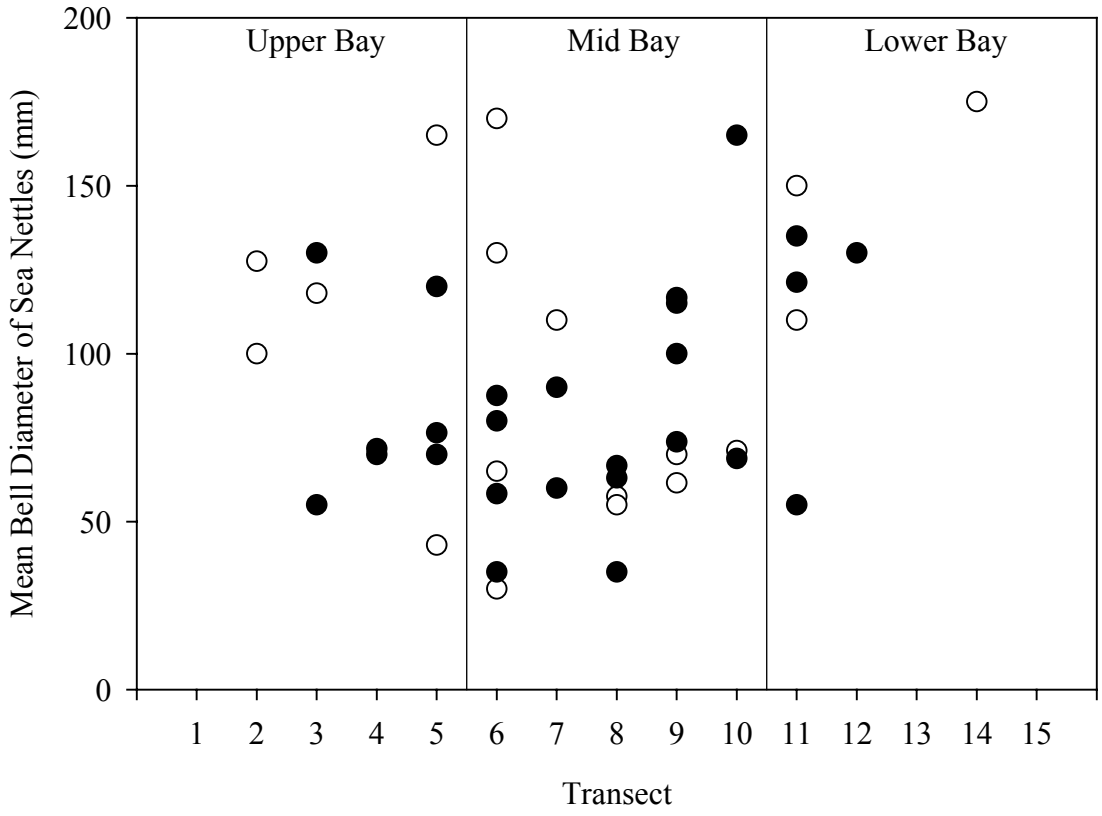

Figure A6: Mean initial lengths of sea nettles at each station for July. Closed circles indicate mean initial lengths of sea nettles at surface-layer stations while open circles indicate mean initial lengths of sea nettles at bottom-layer stations.

Figure A7: Combined densities of zooplankton in terms of dry weights of zooplankton per liter at a site. The density of each zooplankton group was multiplied by the dry weigh per individual of that type to obtain a total weight for each group. The dry weights of the four zooplankton types were added together to get a single measure of zooplankton density in terms of dry weight at each site. Closed circles indicate the density of zooplankton at surface-layer stations while open circles indicate the density of zooplankton at bottom-layer stations.

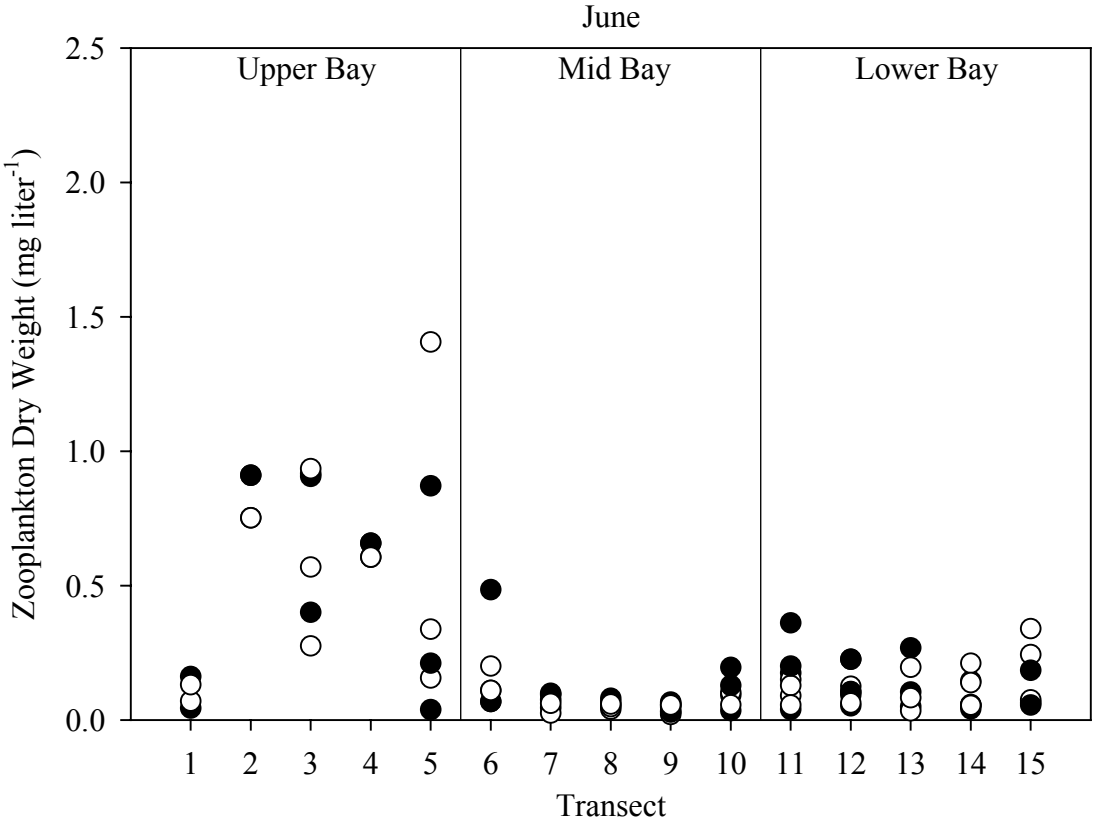
June
Upper Bay
Mid Bay
Lower Bay
Zooplankton Dry Weight (mg liter-1)
2.5
2.0
1.5
1.0
0.5
0.0
1 2 3 4 5 6 7 8 9 10 11 12 13 14 15
Transect

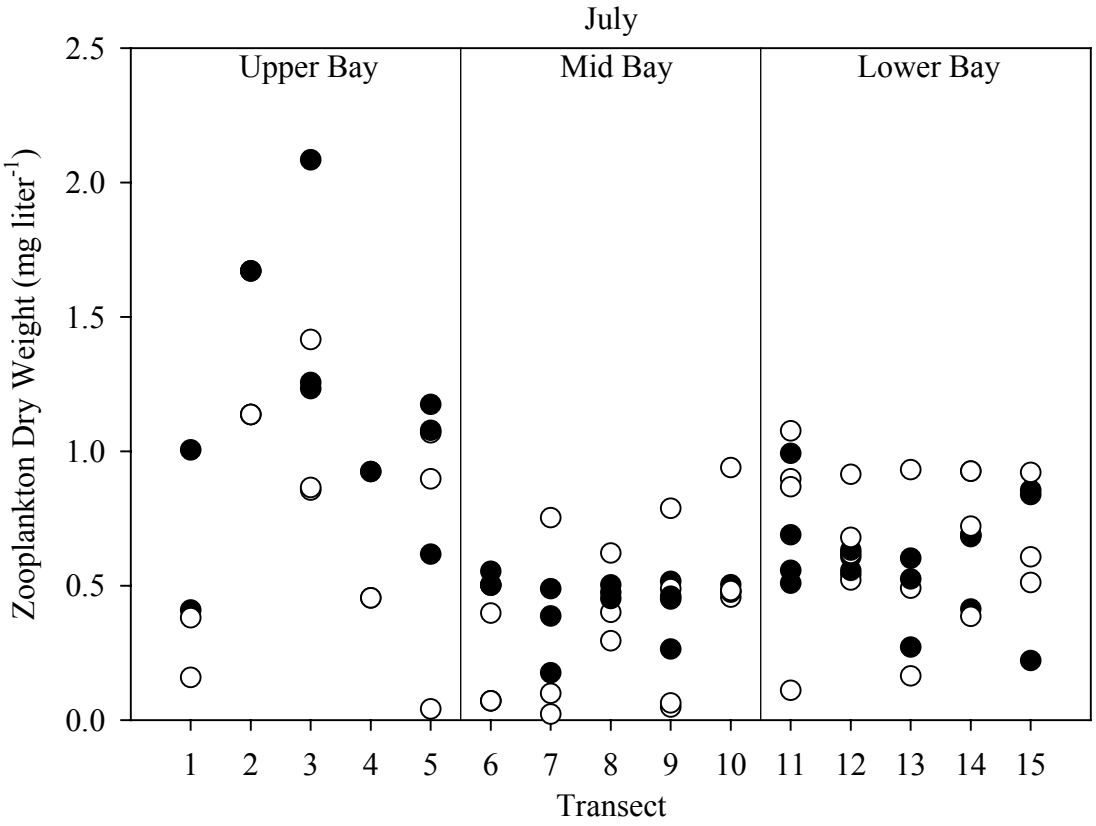
July
Upper Bay
Mid Bay
Lower Bay
Zooplankton Dry Weight (mg liter-1)
2.5
2.0
1.5
1.0
0.5
0.0
1 2 3 4 5 6 7 8 9 10 11 12 13 14 15
Transect

Figure A8: Temperature at each station for the months of June and July. Temperatures are the mean of all temperature readings taken by a CTD cast within a layer weighted by the depth interval covered by each reading. Closed circles are temperature readings for the surface-layer stations while open circles are temperatures for bottom-layer stations.

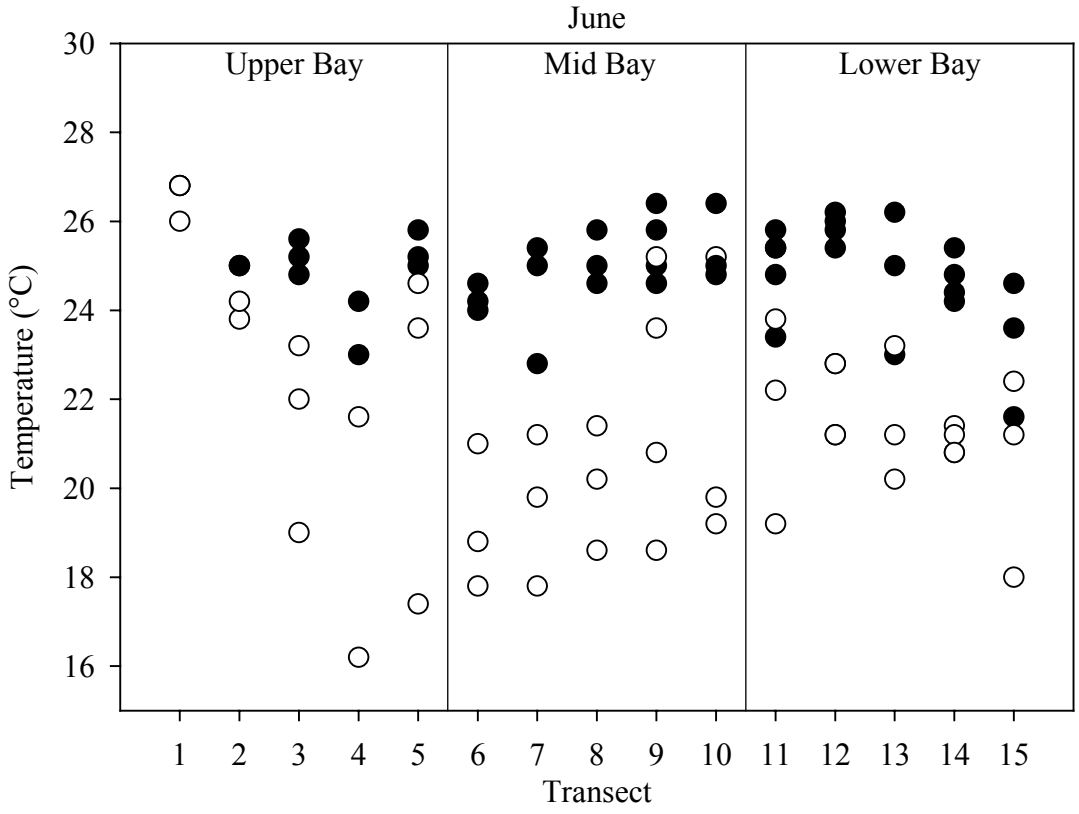
June
Upper Bay
Mid Bay
Lower Bay
Temperature (°C)
30
28
26
24
22
20
18
16
1 2 3 4 5 6 7 8 9 10 11 12 13 14 15
Transcect

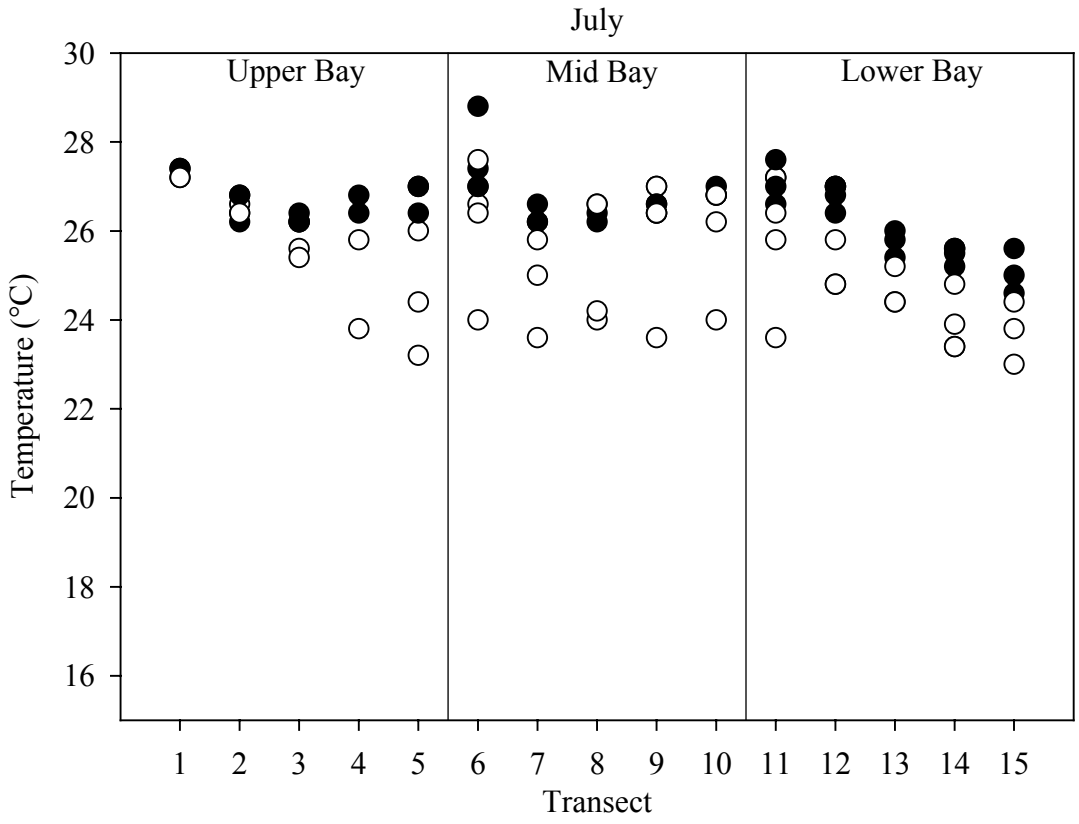
July
Upper Bay
Mid Bay
Lower Bay
Temperature (°C)
30
28
26
24
22
20
18
16
1 2 3 4 5 6 7 8 9 10 11 12 13 14 15
Transcect

VITA

Aaron Thomas Adamack was born in Fernie, British Columbia, Canada, on January 17, 1976, the son of Beverly E. Adamack and Dr. Thomas L. Adamack and the brother of Denene C. Adamack. He attended school in Fernie, British Columbia, before moving to Kelowna, British Columbia, where he attended Mt. Boucherie Secondary School, graduating in 1994. He then attended Okanagan University College from 1994-1996 before transferring to the University of British Columbia, which he attended from 1996-1999, and received a Bachelor of Science in animal biology. He entered the Department of Oceanography and Coastal Sciences at the Louisiana State University in August 1999 as a graduate research assistant under the direction of Dr. Kenneth A. Rose and as a candidate for the degree of Master of Science. Aaron will receive a Master of Science degree in oceanography and coastal sciences in December 2003.